

CONSTANT ENERGY SYNCHRONOUS LUMINESCENCE SPECTROSCOPY:  
THEORY AND APPLICATIONS

By

LEIGH ANN FILES

A DISSERTATION PRESENTED TO THE GRADUATE SCHOOL  
OF THE UNIVERSITY OF FLORIDA IN  
PARTIAL FULFILLMENT OF THE REQUIREMENTS  
FOR THE DEGREE OF DOCTOR OF PHILOSOPHY

UNIVERSITY OF FLORIDA

1986

dedicated to my parents  
with all my love

#### ACKNOWLEDGEMENTS

First I would like to thank my parents, brothers, and grandparents for all their support and love. Their faith in me allowed me to have enough confidence to complete a task which I never could have accomplished otherwise.

I would also like to express my appreciation for the wonderful instructors; Dr. J. E. Bennett, Mrs. M. Cooper, Dr. N. L. Trautwein, Mr. L. Battles, and Dr. L. D. Kispert, who encouraged me to pursue research in chemistry.

I am deeply grateful to all the people I have worked with during my stay at the University of Florida. I would especially like to thank Jonell Kerkhoff, Ben Smith, Ed Voigtman, and Linda Hirshy for their input and guidance in helping to establish my research system. I would also like to acknowledge Brad Jones and Monica Moore for their assistance with the PAH studies. Best wishes go to Mike Mignardi in his future work with CESLS, and many thanks for his help with the final project involving phosphorescence.

The acceptance and guidance as well as the invaluable friendship of the people I have worked with at the University of Florida have made my stay not only successful, but very enjoyable. Among these people I must mention Kathy, Jonell, Doug, Jose, Brad, Moi, and Keith. I can never express how much these people have meant to me.

Finally, I would like to say a very special thank you to Dr. Winefordner. His dedication and enthusiasm for research as well as his sincere interest in his students and colleagues are an example which I will always admire and strive to emulate.

## TABLE OF CONTENTS

	<u>Page</u>
ACKNOWLEDGEMENTS.....	iii
LIST OF TABLES.....	vi
LIST OF FIGURES.....	vii
ABSTRACT.....	xi
 CHAPTERS	
 1 MIXTURE ANALYSIS	
Introduction.....	1
Goals.....	8
 2 THEORETICAL OPTIMIZATION OF PARAMETER SELECTION IN CONSTANT ENERGY SYNCHRONOUS LUMINESCENCE SPECTROMETRY	
Introduction.....	11
Theory.....	12
Discussion.....	20
Conclusions.....	39
 3 ANALYSIS OF ENVIRONMENTAL SAMPLES CONTAINING POLYCYCLIC AROMATIC HYDROCARBONS	
Introduction.....	41
Experimental.....	42
PAH Mixture Analysis.....	45
Gasoline Engine Exhaust Analysis.....	46
Gasoline and Crude Oil Fingerprinting.....	55
Conclusions.....	68
 4 FEASIBILITY STUDY OF CONSTANT ENERGY SYNCHRONOUS LUMINESCENCE SPECTROMETRY FOR PESTICIDE DETERMINATION	
Introduction.....	69
Experimental.....	70
Results and Discussion.....	71

## CHAPTERS

### 5 TIME RESOLVED PHOSPHORIMETRY

Introduction.....	85
Experimental.....	88
Results and Discussion.....	90

### 6 CONCLUSION

Summary.....	96
Future Work.....	99

GLOSSARY.....	100
---------------	-----

REFERENCES.....	102
-----------------	-----

BIOGRAPHICAL SKETCH.....	106
--------------------------	-----

## List of Tables

<u>Table</u>	<u>Page</u>
I      Spectral Data for Three Model Compounds.....	22
II     Limiting Cases.....	26
III    Spectral Data for Two Model Compounds.....	32
IV     Experimental Components for CESLS.....	44
V      Calculated Energy Transitions (in $\text{cm}^{-1}$ ) for Carbaryl.....	74
VI     Calculated Energy Transitions (in $\text{cm}^{-1}$ ) for Naphthol.....	75
VII    Limits of Detection for Pesticides with Variable Parameters.....	79

## List of Figures

<u>Figure</u>		<u>Page</u>
1	Energy level diagram illustrating the luminescence processes for an idealized molecule.....	3
2	CESLS spectra of anthracence. (A) $\Delta\bar{\nu} = 1$ vibrational quantum, (B) $\Delta\bar{\nu} = 3$ vibrational quanta, (C) Jablonski diagram illustrating $\Delta\bar{\nu} = 1$ vibrational quantum, (D) Jablonski diagram illustrating $\Delta\bar{\nu} = 3$ vibrational quanta.....	9
3	Geometric model for CESLS. The ellipse defines the contour equivalent to half the maximum peak intensity. The dashed line defines a CESLS scan with $\Delta\bar{\nu} = \bar{\nu}_{i_0} - \bar{\nu}_{j_0}$ .....	18
4	Graphical representation of various values of $\Delta\bar{\nu}$ (— —) and the line (— — —) defining the position of the CESLS maxima for this scan.....	19
5	Graphical representation of three special cases for a) $\sigma_i = \sigma_j$ , b) $\sigma_i \ll \sigma_j$ , c) $\sigma_i \gg \sigma_j$ .....	25
6	Comparison of peaks generated by using a variety of $\Delta\bar{\nu}$ values ( $\text{cm}^{-1}$ ) for compound A. See Table II. $\Delta\bar{\nu} = 15,000$ (----), $14,000$ (— — —), $13,000$ (— — —), $16,000$ (— · —), and $17,000$ (— — —).....	27
7	Excitation, $A_x$ , (— —) and emission, $A_m$ , (——) peaks for compound A. $\sigma_i = \sigma_j$ . The CESLS spectra, $A_s$ , (----) is shown for the scan path $\Delta\bar{\nu} = \bar{\nu}_{i_0} - \bar{\nu}_{j_0}$ .....	29
8	Excitation, $B_x$ , (— —) and emission, $B_m$ , (——) peaks for compound B. $\sigma_i = \sigma_j/2$ . The CESLS spectrum, $B_s$ , (----) is shown for the scan path $\Delta\bar{\nu} = \bar{\nu}_{i_0} - \bar{\nu}_{j_0}$ .....	30
9	Excitation, $C_x$ , (— —) and emission, $C_m$ , (——) peaks for compound C. $\sigma_i = 2\sigma_j$ . The CESLS spectrum, $C_s$ , (----) is shown for the scan path $\Delta\bar{\nu} = \bar{\nu}_{i_0} - \bar{\nu}_{j_0}$ .....	31
10	Excitation (— —) and emission (——) peaks for model compounds D ( $D_x, D_m$ ) and E ( $E_x, E_m$ ). See Table III. CESLS spectrum (— · —) with $\Delta\bar{\nu} = \Delta\bar{\nu}_{\text{max}}$ for both compounds (D and E), arbitrarily plotted in terms of excitation energy.....	33

11	Peaks described in Figure 10 with x-axis in units of wavelength (nm).....	34
12	Excitation (— —) and emission (————) peaks for compounds D and E as described in Table III. CWSLS spectrum with $\Delta\lambda = \Delta\lambda_{\max}$ for compound D (85.227 nm) (---).....	35
13	Excitation (— —) and emission (————) peaks for compounds D and E. CWSLS spectrum with $\Delta\lambda = \Delta\lambda_{\max}$ for compound E (121.457 nm) (---).....	36
14	Scans defined by $\Delta\bar{\nu} = 12,000 \text{ cm}^{-1}$ (————), $\Delta\lambda = 85.227 \text{ nm}$ (---), and $\Delta\lambda = 121.457 \text{ nm}$ (— —). For compounds D and E as described in Table III.....	37
15	Schematic diagram of experimental system for obtaining CESLS spectra.....	43
16	CESLS scan of 16 component PAH mixture $\Delta\bar{\nu} = 1400 \text{ cm}^{-1}$ .....	47
17	CESLS scan of 16 component PAH mixture $\Delta\bar{\nu} = 4800 \text{ cm}^{-1}$ .....	48
18	CESLS scan of leaded gasoline exhaust extracts obtained using multiple sample collection system ( $\Delta\bar{\nu} = 1400 \text{ cm}^{-1}$ ). Compounds identified include benzo(a)pyrene (BAP), benzo(k)fluoranthene (BKF), anthracene (A), coronene (COR), and perylene (PER).....	50
19	CESLS scan of leaded gasoline exhaust extracts obtained using multiple sample collection system ( $\Delta\bar{\nu} = 2800 \text{ cm}^{-1}$ ). Compounds identified include phenanthrene (PHE), chrysene (CHR), pyrene (PYR), anthracene (A), benzo(a)pyrene (BAP), benzo(k)fluoranthene (BKF), and anthanthrene (ANT).....	51
20	CESLS scan of exhaust from different gasoline samples <sub>1</sub> obtained using a U-tube collection system at $1400 \text{ cm}^{-1}$ . Samples: (a) Brand A Super Unleaded, (b) Brand A Unleaded, (c) Brand B Super Unleaded with Ethanol, (d) Brand B Unleaded with Ethanol, and (e) Brand C Regular Leaded.....	53
21	CESLS scan of exhaust from different gasoline samples <sub>1</sub> obtained using a U-tube collection system at $4800 \text{ cm}^{-1}$ . Samples: (a) Brand A Super Unleaded, (c) Brand B Super Unleaded with Ethanol, and (e) Brand C Regular Leaded.....	54
22	CESLS scans at 77 K and $1400 \text{ cm}^{-1}$ for a) Brand D gasoline (1:10 dilution), b) mixture containing benzo(a)pyrene (BAP) and anthracene (A), and c) mixture containing pyrene (PYR) and fluoranthene (FLU).....	57

23	CESLS scans at 77 K and $4800\text{ cm}^{-1}$ for samples identified in Figure 22.....	58
24	CESLS scans at 77 K and $1400\text{ cm}^{-1}$ for 1:50 dilutions of a) Brand E Super Unleaded Gasoline, b) Brand E Regular Gasoline, and c) Brand F Regular Gasoline.....	59
25	CESLS scans at 298 K and $1400\text{ cm}^{-1}$ for samples identified in Figure 24 (no dilutions required).....	60
26	CESLS scans at 77 K and $1400\text{ cm}^{-1}$ for 1:50 dilutions of a) Brand G Diesel and b) Brand G Regular Gasoline.....	62
27	CESLS scans at 298 K and $1400\text{ cm}^{-1}$ for samples identified in Figure 26 (no dilutions required).....	63
28	CESLS scans at 77 K and $1400\text{ cm}^{-1}$ for 1:1000 dilutions of crude oil number one distillation fractions a) below $350^{\circ}\text{C}$ , b) 160 to $240^{\circ}\text{C}$ , and c) 240 to $350^{\circ}\text{C}$ .....	64
29	CESLS scans at 298 K and $1400\text{ cm}^{-1}$ for 1:10 dilutions of crude oil number one fractions described in Figure 28.....	65
30	CESLS scans at 77 K and $1400\text{ cm}^{-1}$ for 1:1000 dilutions of crude oil number two fractions a) below $350^{\circ}\text{C}$ , b) 160 to $240^{\circ}\text{C}$ , and c) 240 to $350^{\circ}\text{C}$ .....	66
31	CESLS scans at 298 K and $1400\text{ cm}^{-1}$ for 1:10 dilutions of crude oil number two fractions described in Figure 30.....	67
32	Excitation and emission scans of carbaryl. Prominent peaks are listed in Table V.....	72
33	Excitation and emission scans of naphthol. Prominent peaks are listed in Table VI.....	73
34	CESLS scan of naphthol with $\Delta\bar{\nu} = 1400\text{ cm}^{-1}$ . Excitation wavelength range 250-350 nm. Excitation and emission bandpasses 1.5 nm.....	76
35	CESLS scans of a mixture of carbaryl, naphthol, and carbofuran with $\Delta\bar{\nu} = 1400$ and $2650\text{ cm}^{-1}$ . Excitation and emission bandpasses 1.5 nm.....	78
36	Constant energy scans of naphthol with $\Delta\bar{\nu} = 2650\text{ cm}^{-1}$ . Demonstrating the comparison between spectra obtained with bandpasses of 1.5 nm on both monochromators versus a) maintaining a 1.5 nm emission bandpass and opening the excitation bandpass to 4 nm, and b) maintaining a 1.5 nm excitation bandpass and opening the emission bandpass to 4 nm.....	81
37	Constant energy scans of carbaryl with $\Delta\bar{\nu} = 2650\text{ cm}^{-1}$ . Showing the results obtained with the same variation in parameters described in Figure 36.....	82

38	Constant energy scans of a mixture of carbaryl, naphthol, and carbofuran with a) bandpasses of 1.5 nm on both monochromators, b) excitation bandpass of 2.5 nm and emission bandpass of 1.5 nm, and c) excitation bandpass of 1.5 nm and emission bandpass of 2.5 nm.....	84
39	Illustration demonstrating the ability to obtain more selective spectra through the use of time resolution. FL--flash lamp pulse, BC--boxcar, f--fluorescence, p--phosphorescence, $t_d$ --delay time, $t_g$ --gate time. Subscripts used to denote compounds with different excited state lifetimes.....	86
40	Schematic diagram of experimental system modified to allow one to obtain time-resolved CESLS spectra.....	89
41	Constant energy scans with $\Delta\bar{\nu} = 12,000 \text{ cm}^{-1}$ for benzo(e)pyrene obtained using (a) a continuous source and measuring emission directly, and (b) a flashlamp as the source and measuring emission with gated detection.....	91
42	Constant energy scans with $\Delta\bar{\nu} = 12,000 \text{ cm}^{-1}$ for a mixture of benzo(e)pyrene and phenanthrene obtained using (a) a continuous source and measuring emission directly, and (b) a flashlamp as the source and measuring emission with gated detection.....	92
43	Constant energy scans with $\Delta\bar{\nu} = 12,000 \text{ cm}^{-1}$ for a mixture of benzo(a)pyrene and carbazole obtained using (a) a continuous source and measuring emission directly, and (b) a flashlamp as the source and measuring emission with gated detection.....	93

Abstract of Dissertation Presented to the Graduate School  
of the University of Florida in Partial Fulfillment of the  
Requirements for the Degree of Doctor of Philosophy

CONSTANT ENERGY SYNCHRONOUS LUMINESCENCE SPECTROSCOPY:  
THEORY AND APPLICATIONS

By

Leigh Ann Files

August 1986

Chairman: James D. Winefordner  
Major Department: Chemistry

Constant energy synchronous luminescence spectroscopy (CESLS) is a simple, inexpensive method which demonstrates excellent selectivity for mixture analysis. The spectral parameters of CESLS have been evaluated for optimization of experimental variables. Mathematical relationships have been derived for peak wavelength maximum, intensity maximum, and peak bandwidth, defining their dependence upon the luminescence excitation and emission spectral characteristics and the selected scan path.

CESLS at low temperature (77 K) has been applied to environmental analysis involving fingerprinting gasoline exhaust samples containing polyaromatic hydrocarbons (PAHs). Combining this technique with a system which allowed a crude sample separation based on temperature provided increased selectivity and sample information.

CESLS was also applied to analysis of gasoline and crude oil samples containing PAHs. Sample identification at low temperature (77 K) with quartz tubes and at room temperature on filter paper was

compared. The ability to identify individual PAHs in samples as well as fingerprint different samples based on total PAH content was demonstrated.

The results obtained theoretically involving optimization of experimental parameters have been applied to determination of pesticides. Limits of detection, analytically useful ranges, and results obtained using a variety of scan parameters have been determined for carbaryl, naphthol, and carbofuran. Results showed promise and indicated that CESLS has great potential for a wide variety of applications involving complex mixture analysis.

An experimental system has been developed to allow time-resolved measurements in combination with constant energy scanning. Time-resolution further enhances the selectivity of constant energy synchronous luminescence spectra. The system has been designed for maximum versatility. Room and low temperature measurements as well as fluorescence and phosphorescence spectra can be obtained with minimal instrumentation rearrangement required.

## CHAPTER 1 MIXTURE ANALYSIS

### Introduction

Luminescence techniques have often been used for detection of polycyclic aromatic hydrocarbons (1-6), pesticides (7-12), and pharmaceuticals (13-16). These methods are very sensitive due to the high quantum yields of many compounds in these classes. Conventional luminescence methods can be used to identify and quantitate species in such mixtures, however, overlap in spectra often becomes a problem, especially with complex mixtures or a mixture containing compounds with similar structures. Mixture analysis is often done by first separating the sample into its individual components through the use of separation techniques such as HPLC, GC, or TLC, and then detecting the analytes with another technique such as fluorescence, phosphorescence, infrared, or mass spectrometry. Combining techniques in this manner provides the desired selectivity at the expense of increased time and cost required for each sample. Other approaches to mixture analysis focus on increasing the selectivity of the detection method, and eliminating the need for a separation technique. To appreciate the methods which can be implemented to increase the selectivity of a particular technique, it is necessary to understand the fundamentals of the process being monitored. Therefore, a brief explanation of molecular luminescence will be presented. For more detailed descriptions the reader is referred to books by Schulman (17), Turro (18), Parker (19), and Winefordner, O'Haver, and Schulman (20).

Figure 1 presents a Jablonski diagram illustrating the luminescence processes for an organic molecule. Transitions labelled A refer to the absorption process. An absorption spectrum corresponds to the decrease in the intensity of the light passing through a sample due to its absorption by the sample. The wavelength of light being absorbed corresponds to the amount of energy required to excite the molecule from the ground state to an excited state.

Once the molecule is in the excited state many processes are available. One possibility is intersystem crossing, IS, to the triplet state where it may then undergo internal conversion, IC, (nonradiative decay), or it may undergo radiative decay in a process termed phosphorescence, P. Phosphorescence occurs at wavelengths longer than those of excitation and fluorescence--longer wavelengths correspond to lower energy.

Another possibility for the molecule in the excited state is for it to undergo vibrational relaxation, VR, to the lowest excited state--at this point if the molecule decays radiatively to one of the ground state levels this transition is described as fluorescence, F.

Molecular luminescence spectroscopy is the measurement of emission accompanying the deexcitation of a molecule from an excited electronic state, i.e. fluorescence and phosphorescence. Luminescence signals are measured against essentially a zero background, whereas absorption measurements involve small differences in two large signals. Therefore, luminescence spectroscopy often provides an enhancement in detection power. The low limits of detection generally obtained produce large linear dynamic ranges--usually in the range of five orders of magnitude. Also, detection systems involving fluorescence

# JABLONSKI DIAGRAM

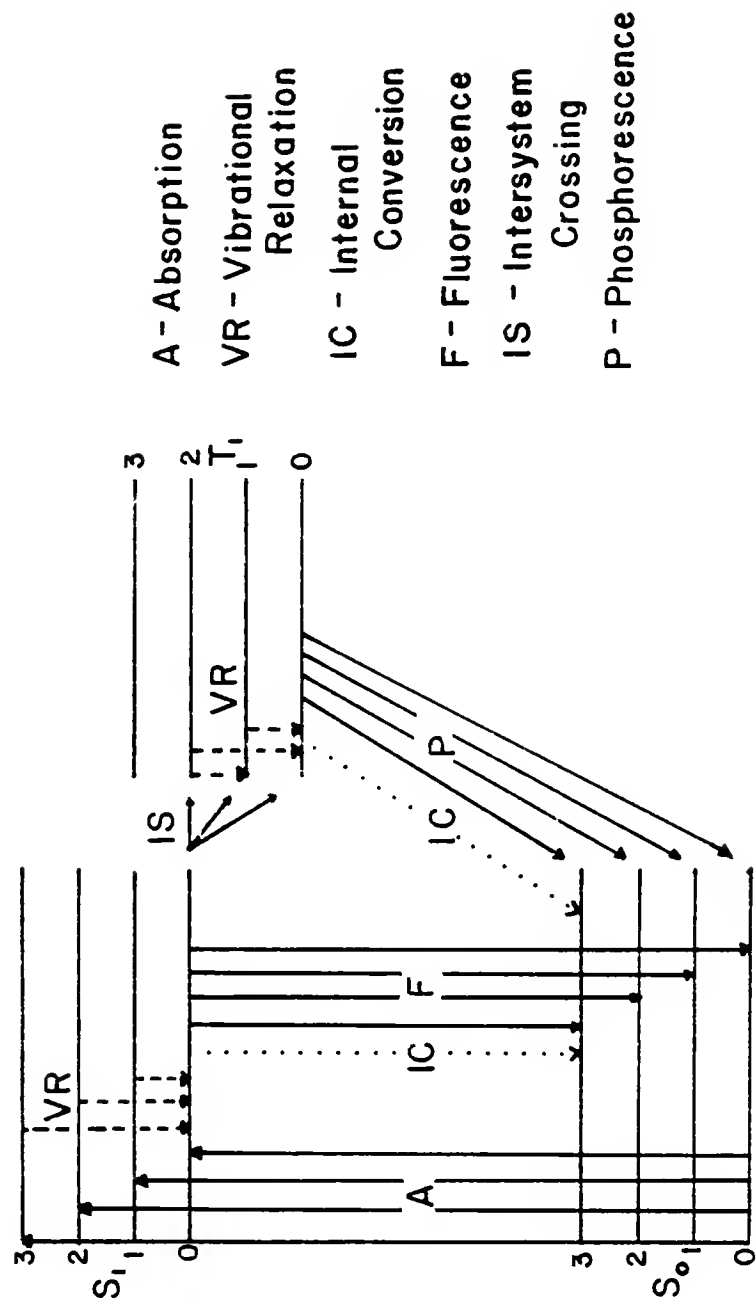


Figure 1. Energy level diagram illustrating the luminescence processes for an idealized molecule.

and phosphorescence are inherently selective in that they determine only those compounds which are excited by absorbing light and then decay radiatively to the ground state. Two degrees of selectivity are possible in such detection schemes due to the ability to select the energy of the exciting light and the energy of the emitted light. Still another degree of selectivity involves the use of delayed and gated detection to monitor the lifetimes of the excited states of the analytes. This aspect will be dealt with later.

The differences in the excitation and emission wavelengths for different compounds are based on the relative positions of the ground and excited states and the energy spacings between the levels in these states. Many different techniques are used to exploit these differences, and the choice of techniques is based on considerations such as speed, resolution, and the number of components of interest.

One of the most widely used techniques for increasing selectivity is the use of measurement at low temperature ( $\leq 77$  K). Examples of such methods include matrix isolation, supersonic jet expansion, and the use of glassy and Shopolskii solvents. Lowering the temperature of a sample reduces the internal degrees of freedom, molecular rotation, and vibration. The lower the temperature, the narrower the energy distribution profile of molecules within vibrational energy levels. This narrowing effect reduces overlap between neighboring levels. Increased sample information can then be obtained by selectively monitoring transitions between specific energy levels, provided the instrumentation is capable of accurately interrogating the exciting energy and emitted radiation. When one increases the selectivity of detection to the point at which it is possible to excite only those

molecules which inhabit very similar matrix sites, the term site selection is applied. Lasers are generally used as sources of excitation in site selection due to the intense, narrow bands which they provide. However, xenon arc lamps are also used as sources at low temperature, due to their low cost, reliability, and broad band emission. Through the use of a monochromator, a xenon arc lamp can be used to interrogate a wide range of excitation transitions. Xenon lamps are especially useful in conjunction with Shopolskii spectroscopy where the analyte and solvent are matched to produce a reduction in the total number of possible orientations for a molecule. Wehry and Mamantov (21) give more complete explanations of the theory and advantages of the use of low temperature for enhanced spectral resolution, as well as references demonstrating the use of such techniques.

An added advantage of analysis at low temperatures is the increase in quantum yields due to a decrease in nonradiative collisional deactivation of analytes in the excited state. For a detailed discussion of the radiative and nonradiative electronic decay processes, the reader is referred to Jaffe and Orchin (22).

Still another method for improving the selectivity of a detection system involves the options available for monitoring excitation and emission energies. The most simple method of luminescence detection involves fixed excitation and emission wavelengths, and monitoring the luminescence signal intensity (typically through the use of a photomultiplier tube). This method requires prior knowledge of system response to individual analytes, and it must be verified that the response is proportional to analyte concentration and independent of

sample matrix and other variables. It is also essential in such measurements that a true, consistent blank be determined. These requirements generally limit measurements of this type to determination of one known analyte in a mixture, or require that the sample be separated into relatively pure components prior to detection.

Another approach to luminescence measurement involves using either a fixed excitation or emission wavelength and scanning to determine the corresponding response. Spectra obtained in this manner provide information concerning the vibrational energy spacings in the excited electronic state, excitation/ absorption spectra, and the ground electronic state, emission spectra. Often spectra obtained in this manner are used for identification as well as quantitation. Through the use of more advanced electronic design and computer interfaces, spectra corrected for system response have been obtained for a wide variety of compounds (23,24). It is expected that in the future libraries containing luminescence spectra similar to Sadtler indices for IR, NMR, and UV absorption will be available.

More recent attempts at selectivity enhancement for multicomponent analysis have included such methods as total luminescence spectroscopy, TLS, and synchronous luminescence spectroscopy, SLS. TLS involves the use of multichannel analyzers and/or computers to obtain emission spectra of a sample over a range of excitation wavelengths. One of the major advantages of TLS is that it requires minimal prior knowledge concerning the luminescence characteristics of an unknown. Disadvantages of TLS include the cost of equipment required to obtain and store the extensive data corresponding to total luminescence spectra. Also, the amount of information in a TLS spectrum can often

be of such a magnitude that it is difficult to interpret. For a more complete review and explanation of the theory, advantages, and applications of total luminescence spectroscopy the reader is referred to Inman (25) and included references.

Synchronous luminescence spectroscopy is a technique which involves measuring luminescence as the excitation and emission monochromators are scanned simultaneously while maintaining a well-defined relationship between the wavelengths of the monochromators (26). Conventionally this relationship is a constant wavelength difference,  $\Delta\lambda$ . Alternately, variable-angle synchronous luminescence spectroscopy implements different scan speeds between the monochromators, thus providing a variable wavelength difference during the scan (27,28). Recently, constant energy synchronous luminescence spectroscopy (CESLS) has been described where a constant energy difference is maintained between the monochromators (29). In this way, the natural energy relationships fundamental to spectroscopic evaluation of fluorescent compounds are instrumentally exploited. These energy relationships are represented in the Jablonski diagram presented in Figure 1. The energy separation maintained between the monochromators in CESLS is chosen to correspond to the overall vibrational energy loss of an absorption-fluorescence transition. The energy difference for a particular transition can be experimentally determined by solving the equation

$$\Delta\bar{\nu} = (1/\lambda_{\text{ex}} - 1/\lambda_{\text{em}}) * 10^7$$

where  $\lambda_{\text{ex}}$  = excitation peak maximum in nm,  $\lambda_{\text{em}}$  = emission peak maximum in nm, and  $\Delta\bar{\nu}$  = energy difference for the transition in  $\text{cm}^{-1}$ .

The ability to selectively monitor transitions with CESLS is illustrated in Figure 2 (30). Here constant energy scans of anthracene are shown with their respective Jablonski diagrams depicting the absorption-fluorescence transitions being observed. The  $1400\text{ cm}^{-1}$  scan yields two peaks, which are attributed to transitions resulting in an overall vibrational energy loss of one quantum. The  $4800\text{ cm}^{-1}$  scan yields four peaks. These peaks are assigned to transitions which involve a loss of three vibrational quanta.

The advantages of synchronous techniques have been discussed, with examples demonstrating qualitative spectral improvements (31). These advantages include a reduction in spectral complexity, a reduction in peak bandwidths, and a decrease in interference from Rayleigh scatter (32) and even Raman scatter (33).

### Goals

The initial goal of this work is to provide a theoretical and practical evaluation of constant energy synchronous luminescence spectrometry (CESLS). The spectral parameters of CESLS will be evaluated for optimization of experimental variables. Mathematical relationships will be given for determining location of synchronous peak maximum, maximum intensity, and peak bandwidth; defining their dependence upon the luminescence excitation and emission spectral characteristics and the selected scan path. Graphical representations of CESLS scans illustrate these relationships, with hypothetical compounds used to demonstrate their application.

The feasibility of fingerprinting and identifying PAHs in environmental samples and analyzing synthetic mixtures of pesticides and pharmaceuticals using CESLS will be demonstrated. Special emphasis

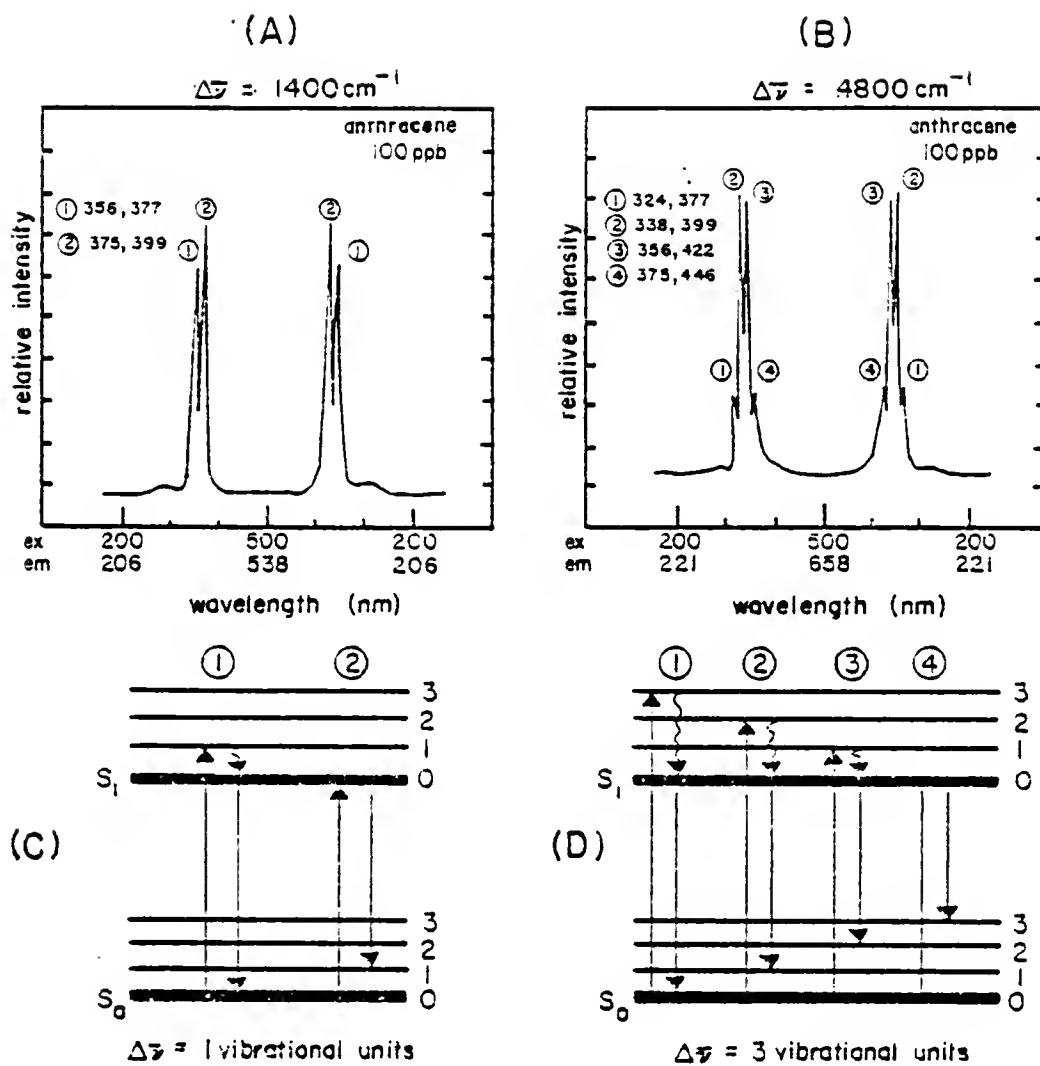


Figure 2. CESLS spectra of anthracene. (A)  $\Delta\bar{\nu} = 1$  vibrational quantum, (B)  $\Delta\bar{\nu} = 3$  vibrational quanta, (C) Jablonski diagram illustrating  $\Delta\bar{\nu} = 1$  vibrational quantum, (D) Jablonski diagram illustrating  $\Delta\bar{\nu} = 3$  vibrational quanta. Taken from M. J. Kerkhoff, reference (30).

is placed on combining techniques and implementing novel sampling systems for acquiring maximum sample information.

The final goal of this work is to develop and evaluate a system capable of constant energy synchronous phosphorescence spectrometry.

CHAPTER 2  
THEORETICAL OPTIMIZATION OF PARAMETER SELECTION IN  
CONSTANT ENERGY SYNCHRONOUS LUMINESCENCE SPECTROSCOPY

Introduction

The advantages of synchronous techniques include a reduction in spectral complexity; a reduction in peak bandwidths; and a reduction in interference by Rayleigh (32) and Raman (33) scatter. Full realization of these advantages has been limited due to the lack of a thorough theoretical evaluation and subsequent parameter optimization to aid in the routine application of these techniques. The characteristics of the luminescence excitation and emission spectra and their effect on the selection of scan parameters, and the resultant synchronous spectral features are considered here.

The prediction of peak wavelength maxima, intensity maxima, and peak bandwidths in conventional constant wavelength synchronous luminescence (CWSLS) spectra have been described (34,35). However, these have included approximations due to the complexity of the mathematical manipulations necessary when assuming excitation and emission peaks to be Gaussian in frequency and determining their response in terms of constant wavelength scanning (i.e. the reciprocal relationship between wavelength and frequency). The calculations are less formidable for CESLS and exact relationships can be obtained. Thus, the spectral advantages of CESLS can be quantitated and utilized for scan selection, providing for systematic parameter optimization. These will be presented, along with a discussion of the experimental consequences of these relationships.

### Theory

The fundamental spectral parameters of interest in CESLS include the location of the synchronous peak maximum, its relative intensity and its bandwidth as functions of luminescence excitation band characteristics, emission band characteristics, and scan parameters. Lloyd and Evett (34) obtained the following relationship for the synchronous peak wavelength maximum,  $\lambda_{s_o}$ , in CWSLS:

$$\lambda_{s_o} = 2\lambda_{i_o}\lambda_{j_o}(\lambda_{i_o} + \lambda_{j_o} - \Delta\lambda)^{-1} \quad (1)$$

where  $\lambda_{i_o}$  is the wavelength of maximum luminescence intensity in the excitation spectrum,  $\lambda_{j_o}$  is the wavelength of maximum intensity in the luminescence excitation spectrum, and  $\Delta\lambda$  is the wavelength difference in the conventional synchronous (CWSLS) scan mode. An assumption is made in their treatment that the bandwidths of the excitation and emission peaks are equivalent when expressed in energy terms. Satisfactory agreement was observed with experimental data for a number of compounds over a range of  $\Delta\lambda$  values. From the experimental data, an empirical relationship was derived for the synchronous bandwidth

$$\delta\lambda_s = 0.364 (\delta\lambda_i + \delta\lambda_j) - 3.309 \quad (2)$$

where  $\delta\lambda_s$  is the synchronous bandwidth,  $\delta\lambda_i$  is the luminescence excitation bandwidth, and  $\delta\lambda_j$  is the luminescence emission bandwidth. Andre et al. (36) approximated the bandwidths of synchronous peaks as

$$\delta\lambda_s = \delta\lambda_i + \delta\lambda_j - (\delta\lambda_i^2 + \delta\lambda_j^2)^{1/2} \quad (3)$$

While no derivation was provided for this expression, it seemed to agree with observed experimental data. It was noted that  $\delta\lambda_s$  was

always less than  $\delta\lambda_j$ , confirming the bandwidth reduction observed for synchronous techniques. Thus, experimental data have suggested the direction for parameter optimization for synchronous techniques.

For the discussion to follow, luminescence excitation and emission peaks are represented as single Gaussian functions of frequency (wavenumbers) or reciprocal wavelength. A range of energy differences ( $\Delta\bar{\nu}$  values) is considered where the scan path does not cross the excitation-emission peak maxima. The peak location and the bandwidth of the CESLS peak,  $\bar{\nu}_{js_o}$  and  $\delta\bar{\nu}_s$ , respectively, are derived in the discussion to follow. Appropriate modification is necessary when the derived expressions are used with other SLS scanning techniques.

#### Peak Maximum Location and Relative Intensity

To obtain equations which will define the location,  $\bar{\nu}_{s_o}$ , and intensity,  $M_{ijs_o}$ , of peak maxima in constant energy scans, it is necessary to establish functions which describe the intensity of these scans. To determine these functions in terms of the excitation and emission spectra assuming peaks which are Gaussian in frequency, the following definitions and substitutions were required.

The terms used throughout this discussion were selected in an attempt to maintain consistency throughout the literature and are defined in a Glossary. The general equation defining a Gaussian distribution can be written as

$$y = \frac{1}{\sigma(2\pi)^{1/2}} \exp[-(x - \mu)^2/2\sigma^2] \quad (4)$$

where  $y$  is the normalized peak intensity,  $\sigma$  is the standard deviation of the peak,  $x$  is an independent variable, and  $\mu$  is the average value

of  $x$  over the peak. If the luminescence excitation and emission spectral band shapes are Gaussian functions, then

$$x_i = x_{i_o} \exp[-(\bar{\nu}_i - \bar{\nu}_{i_o})^2 / 2\sigma_i^2] \quad (5)$$

and

$$y_j = y_{j_o} \exp[-(\bar{\nu}_j - \bar{\nu}_{j_o})^2 / 2\sigma_j^2] \quad (6)$$

The relative luminescence measured for a single component sample can be written as

$$M_{ij} = \alpha x_i y_j \quad (7)$$

where  $\alpha$  is the product of wavelength independent terms,  $x_i$  is the product of excitation wavelength dependent terms, and  $y_j$  is the product of emission wavelength dependent terms (37). The conversion from wavelength (nm) to frequency ( $\text{cm}^{-1}$ ) is written as

$$\bar{\nu} = 10^7 / \lambda \quad (8)$$

Substitution of Equations 5 and 6 into 7 yields

$$M_{ij} = \alpha x_{i_o} y_{j_o} \exp[-(\bar{\nu}_i - \bar{\nu}_{i_o})^2 / 2\sigma_i^2 - (\bar{\nu}_j - \bar{\nu}_{j_o})^2 / 2\sigma_j^2] \quad (9)$$

Equation 9 defines the intensity at any excitation and emission wavelength relative to the maximum peak wavelengths. The wavenumber difference between the excitation and emission monochromators in a CESLS scan is defined as:

$$\Delta\bar{\nu} = \bar{\nu}_i - \bar{\nu}_j \quad (10)$$

where  $\Delta\bar{\nu}$  is the constant frequency difference maintained between the

excitation and emission monochromators during the CESLS spectral measurements. Placing this restriction on Equation 9 gives

$$M_{ijs} = \alpha x_{i_o} y_{j_o} \exp[-(\bar{\nu}_j + \Delta\bar{\nu} - \bar{\nu}_{i_o})^2/2\sigma_i^2 - (\bar{\nu}_j - \bar{\nu}_{j_o})^2/2\sigma_j^2] \quad (11)$$

This equation defines the synchronous spectrum as a function of only the emission wavenumber,  $\bar{\nu}_j$ , at a selected energy difference,  $\Delta\bar{\nu}$ .

To determine the location of the intensity maximum of the CESLS scan,  $M_{ijs_o}$ , the CESLS intensity function is differentiated with respect to emission frequency and set equal to zero. Therefore,

$$dM_{ijs}/d\bar{\nu}_j = 0$$

This results in a peak wavenumber maximum,  $\bar{\nu}_{js_o}$  of

$$\bar{\nu}_{js_o} = (\bar{\nu}_{j_o} (\sigma_i^2/\sigma_j^2) + \bar{\nu}_{i_o} - \Delta\bar{\nu}) / (1 + \sigma_i^2/\sigma_j^2) \quad (13)$$

Because  $\delta\bar{\nu}$  by definition is related to  $\sigma$  by

$$\delta\bar{\nu} = (8 \ln 2)^{1/2} \sigma \quad (14)$$

Equation 13 can be rewritten as

$$\bar{\nu}_{js_o} = (\bar{\nu}_{j_o} (\delta\bar{\nu}_i^2/\delta\bar{\nu}_j^2) + \bar{\nu}_{i_o} - \Delta\bar{\nu}) / (1 + \delta\bar{\nu}_i^2/\delta\bar{\nu}_j^2) \quad (15)$$

Equation 15 defines the location of the peak maximum in a given constant energy scan in terms of the emission wavenumber. Therefore, the intensity of the CESLS maximum in a specific constant energy scan is given from Equation 11 by

$$M_{ijs_o} = \alpha x_{i_o} y_{j_o} \exp[-(\bar{\nu}_{js_o} + \Delta\bar{\nu} - \bar{\nu}_{i_o})^2/2\sigma_i^2 - (\bar{\nu}_{js_o} - \bar{\nu}_{j_o})^2/2\sigma_j^2] \quad (16)$$

### CESLS Bandwidths

To calculate the bandwidth of a constant energy peak,  $\delta\bar{v}_s$ , one can determine the location of the peak maximum at  $\bar{v}_{js_o}$  and the location at which the intensity is half the maximum value. The difference in these two locations is equal to half the CESLS bandwidth. This goal is accomplished through the use of Equation 16 and an analogous equation for the relative intensity at half the maximum intensity

$$M_{ijs_h} = \alpha x_{i_o} y_{j_o} \exp[-(\bar{v}_{js_h} + \Delta\bar{v} - \bar{v}_{i_o})^2 / 2\sigma_i^2 - (\bar{v}_{js_h} - \bar{v}_{j_o})^2 / 2\sigma_j^2] \quad (17)$$

Under these conditions

$$M_{ijs_o} / M_{ijs_h} = 2 \quad (18)$$

Substitution and simplification results in

$$\begin{aligned} 0 = & (\bar{v}_{js_h}^2 - \bar{v}_{js_o}^2)(\sigma_i^2 + \sigma_j^2) + (\bar{v}_{js_h} - \bar{v}_{js_o})(2\sigma_j^2\Delta\bar{v} - 2\sigma_j^2\bar{v}_{i_o} - 2\sigma_i^2\bar{v}_{j_o}) \\ & - (2\sigma_i^2\sigma_j^2 \ln 2) \end{aligned} \quad (19)$$

The bandwidth,  $\delta\bar{v}_s$ , is introduced and defined as

$$\delta\bar{v}_s = 2\bar{v}_{js_h} - \bar{v}_{js_o} \quad (20)$$

Solving Equation 19 for  $\delta\bar{v}_s$  gives the CESLS bandwidth

$$\delta\bar{v}_s = 8 \ln 2 [\sigma_i\sigma_j / (\sigma_i^2 + \sigma_j^2)^{1/2}] \quad (21)$$

and so

$$\delta\bar{v}_s = \delta\bar{v}_i\delta\bar{v}_j / (\delta\bar{v}_i^2 + \delta\bar{v}_j^2)^{1/2} \quad (22)$$

### Geometric Representation

The total luminescence spectrum provides a clear picture of the CESLS scanning procedure. This spectrum includes the relative luminescence intensity contours measured as a function of excitation and emission wavelengths (38). For this discussion, this spectrum can be plotted in frequency units, maintaining spectral symmetry (29). For simplicity, Figure 3 illustrates the total luminescence spectrum of a single peak, where the ellipse defines the contour equivalent to half the maximum peak intensity. The following terms are used for this model:

$$x = \bar{\nu}_i - \bar{\nu}_{i_0} \quad (23)$$

$$y = \bar{\nu}_j - \bar{\nu}_{j_0} \quad (24)$$

$$2a = \delta\bar{\nu}_i \quad (25)$$

$$2b = \delta\bar{\nu}_j \quad (26)$$

The dashed line represents the CESLS scan path for the special case

$$\Delta\bar{\nu} = \bar{\nu}_{i_0} - \bar{\nu}_{j_0} \quad (27)$$

The ellipse can be expressed as

$$x^2/a^2 + y^2/b^2 = 1 \quad (28)$$

or

$$x^2/b^2 + y^2/a^2 = a^2/b^2 \quad (29)$$

As  $\Delta\bar{\nu}$  is varied, a number of scan paths are defined as shown in Figure 4, each with a slope of 1, or:

$$dy/dx = 1 \quad (30)$$

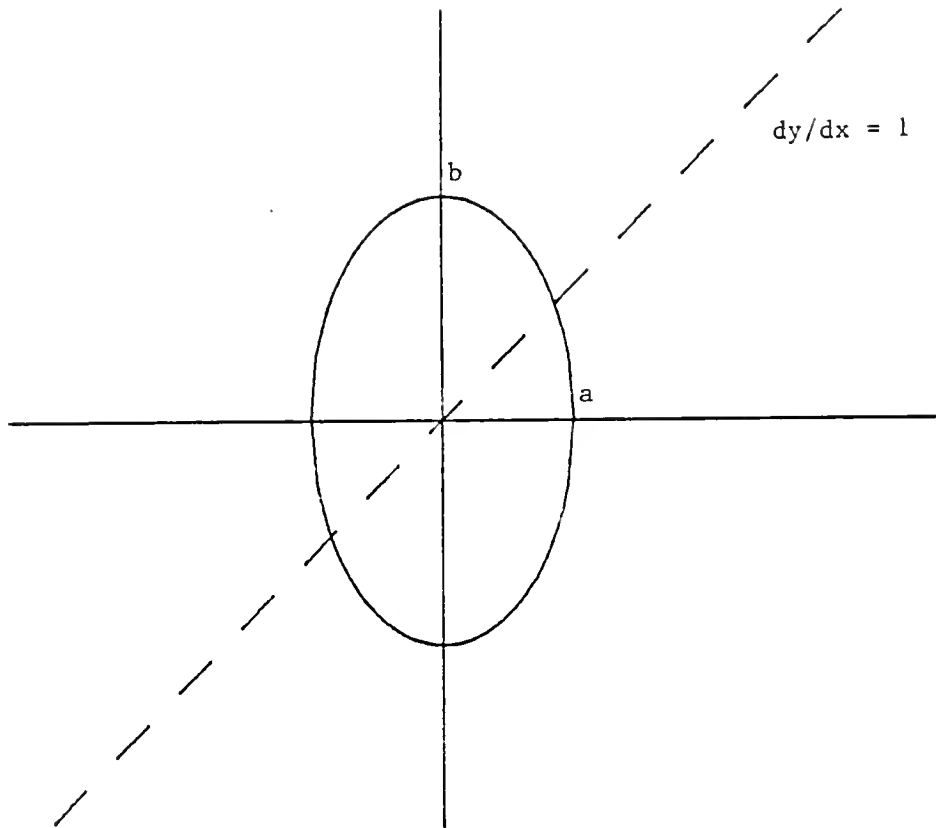


Figure 3. Geometric model for CESLS. The ellipse defines the contour equivalent to half the maximum peak intensity. The dashed line defines a CESLS scan with  $\Delta v = v_{i_o} - v_{j_o}$ .

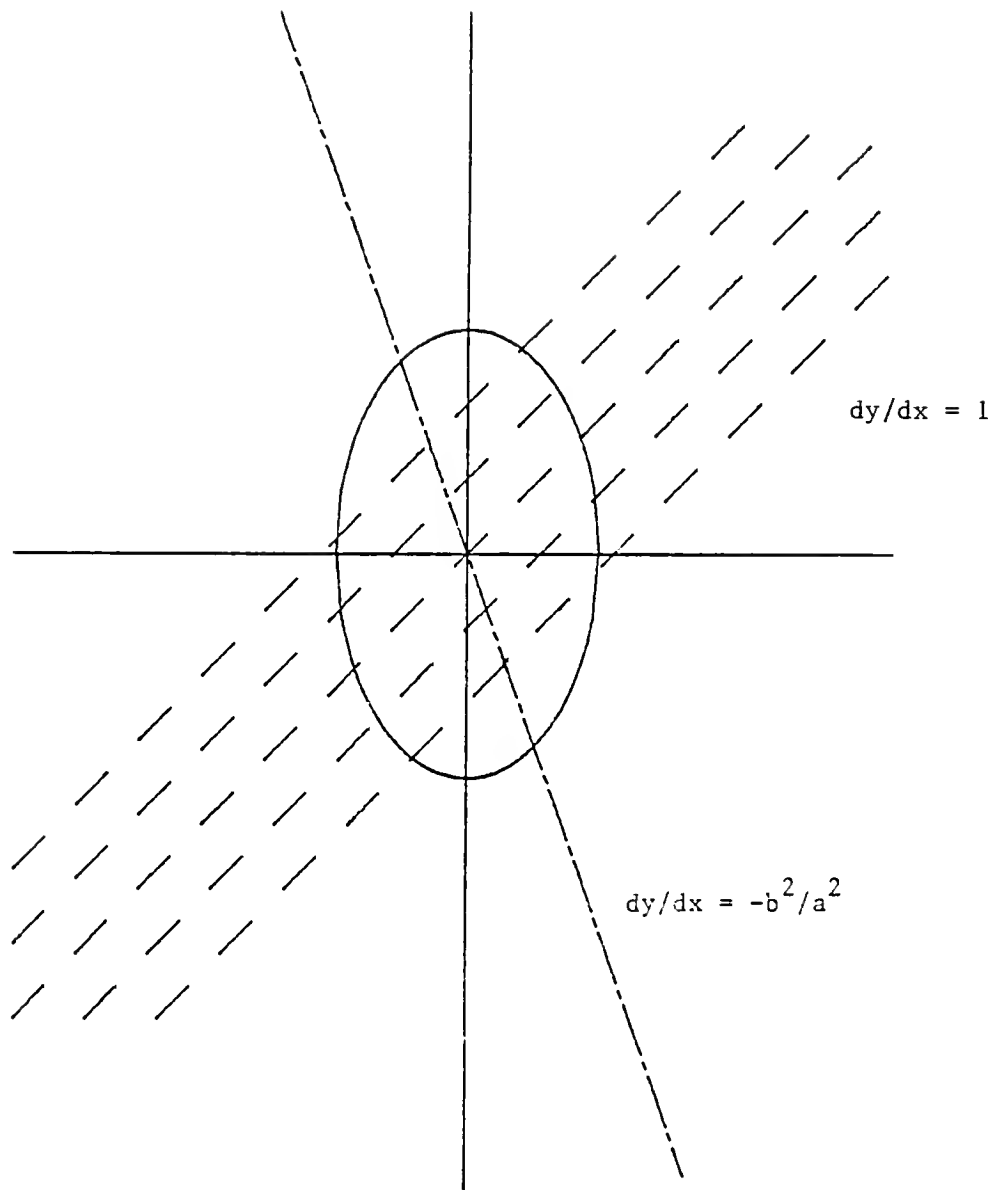


Figure 4. Graphical representation of various values of  $\Delta v$  (—) and the line (---) defining the position of the CESLS maxima for this scan.

These definitions can be used to determine the intensity maximum for each CESLS spectrum. The maxima fall on a line that runs through the origin in Figure 4. The equation for this line can be established using two points, one of these being the origin and the other being determined by finding one of the two points on the ellipse where the scan path intersects the ellipse at a single point. While this may not seem intuitively obvious, the addition of a number of contour lines will verify this conclusion. Differentiating Equation 29 yields

$$y = -(b^2/a^2) x \quad (31)$$

Equation 31 represents the line defining the intensity maxima for CESLS scans. Substituting the appropriate CESLS terms into Equation 31 and solving for  $\bar{\nu}_{js_o}$  gives

$$\bar{\nu}_{js_o} = [\bar{\nu}_j (\delta\bar{\nu}_i^2 / \delta\bar{\nu}_j^2) + \bar{\nu}_{i_o} - \Delta\bar{\nu}] / (1 + \delta\bar{\nu}_i^2 / \delta\bar{\nu}_j^2) \quad (32)$$

Equation 32 represents the location of the CESLS peak maximum in terms of the emission wavenumber,  $\bar{\nu}_j$ . Note that this result agrees with Equation 15.

### Discussion

From these expressions, a number of observations can be made concerning CESLS spectral characteristics. For illustration, a number of hypothetical compounds were evaluated. These observations will provide guidelines for experimental design of CESLS applications.

### Peak Wavelength and Intensity Maxima

The shape and location of each CESLS peak is a function of the intensity maxima of the excitation and emission bands and the selected  $\Delta\bar{\nu}$ . Thus, for a specific compound, the synchronous spectrum intensity maximum and location varies only with the scan parameter,  $\Delta\bar{\nu}$ . The peak characteristics of three hypothetical compounds are shown in Table I. For each compound,  $\Delta\bar{\nu}$  is varied to compare the peak maximum locations, relative intensities, and peak bandwidths. The values of  $\Delta\bar{\nu}$  were selected to coincide with  $\bar{\nu}_{i_o} - \bar{\nu}_{j_o}$  and reasonable variation around this value. Equation 15 suggests that if  $\Delta\bar{\nu}$  is chosen to coincide with  $\bar{\nu}_{i_o} - \bar{\nu}_{j_o}$ , then  $\bar{\nu}_{js_o}$  is equivalent to  $\bar{\nu}_{j_o}$ . That is, if the scan path passes through the peak maximum, the synchronous and emission peak maxima are identical. If  $\Delta\bar{\nu}$  is less than  $\bar{\nu}_{i_o} - \bar{\nu}_{j_o}$ , then  $\bar{\nu}_{js_o}$  is greater than  $\bar{\nu}_{j_o}$  (thus shorter in wavelength terms), and the scan crosses the x-axis in Figure 4 to the left of the origin. If  $\Delta\bar{\nu}$  is greater than  $\bar{\nu}_{i_o} - \bar{\nu}_{j_o}$ , then  $\bar{\nu}_{js_o}$  is less than  $\bar{\nu}_{j_o}$  and the scan crosses the x-axis in Figure 4 to the right of the origin. If Equation 13 is differentiated, then

$$d\bar{\nu}_{js_o}/d\Delta\bar{\nu} = -1/(1 + \sigma_i^2/\sigma_j^2) \quad (33)$$

This defines the slope of the line of CESLS maxima. This line is also depicted in Figure 4.

The three compounds in Table I represent three cases for relative values of  $\sigma_i$  and  $\sigma_j$ . These are

1.  $\sigma_i = \sigma_j$
2.  $\sigma_i \ll \sigma_j$
3.  $\sigma_i \gg \sigma_j$

Table I. Spectral Data for Three Model Compounds<sup>\*</sup>

## Compound A

$\Delta\bar{\nu}(\text{cm}^{-1})$	$\bar{\nu}_{\text{js}_o}(\text{cm}^{-1})$	$\delta\bar{\nu}_s(\text{cm}^{-1})$	$M_{\text{ijs}_o}/M_o$
-----	-----	-----	-----
13,000	28,500	1,061	0.641
14,000	28,000	1,061	0.895
15,000	27,500	1,061	1.000
16,000	27,000	1,061	0.895
17,000	26,500	1,061	0.641

## Compound B

$\Delta\bar{\nu}(\text{cm}^{-1})$	$\bar{\nu}_{\text{js}_o}(\text{cm}^{-1})$	$\delta\bar{\nu}_s(\text{cm}^{-1})$	$M_{\text{ijs}_o}/M_o$
-----	-----	-----	-----
13,000	29,100	671	0.491
14,000	28,300	671	0.837
15,000	27,500	671	1.000
16,000	26,700	671	0.837
17,000	25,900	671	0.491

## Compound C

$\Delta\bar{\nu}(\text{cm}^{-1})$	$\bar{\nu}_{\text{js}_o}(\text{cm}^{-1})$	$\delta\bar{\nu}_s(\text{cm}^{-1})$	$M_{\text{ijs}_o}/M_o$
-----	-----	-----	-----
13,000	27,900	671	0.491
14,000	27,700	671	0.837
15,000	27,500	671	1.000
16,000	27,300	671	0.837
17,000	27,100	671	0.491

Table I. Continued

\*

	<u>Compound A</u>	<u>Compound B</u>	<u>Compound C</u>
$\bar{\nu}_{i_o} \text{ (cm}^{-1}\text{)}$	42,500	42,500	42,500
$\bar{\nu}_{j_o} \text{ (cm}^{-1}\text{)}$	27,500	27,500	27,500
$\sigma_i \text{ (cm}^{-1}\text{)}$	1,500	750	1,500
$\sigma_j \text{ (cm}^{-1}\text{)}$	1,500	1,500	750

The total luminescence spectra for these cases are illustrated in Figure 5. Case 1 is representative of the solution fluorescence spectra of the majority of common fluorescent compounds. If  $\sigma_i = \sigma_j$ , then Equation 13 reduces to

$$\bar{\nu}_{js_o} = (\bar{\nu}_{j_o} + \bar{\nu}_{i_o} - \Delta\bar{\nu})/2 \quad (34)$$

From Equation 33,  $d\bar{\nu}_{js_o}/d\Delta\bar{\nu}$  reduces to  $-1/2$ . The data for compound A in Table I confirms these relationships. For Case 2,  $\bar{\nu}_{js_o}$  approaches  $\bar{\nu}_{i_o} - \bar{\nu}_{j_o}$ . That is, the synchronous maximum is proportional to  $\Delta\bar{\nu}$ , representing the conditions for maximum change in  $\bar{\nu}_{js_o}$  as  $\Delta\bar{\nu}$  is varied; also from Equation 33,  $d\bar{\nu}_{js_o}/d\Delta\bar{\nu}$  approaches  $-1$ . For Case 3,  $\bar{\nu}_{js_o}$  approaches  $\bar{\nu}_{j_o}$ . That is, the synchronous maximum does not deviate significantly from the emission maximum as  $\Delta\bar{\nu}$  is varied. This is readily apparent from Figure 5C, and is further proven by Equation 33, since  $d\bar{\nu}_{js_o}/d\Delta\bar{\nu}$  approaches 0. These three cases are summarized in Table II.

#### CESLS Bandwidths

Several observations can be made about CESLS bandwidths. Note that from Equation 22,  $\delta\bar{\nu}_s$  is independent of  $\Delta\bar{\nu}$ . This is also confirmed by the data in Table I. This is graphically illustrated in Figure 6 where five CESLS spectra are shown with varying values of  $\Delta\bar{\nu}$ . The bandwidth at half maximum is identical for each peak. In conventional synchronous (CWSLS) techniques, it has been observed that  $\delta\lambda_s$  is dependent upon  $\Delta\lambda$  (36). The three cases previously described are also important in this discussion. For Case 1,  $\sigma_i = \sigma_j$  and  $\delta\lambda_s$  is equivalent to  $\delta\lambda_j/2$ . This effect is clearly seen in the example

## SPECIAL CASES

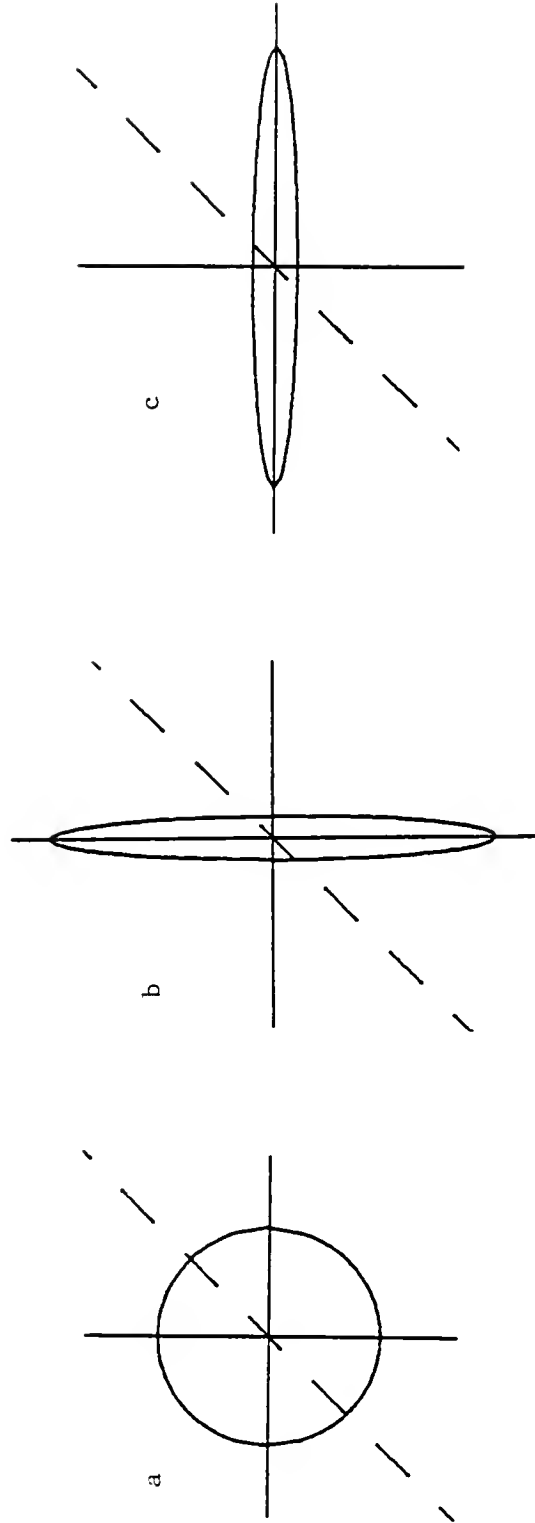


Figure 5. Graphical representation of three special cases for  
a)  $\sigma_i = \sigma_j$ ,  $\sigma_i < \sigma_j$ , and c)  $\sigma_i \gg \sigma_j$ .

Table II. Limiting Cases

	Case 1 ( $\sigma_i = \sigma_j$ ) -----	Case 2 ( $\sigma_i \ll \sigma_j$ ) -----	Case 3 ( $\sigma_i \gg \sigma_j$ ) -----
$d\bar{v}_{js_o}/d\Delta\bar{v}$	-1/2	-1	0
$\bar{v}_{js_o}$	$(\bar{v}_{j_o} + \bar{v}_{i_o} - \Delta\bar{v})/2$	$\bar{v}_{i_o} - \Delta\bar{v}$	$\bar{v}_{j_o}$
$\sigma_s$	$\sigma_j / \sqrt{2}$	$\sigma_i$	$\sigma_j$
$\delta\bar{v}_s$	$\delta\bar{v}_j / \sqrt{2}$	$\delta\bar{v}_i$	$\delta\bar{v}_j$

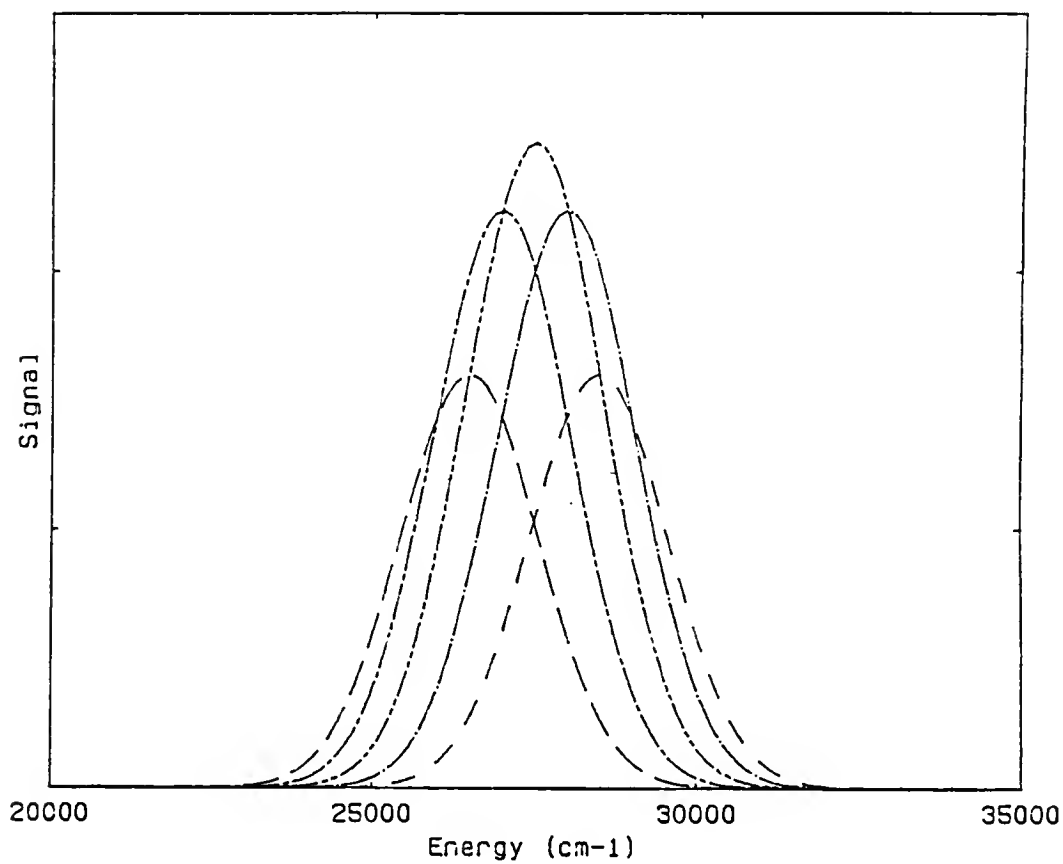


Figure 6. Comparison of peaks generated by using a variety of  $\Delta v$  values ( $\text{cm}^{-1}$ ) for compound A. See Table II.  
 $\Delta v = 15,000$  (— · —),  $14,000$  (— — —),  $13,000$  (— — —),  $16,000$  (— · —), and  $17,000$  (— — —).

shown in Figure 7. For Case 2,  $\sigma_i \ll \sigma_j$  and  $\delta\bar{\nu}_s$  approaches  $\delta\bar{\nu}_i$  as this difference increases. An example of this is shown in Figure 8 where  $\sigma_i = \sigma_j/2$ . Correspondingly for Case 3,  $\sigma_i \gg \sigma_j$  and  $\delta\bar{\nu}_s$  approaches  $\delta\bar{\nu}_j$ . An example of this is shown in Figure 9 where  $\sigma_i = 2\sigma_j$ . These two cases have significant experimental consequences. This suggests that the CESLS bandwidth corresponds to the narrower of the excitation and emission bandwidths as one becomes much larger than the other. Therefore,  $\delta\bar{\nu}_s$  is theoretically always less than or equal to  $\delta\bar{\nu}_j$ .

#### CESLS vs CWSLS

For comparison of CESLS and CWSLS two additional hypothetical compounds are evaluated. Relevant spectral characteristics for these compounds, D and E, are given in Table III. For demonstration purposes, peak locations ( $\bar{\nu}$  values) were chosen based on molecular theory, which shows that compounds within a class (such as PAHs) generally exhibit similar vibrational energy separations, and consequently comparable  $\Delta\bar{\nu}_{\max}$  values. Figure 10 compares the excitation and emission spectra for D and E to the synchronous spectra obtained using a constant energy difference equal to  $\Delta\bar{\nu}_{\max}$  for both compounds. Figure 11 demonstrates the change in appearance of spectra presented in Figure 10 when they are plotted in terms of signal vs wavelength rather than energy.

Figure 12 shows the result obtained if a constant wavelength difference is scanned with  $\Delta\lambda = 85.227$  nm (this is  $\Delta\lambda_{\max}$  for compound D). Figure 13 shows the result obtained if a constant wavelength difference is scanned with  $\Delta\lambda = 121.457$  nm (this is  $\Delta\lambda_{\max}$  for compound E). Figure 14 shows on an expanded scale comparison of plots defined

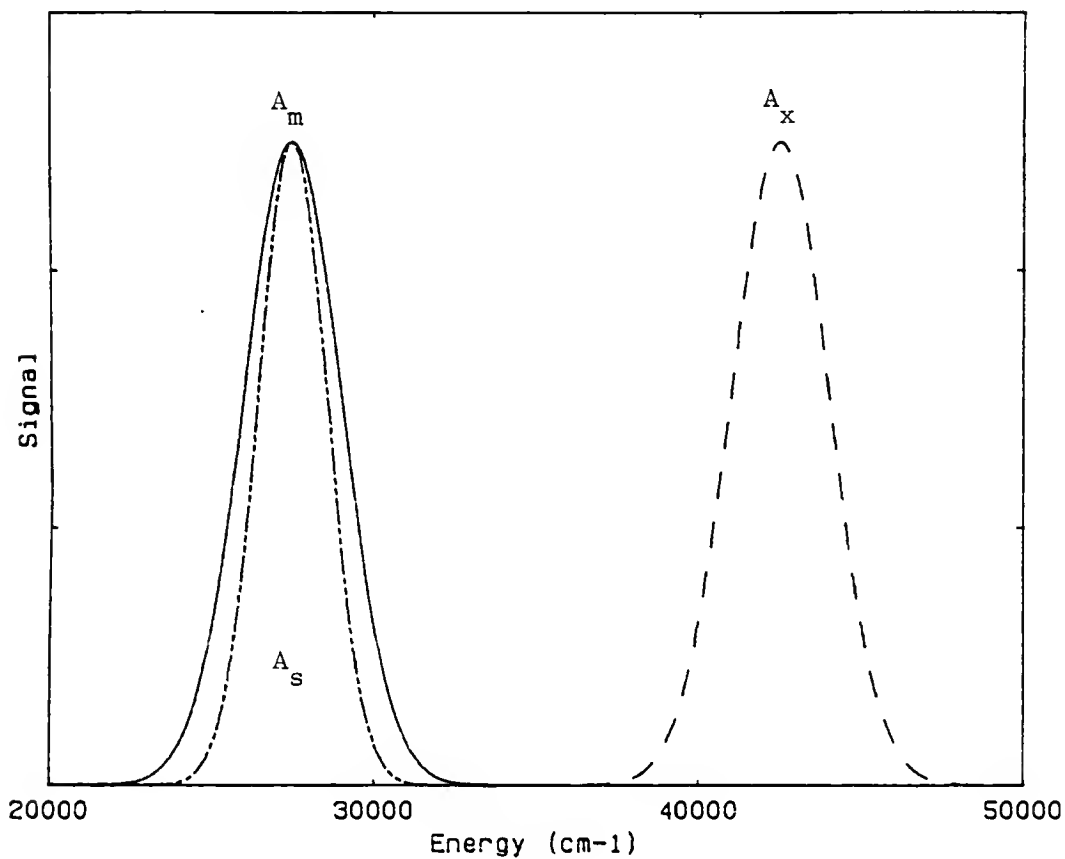


Figure 7. Excitation,  $A_x$ , (— —) and emission,  $A_m$  (——) peaks for compound A.  $\sigma_i = \sigma_j$ . The CESLS spectra,  $A_s$ , (— · —) is shown for the scan path  $\Delta\bar{\nu} = \bar{\nu}_{i_0} - \bar{\nu}_{j_0}$ .

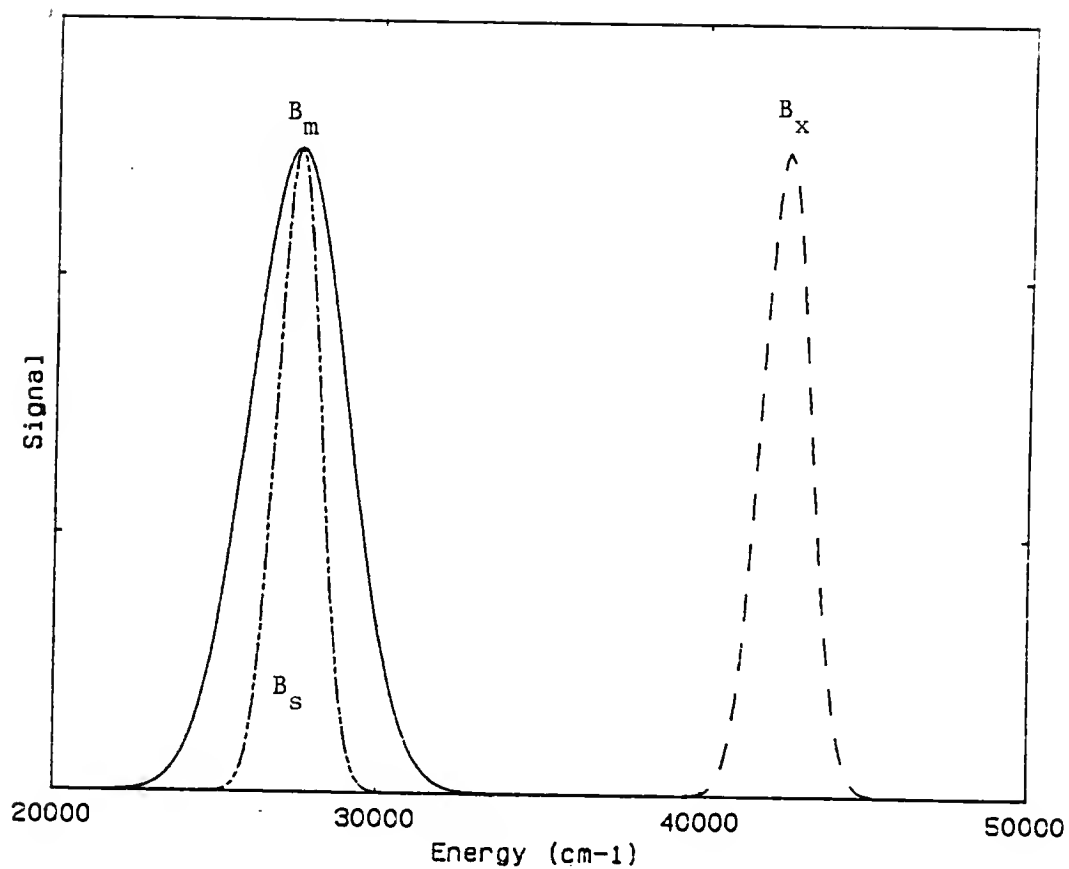


Figure 8. Excitation,  $B_x$ , (— —) and emission,  $B_m$  (——) peaks for compound B.  $\sigma_i = \sigma_j/2$ . The CESLS spectrum,  $B_s$ , (— · —) is shown for the scan path  $\Delta\bar{\nu} = \bar{\nu}_{i_o} - \bar{\nu}_{j_o}$ .

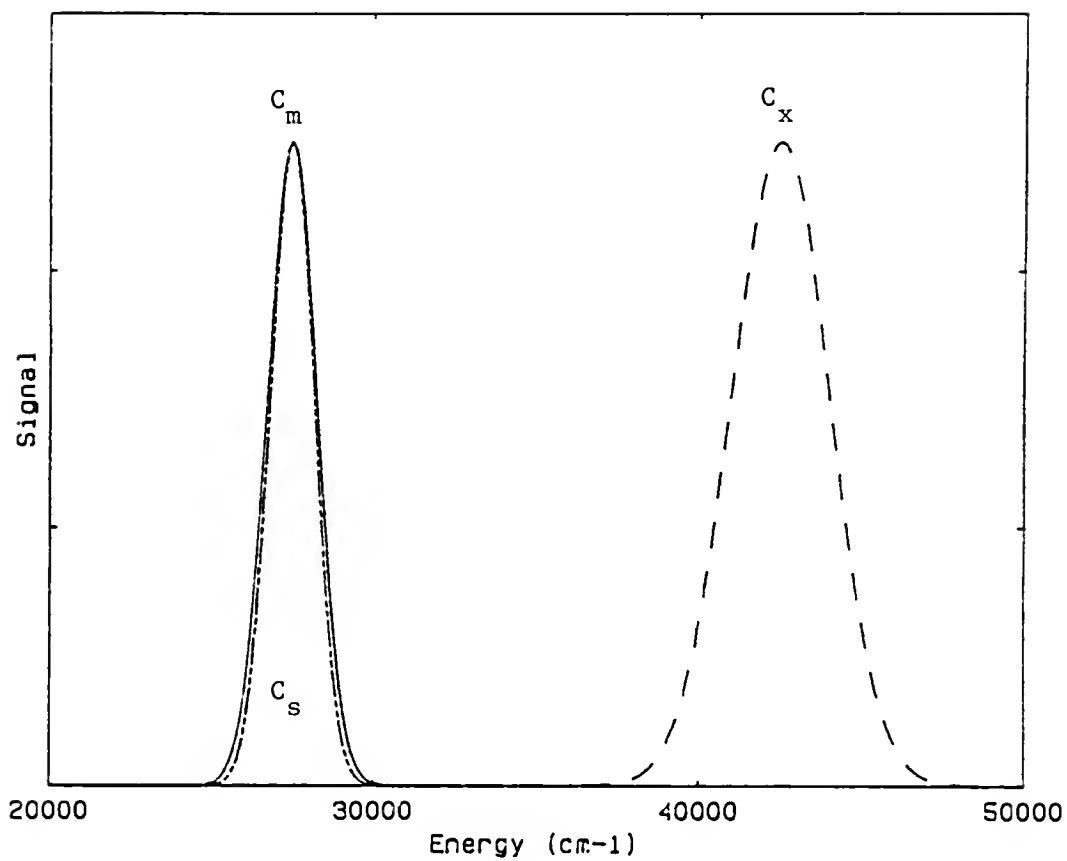


Figure 9. Excitation,  $C_x$ , (— —) and emission,  $C_x$ , (——) peaks for compound C.  $\sigma_i = 2 \sigma_j$ . The CESLS spectrum,  $C_s$ , (— · —) is shown for the scan path  $\Delta \bar{\nu} = \bar{\nu}_{i_o} - \bar{\nu}_{j_o}$ .

Table III. Spectral Data for Two Model Compounds

	<u>Compound D</u>	<u>Compound E</u>
$\bar{\nu}_{\text{ex}_o} \text{ (cm}^{-1}\text{)}$	44,000	38,000
$\bar{\nu}_{\text{em}_o} \text{ (cm}^{-1}\text{)}$	32,000	26,000
$\Delta\bar{\nu}_{\text{max}} \text{ (cm}^{-1}\text{)}$	12,000	12,000
$\lambda_{\text{ex}_o} \text{ (nm)}$	227.273	263.158
$\lambda_{\text{em}_o} \text{ (nm)}$	312.5	384.6
$\Delta\lambda_{\text{max}} \text{ (nm)}$	85.227	121.457
$\sigma_{\text{ex}} \text{ (cm}^{-1}\text{)}$	1,000	1,000
$\sigma_{\text{em}} \text{ (cm}^{-1}\text{)}$	1,000	1,000

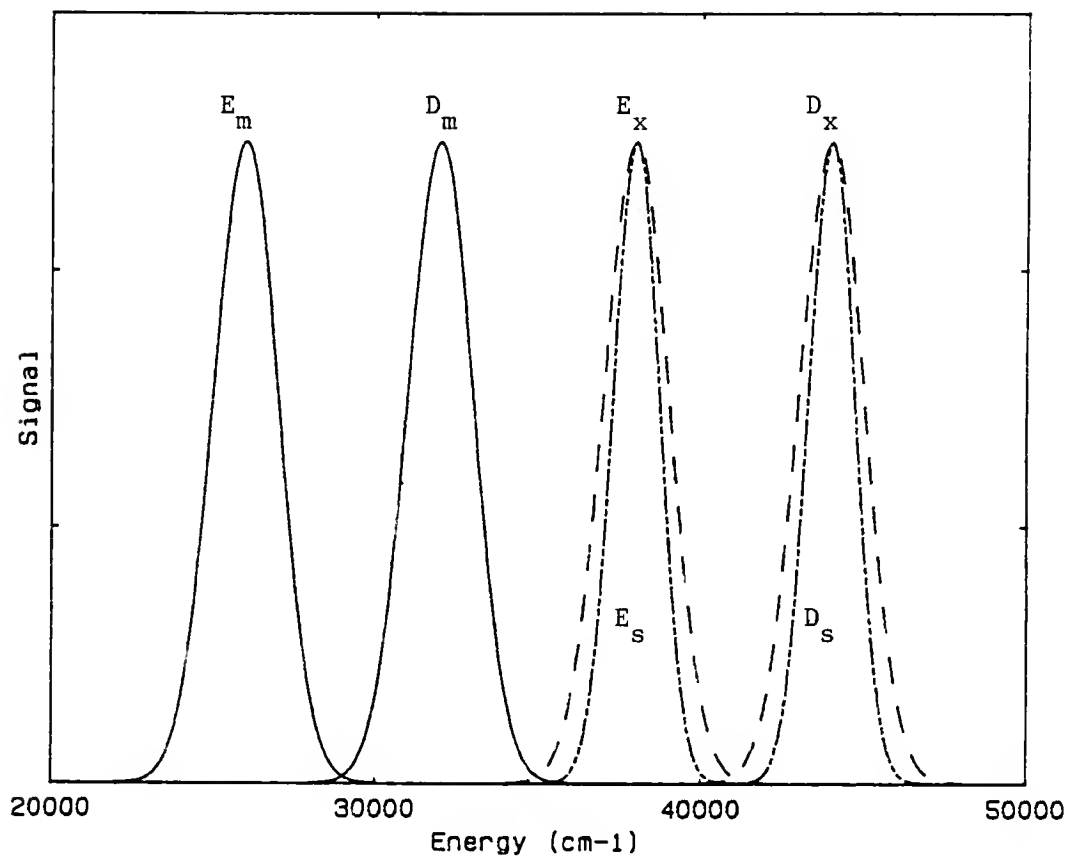


Figure 10. Excitation (— —) and emission (——) peaks for model compounds D ( $D_x, D_m$ ) and E ( $E_x, E_m$ ). See Table III. CESLS spectra (---) with  $\Delta\bar{\nu} = \Delta\bar{\nu}_{\max}$  for both compounds ( $D_s$  and  $E_s$ ), arbitrarily plotted in terms of excitation energy.

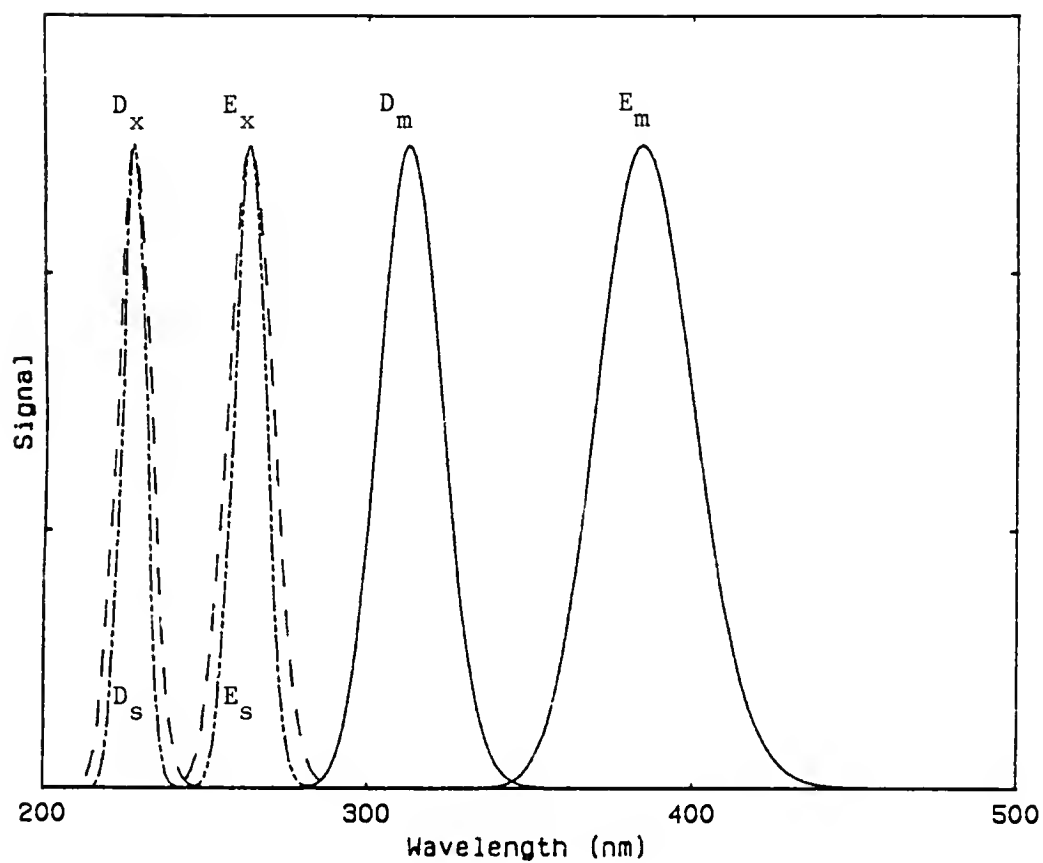


Figure 11. Peaks described in Figure 10, with x-axis plotted in units of wavelength (nm).

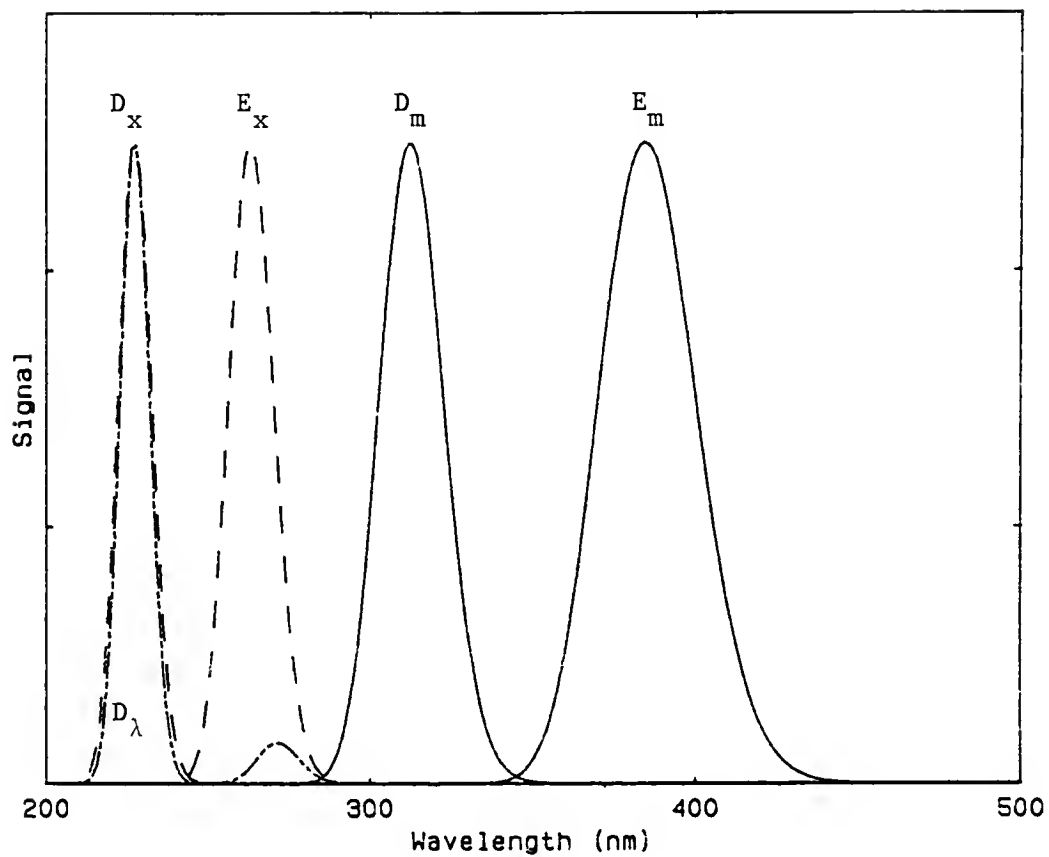


Figure 12. Excitation (— —) and emission (——) peaks for compounds D and E as described in Table III. CWSLS spectrum with  $\Delta\lambda = \Delta\lambda_{\max}$  for compound D (85.227 nm) (---).

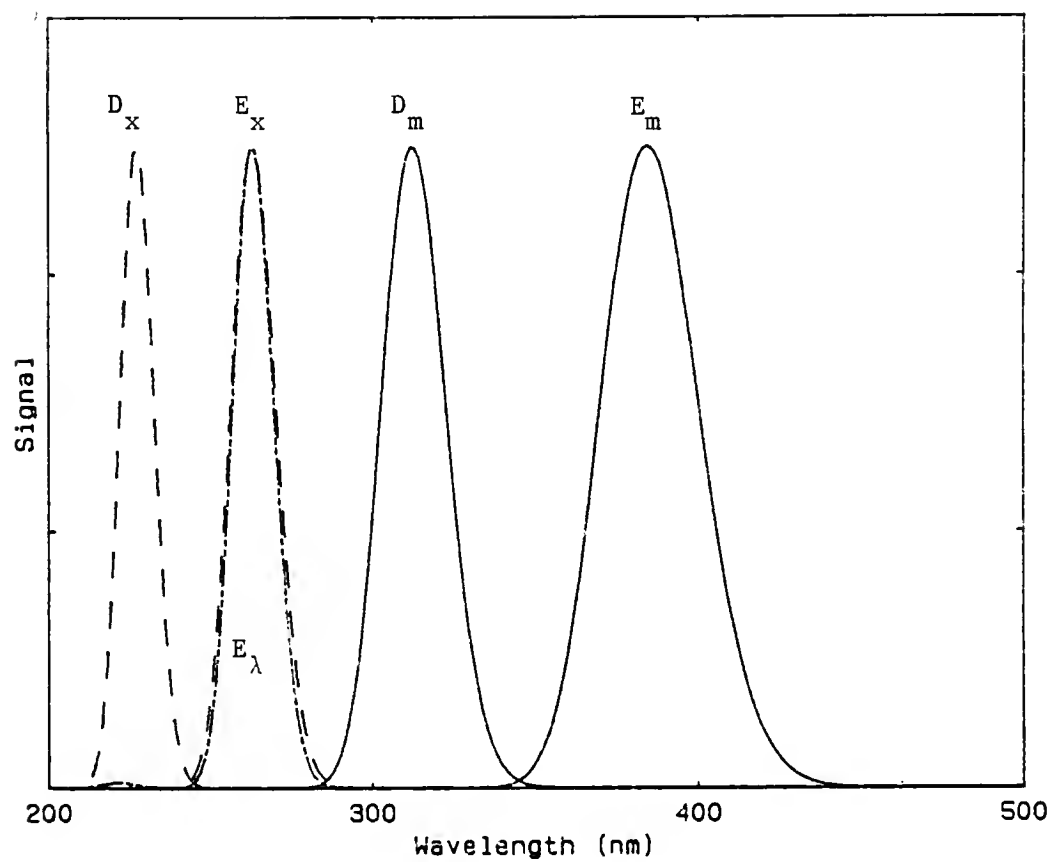


Figure 13. Excitation (— —) and emission (——) peaks for compounds D and E. CWSLS spectrum with  $\Delta\lambda = \Delta\lambda_{\max}$  for compound E (121.457 nm) (--- —).

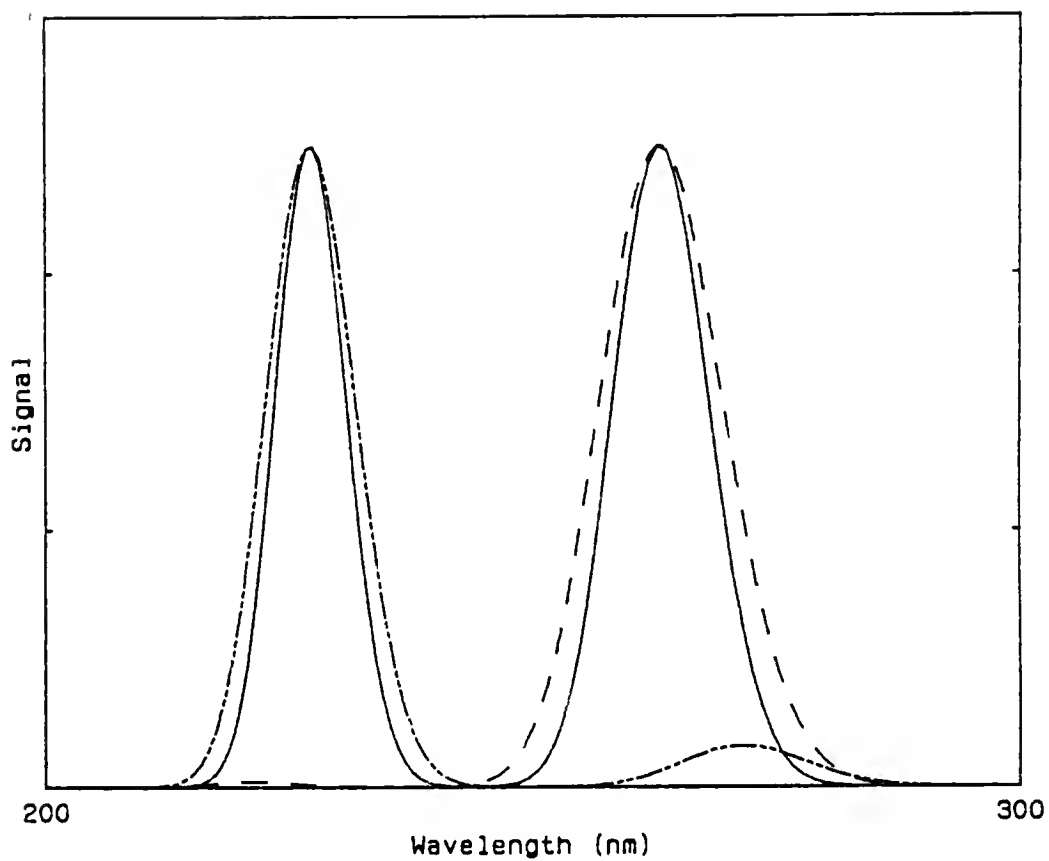


Figure 14. Scans defined by  $\Delta\bar{\nu} = 12,000 \text{ cm}^{-1}$  (—),  $\Delta\lambda = 85.227 \text{ nm}$  (---), and  $\Delta\lambda = 121.457 \text{ nm}$  (- -). For compounds D and E as described in Table III.

by  $\Delta\bar{\nu} = 12,000 \text{ cm}^{-1}$ ,  $\Delta\lambda = 85.227 \text{ nm}$ , and  $\Delta\lambda = 121.457 \text{ nm}$ , for hypothetical compounds D and E.

Figures 10 through 14 demonstrate the superior ability of CESLS over CWSLS to exploit the natural energy relationships in luminescence spectrometry, i.e. peak shapes Gaussian in energy and equivalent vibrational energy spacings exhibited by compounds within a given class.

### Experimental Design

Room temperature fluorescence and phosphorescence spectra generally fall within the Case 1 category where  $\sigma_i = \sigma_j$ . For these spectra, monochromator bandpasses are selected to limit instrumental broadening of the luminescence bands. A reduction of the spectral bandwidth by a factor of 2 can be advantageous. Cases 2 and 3 describe those systems where significant band-narrowing is observed in the luminescence excitation and emission spectra, such as fluorescence observed at reduced temperatures (39,40). The combination of low temperature spectral band narrowing techniques with synchronous scanning provides extensive application of the selectivity advantages described for synchronous techniques. Experimental parameter selection for these combinations requires a careful evaluation of the fundamental relationships as they have been presented above.

The major consideration for synchronous scanning of narrow peaks include insuring that the scan path crosses the peak of interest; providing sufficient light throughput for detection; and maintaining the spectral features provided by the band-narrowing technique. All three objectives are met by maintaining the bandpass of one monochromator at a level where the bandwidth is not instrumentally

broadened and by increasing the bandpass of the other monochromator to a significantly larger value. The narrow bandpass is maintained on the monochromator where narrower bands are observed in the excitation and emission spectra. While a thorough evaluation of experimental parameters was not available at the time, reference 13 demonstrated the effectiveness of this approach. If the excitation and emission spectra are comparable in bandwidth, increasing the excitation monochromator is recommended, forcing the system into the Case 3 category. Case 3 offers several advantages for this application. The CESLS maximum approaches the emission peak maximum, providing a means of peak comparison for identification. Note that the CESLS maximum is independent of  $\Delta\bar{\nu}$ . Also  $\delta\bar{\nu}_s$  is then approximately equal to  $\delta\bar{\nu}_j$ . By increasing the excitation monochromator bandpass, sensitivity is increased for adequate detection. Finally, the luminescence intensity of the synchronous peak relative to the maximum peak intensity is maintained over a wider range of scan values for  $\Delta\bar{\nu}$  using these experimental conditions. Figure 5 demonstrates that a Case 3 peak has a greater probability of being included in a synchronous scan than a Case 1 peak without instrumental broadening.

### Conclusions

The CESLS parameters of peak wavelength maximum, intensity maximum, and peak bandwidth have been evaluated, with mathematical relationships derived for each parameter as it is affected by the luminescence excitation and emission spectral characteristics and the scan path. These relationships are solved without approximation based on the initial assumption of single Gaussian peakshapes. Graphical representations of CESLS scans confirm these relationships, with

hypothetical compounds used to demonstrate their application. Calculations are significantly influenced by the ratio of the excitation and emission bandwidths, resulting in three special cases used for detailed discussion. Observations from three cases were translated into experimental design considerations for CESLS applications. This provides a parameter optimization strategy based on fundamental spectral characteristics rather than empirical determinations. As a result, the combination of synchronous scanning with other luminescence techniques should implement the selectivity advantages.

CHAPTER 3  
ANALYSIS OF ENVIRONMENTAL SAMPLES CONTAINING  
POLYCYCLIC AROMATIC HYDROCARBONS

Introduction

Polycyclic aromatic hydrocarbons are formed during incomplete combustion of fuel in an engine. The concentration of chemical species in vehicle exhaust is dependent upon factors such as engine type, oil and fuel consumption, and operating conditions for the engine. PAHs have also been found to occur naturally in crude oil and gasoline samples (41). The number and quantity of PAHs in such materials depends on a number of variables, including: degree of maturity, temperature fractionation, sampling, and processing parameters. Fuels and exhausts are merely examples of sources of PAHs. The reader is referred to Grimmer (41), Cooke and Dennis (42), and Jacob et al. (43,44) for comprehensive reviews concerning the occurrence and toxicity of PAHs found in the environment.

Due to the documented carcinogenic and mutagenic activity of many PAHs, there is an obvious need for a simple, sensitive, and reliable method for determining these compounds. Also, a simple method capable of fingerprinting a sample based on the PAH content could be used to identify the source of an environmental hazard, (i.e. an oil spill, gasoline leak, etc.). Such a method could also be used to study the metabolism of oil products by marine species, to aid in forensic analysis, and to evaluate systems proposed for reducing PAH production and emission by engines.

Widely employed techniques for analysis of samples containing PAHs include MS/MS (45), GC/MS (46), and luminescence techniques (1-6). Conventional luminescence measurements are generally very sensitive due to the high quantum yields exhibited by PAHs; however, they offer limited application to analysis of complex mixtures containing PAHs due to the broad, overlapping spectral characteristics exhibited by many of these compounds. Methods often used for enhancing the selectivity of luminescence techniques for mixture analysis were outlined in Chapter 1. Constant Energy Synchronous Luminescence Spectrometry (CESLS) is among the more successful techniques used for selectivity enhancement. CESLS has been shown to be useful for identifying and quantitating PAHs (29,39) in mixtures. To further enhance selectivity CESLS has been carried out in a rapid scan mode for HPLC detection (47). This system showed promise and would be especially useful for extremely complex samples. Based on the success achieved for PAH analysis in the past, CESLS is proposed for fingerprinting gasoline and oil samples as well as gasoline engine exhaust particles.

### Experimental

#### Instrumentation

The experimental setup used for this study is shown in Figure 15. Components and manufacturers are listed in Table IV. The scan rate was approximately 50 nm/min allowing a constant energy scan with an excitation range from 200 to 500 nm to be collected in less than 6 min. The excitation monochromator was pulsed at a constant rate while the emission monochromator was pulsed at a variable and faster rate to maintain the desired constant energy difference. Scan rates were controlled by an Apple II plus microcomputer.

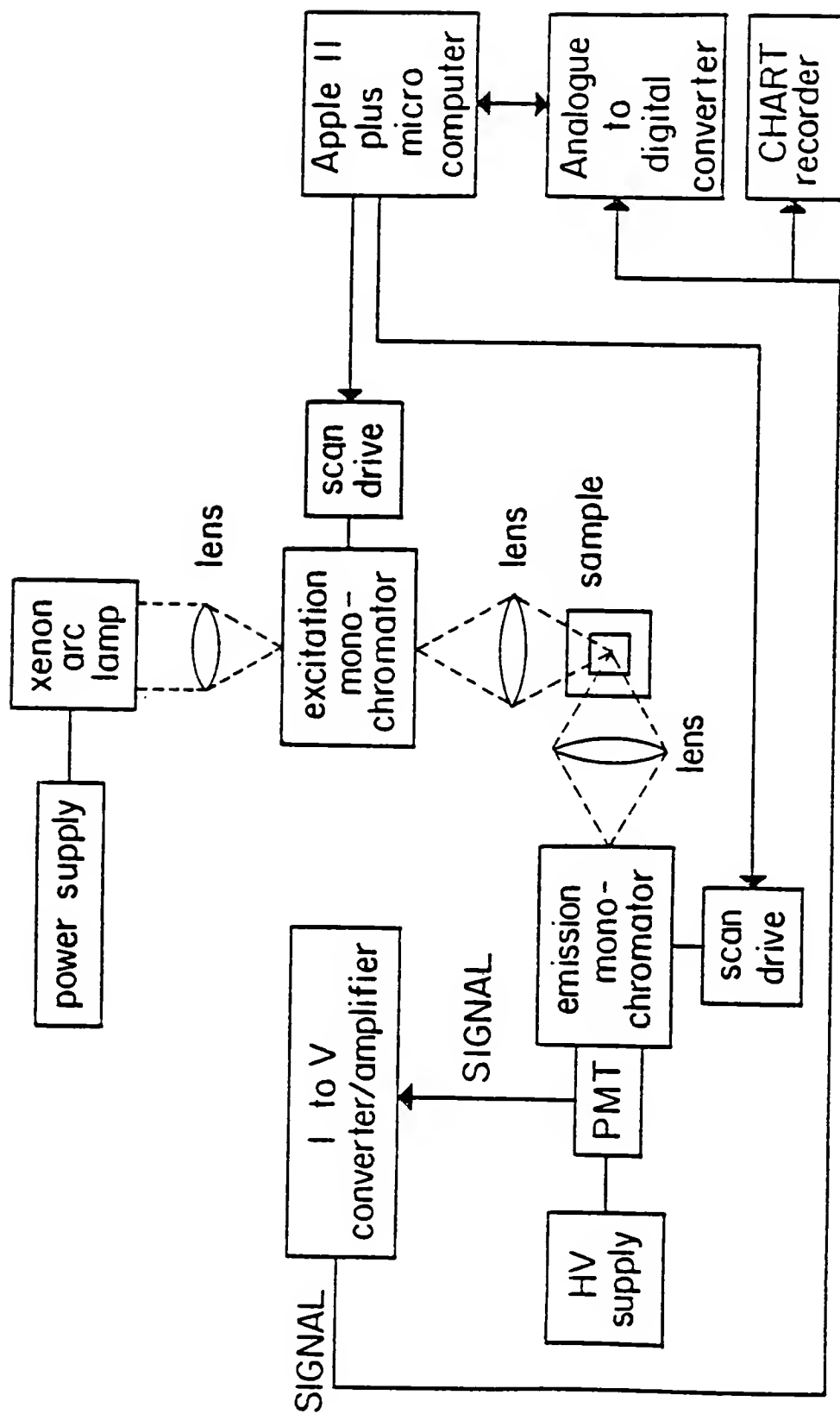


Figure 15. Schematic diagram of experimental system for obtaining CESLS spectra.

Table IV. Experimental Components for CESLS.

<u>Equipment</u>	<u>Model</u>	<u>Manufacturer</u>
Xenon Arc Lamp, 300W	VIX-300UV	EIMAC, Division of Varian, San Carlos CA 94070
Illuminator Power Supply	PS300-1	EIMAC, Division of Varian, San Carlos
Excitation and Emission Monochromators f/3.5 holographic grating 1200 grooves/mm	EU700-56	GCA McPherson Instruments, Acton MA
Monochromator Scan Controls	EU700-51	Heath Co., Benton Harbor, MI 49022
Photomultiplier	1P 28	Hamamatsu, Waltham MA 02154
High Voltage Power Supply operated at 800V	EU701-30	Heath Co., Benton Harbor, MI 49022
Current Voltage Converter/ Amplifier TC 300msec	427	Keithley Instru- ment Inc. 28775 Cleveland, OH 44139
Recorder	Omniscribe	Houston Instrument Austin, TX 78753
Microcomputer	Apple II plus	Apple Computer Cupertino, CA 95014

### Sample Analysis

Measurements at low temperature (77 K) were obtained using quartz tubes immersed in a liquid nitrogen dewar. Room temperature measurements were made on filter paper (Fisher Scientific Company, Pittsburgh, PA) placed at a  $45^{\circ}$  angle with respect to the excitation and emission monochromators. The filter paper was held in position using a device similar to one described previously (48). The holder resembles an aluminum cuvette with the center cut at a  $45^{\circ}$  angle and has a metal plate with a hole in the center to hold the filter paper in place. The metal cuvette was attached to a cover designed to fit over the liquid nitrogen dewar holder. This design allowed us to obtain spectra at room temperature and low temperature with a minimum of alteration in the system. Also, both methods required less than 0.5 mL of sample volume for analysis.

### PAH Mixture Analysis

To determine the suitability of CESLS at low temperature (77 K) for PAH mixture analysis, a 16 component mixture (Chem Service, Westchester, PA) was used. All of these compounds are on the EPA priority pollutant list.

The mixture was first scanned at a variety of constant energy differences ( $\Delta\bar{\nu}$  values). The  $\Delta\bar{\nu}$  values were chosen based on preliminary work determining optimum  $\Delta\bar{\nu}$  values for each compound calculated from excitation and emission spectra (49). The values used for this study included  $\Delta\bar{\nu} = 1400, 2800, \text{ and } 4800 \text{ cm}^{-1}$ . The small number of values necessary for multi-component identification agrees with molecular luminescence theory which shows that compounds within a class (such as PAHs) generally exhibit similar vibrational energy level

spacings and consequently comparable  $\Delta\bar{\nu}$  values. After the mixture was scanned, a library of scans was established containing each of the 16 compounds (obtained from Foxboro Analabs, North Haven, CT, and the EPA Repository, Cincinnati, OH) at the different values. This library was used to identify the peaks in the scans of the mixture. Standard additions were also used when identification was difficult. Results of two of the scans obtained after dilution to a concentration of 200 ppb in each component (with peak identification) are shown in Figures 16 and 17. Thirteen of the compounds in the 16 component mixture are identified in the two scans used for demonstration purposes. The other three compounds were dibenz(a,h)anthracene (which was identifiable in the  $2800\text{ cm}^{-1}$  scan), acenaphthylene, and indeno(1,2,3-cd)pyrene. The last two were not identifiable at the sample concentration chosen for the demonstration scans. These scans were later used for comparison to unknown mixtures for preliminary identification of components.

### Gasoline Engine Exhaust Analysis

#### Sampling Methodology

The samples in this study were collected from the exhaust of a small 4-cycle 1975 model #21 Toro lawn mower. One of the first considerations in identifying and quantitating the components of the exhaust of an engine is the choice of the sampling system. The number and quantity of PAHs measured at a sampling site shows a strong dependence on the sampling methodology (50-54). Two different sampling systems were used in this study. In the first system (outlined in Figure 18), the exhaust was routed through a short (20 cm) flexible metal tube into an open glass tube 120 cm long for 30 min. To determine the effect of sampling location on PAH content, sections 3 cm

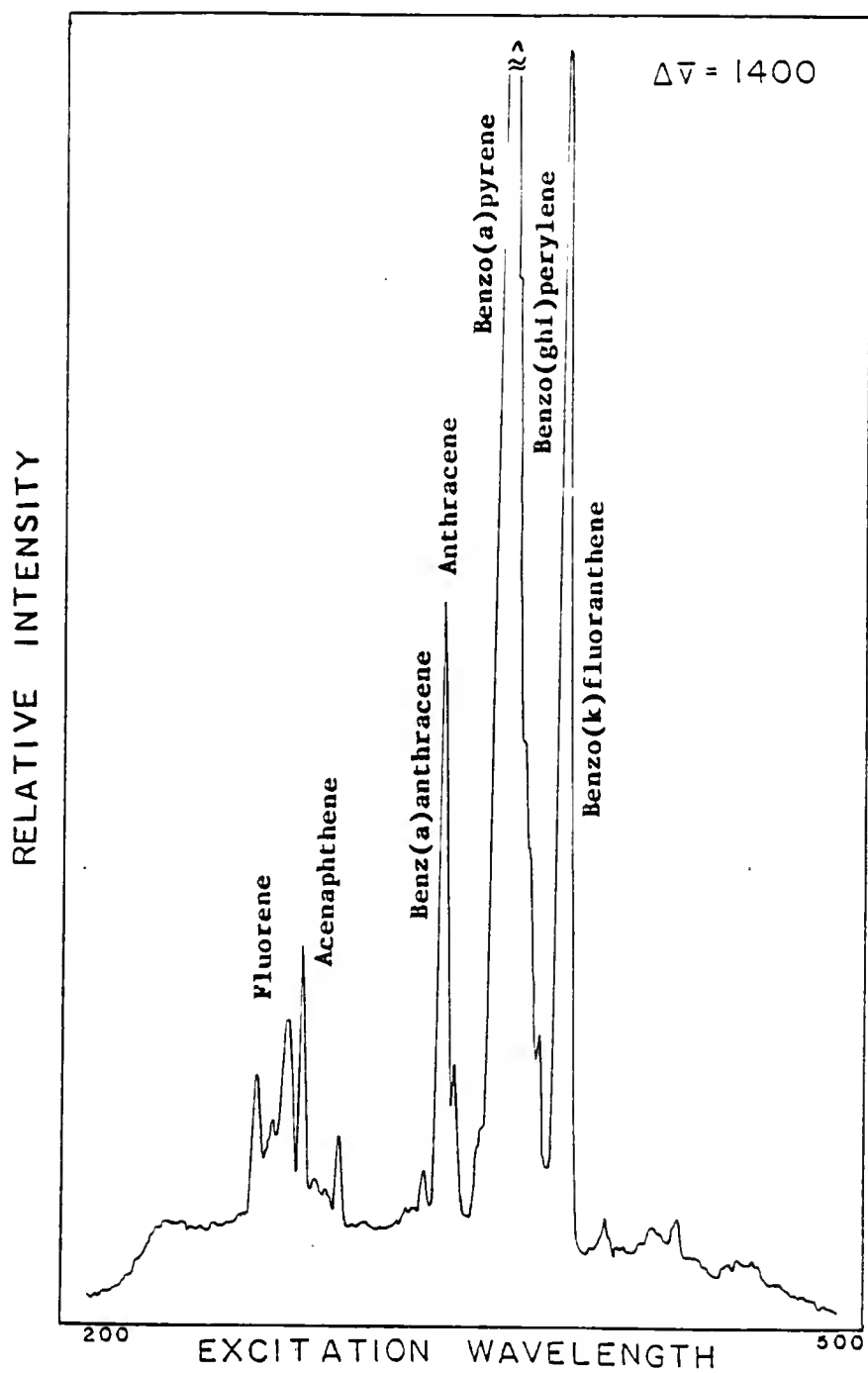


Figure 16. CESLS scan of 16 component PAH mixture  
 $\Delta\bar{\nu} = 1400 \text{ cm}^{-1}$ .

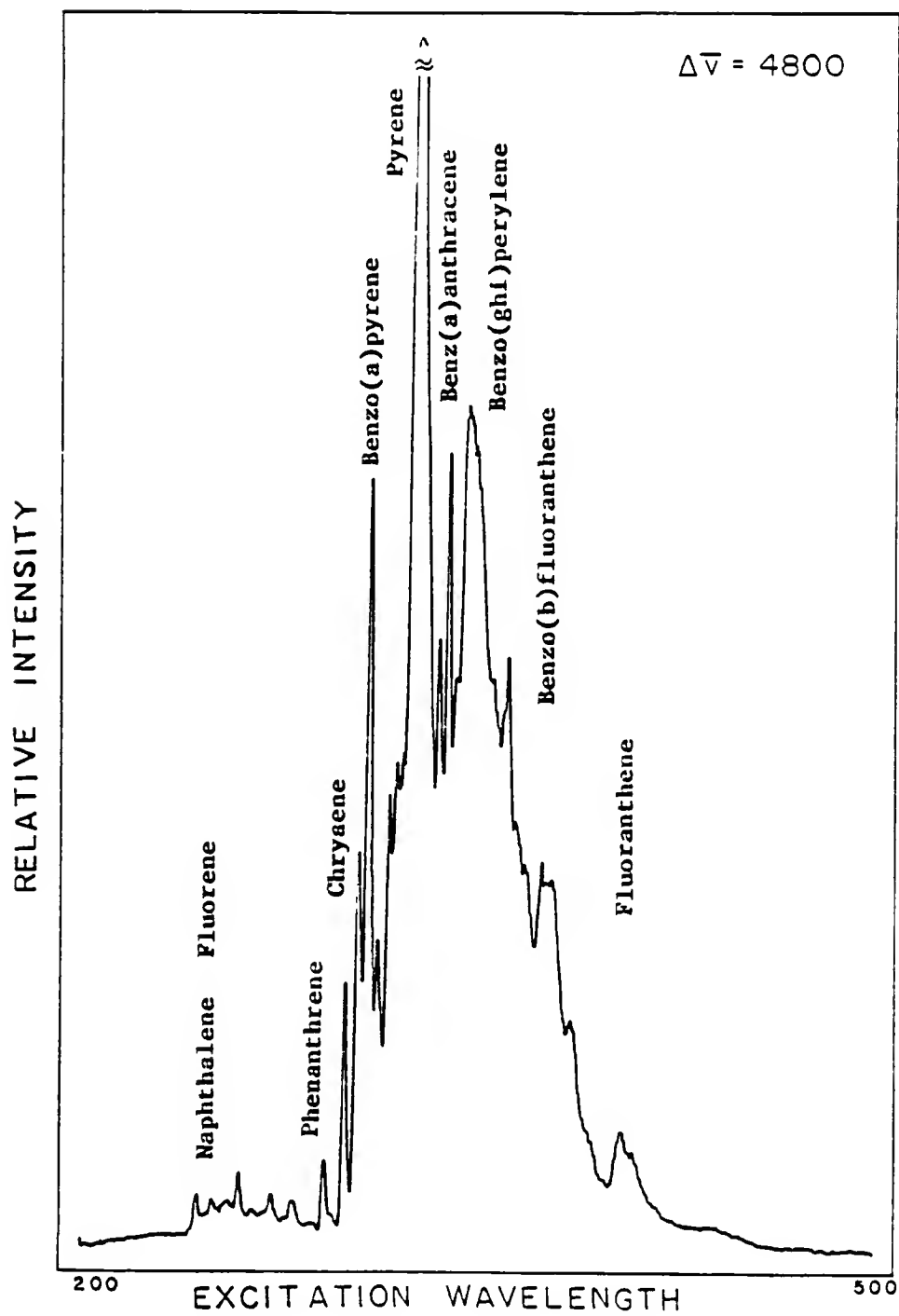


Figure 17. CESLS scan of 16 component PAH mixture  
 $\Delta\bar{\nu} = 4800 \text{ cm}^{-1}$ .

in length were cut from the tube. Three sections were taken; one from the end connected to the metal tube (a), one from the center (b), and one from the open end (c). Although the temperature was not calibrated along the length of the tube, it was expected that this sampling procedure would be equivalent to a crude chromatographic separation based on the volatility of the compounds. The 3 cm sections labelled a, b, and c were each extracted with 25 mL of hexane (obtained from Burdick and Jackson). The extraction process involved immersing the 3 cm sections in hexane contained in amber glass vials and placing them in an ultrasonic bath at room temperature for 30 min. Constant energy scans were then obtained for these samples. The second system for sample collection was designed for qualitative comparison of PAHs produced by different samples. The system involved routing the exhaust into an open 120 cm glass U-tube (i.d. 8 mm o.d. 12 mm) placed in a dewar containing liquid nitrogen. Samples were collected for 6 min and subsequently extracted into 25 mL of hexane by repeated rinsing. The samples included exhaust collected from two different brands of super and regular unleaded and one brand of regular leaded gasoline. The two brands of super and regular unleaded were chosen because although they have comparable octane ratings only one of them contains ethanol.

### Results and Discussion

Figures 18 and 19 show results obtained for exhaust samples collected using the first system described. The  $\Delta\bar{\nu}$  values chosen for demonstration purposes were 1400 and 2800  $\text{cm}^{-1}$ . The exhaust samples shown here were from regular leaded gasoline and the separation results were typical of other gasoline samples which were measured with the

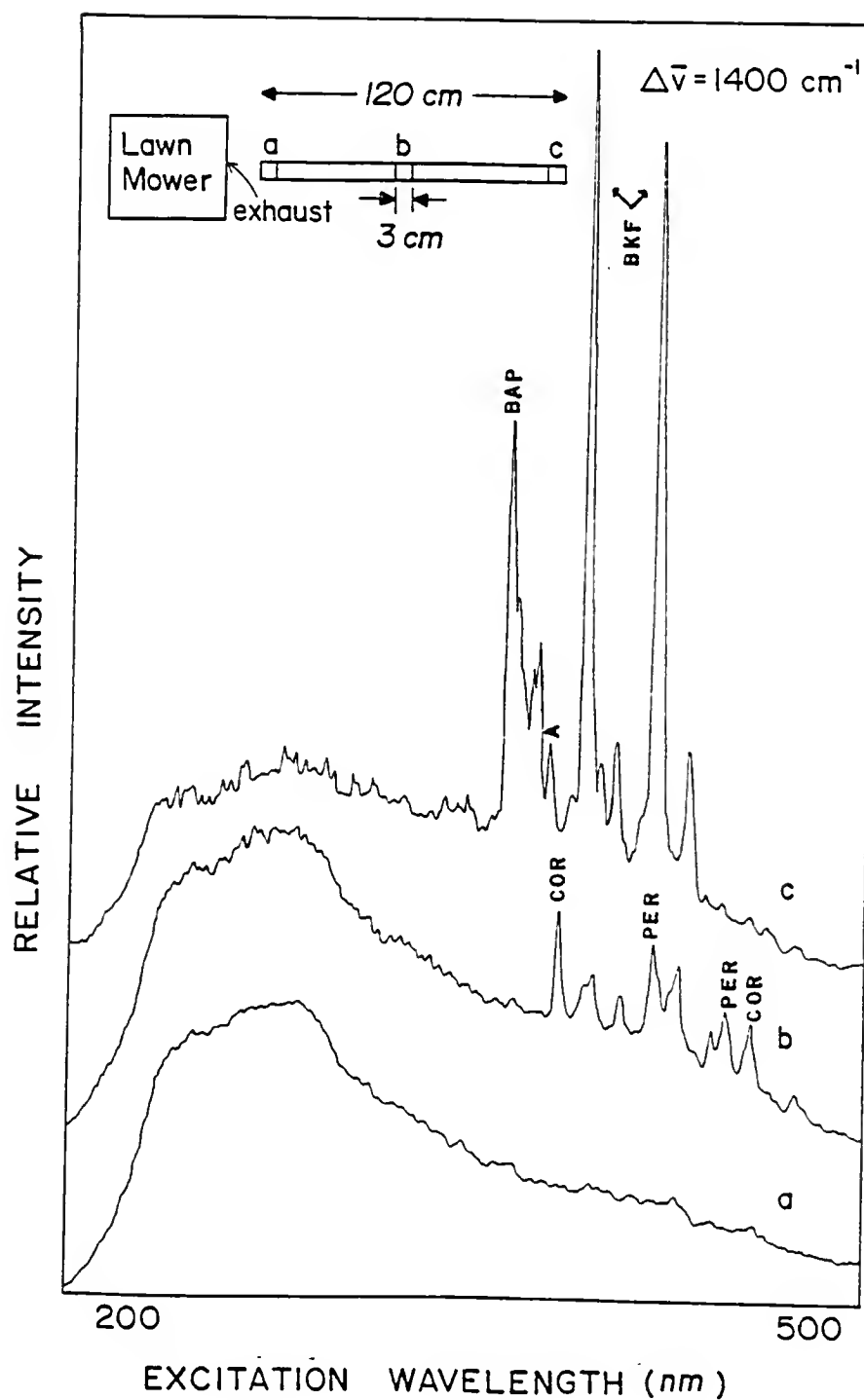


Figure 18. CESLS scan of leaded gasoline exhaust extracts obtained using multiple sample collection system ( $\Delta\bar{\nu} = 1400 \text{ cm}^{-1}$ ). Compounds identified include benzo(a)pyrene (BAP), benzo(k)fluoranthene (BKF), anthracene (A), coronene (COR), and perylene (PER).

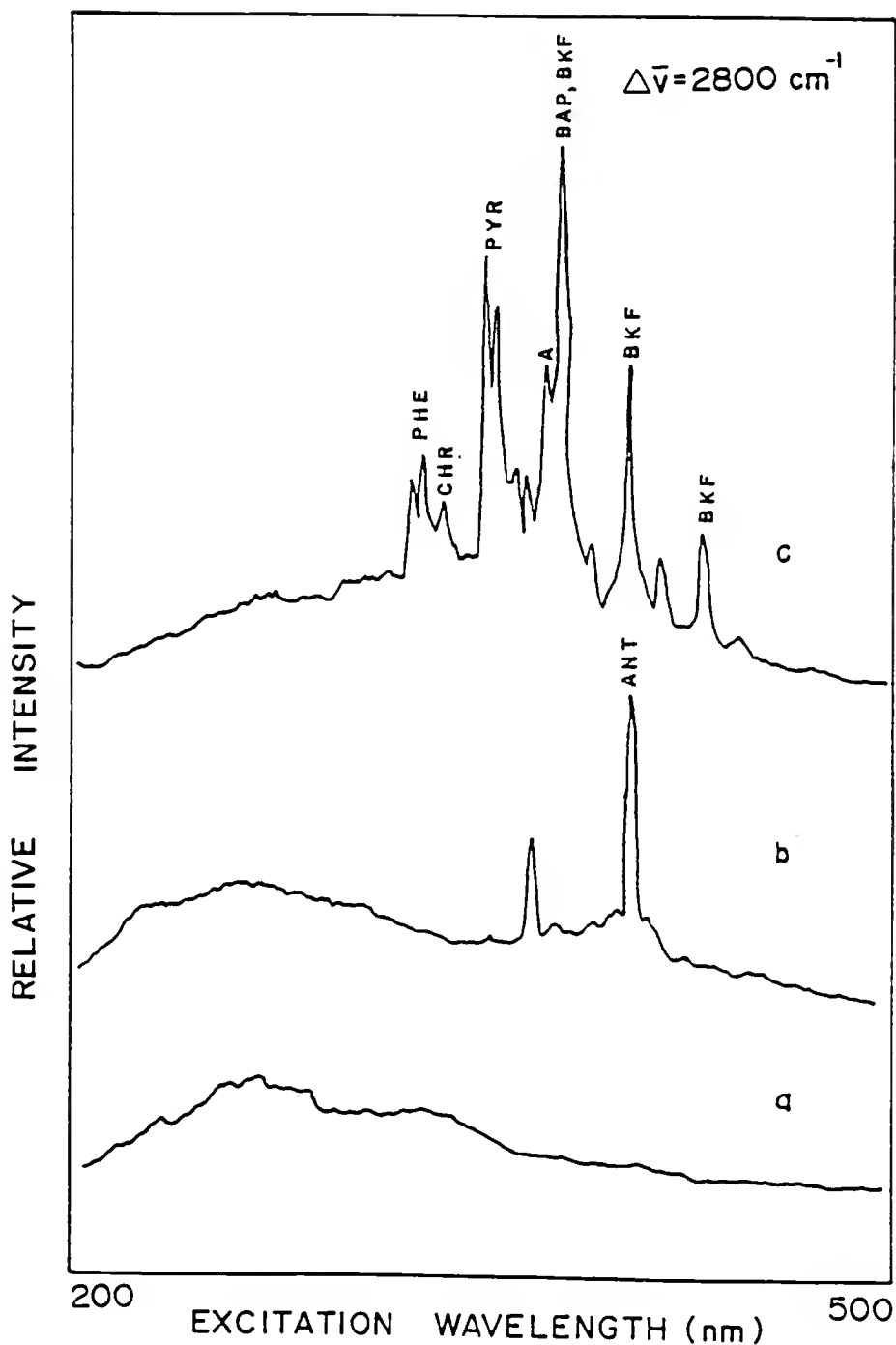


Figure 19. CESLS scan of leaded gasoline exhaust extracts obtained using multiple sample collection system ( $\Delta\bar{\nu} = 2800 \text{ cm}^{-1}$ ). Compounds identified include phenanthrene (PHE), chrysene (CHR), pyrene (PYR), anthracene (A), benzo(a)pyrene (BAP), benzo(k)fluoranthene (BKF), and anthanthrene (ANT).

same sampling system. Results indicate that section a which would be the hottest since it is closest to the engine is too hot to allow significant condensation of any of the PAHs. (Spectra of section a are typical of the background obtained with hexane alone.) The next sections indicate condensation of PAHs in a trend which agrees with their boiling points (41). Identification of PAHs was made through comparison to standard spectra at all  $\Delta\bar{\nu}$  values and confirmed by standard additions. This experiment confirms previous studies which indicate that the results obtained from a particular sampling system may not be indicative of the total PAH content of an exhaust. It also demonstrates the advantage of combining CESLS with a preliminary separation, when one wishes to analyze an especially complex mixture to obtain further information about a sample. Of course, a more elegant separation technique would enhance the information content at the expense of time. Another possibility for information enhancement would be the use of mathematical techniques such as factor analysis.

Figures 20 and 21 show scans of the extracts from the U-tube samples collected for the exhaust of the five different gasolines analyzed in the second system. The  $\Delta\bar{\nu}$  values chosen for demonstration purposes were 1400 and 4800  $\text{cm}^{-1}$ . No attempt was made in this study to label peaks in Figures 20 and 21 because of the confusion which would arise with the need for multiple labeling of individual peaks. However, this system demonstrates the sensitivity of CESLS for PAH analysis, especially for fingerprinting and screening. The results of the study indicate comparable PAH production from different gasoline samples with slight differences in relative concentrations of particular species, such as pyrene, perylene, and acenaphthene.

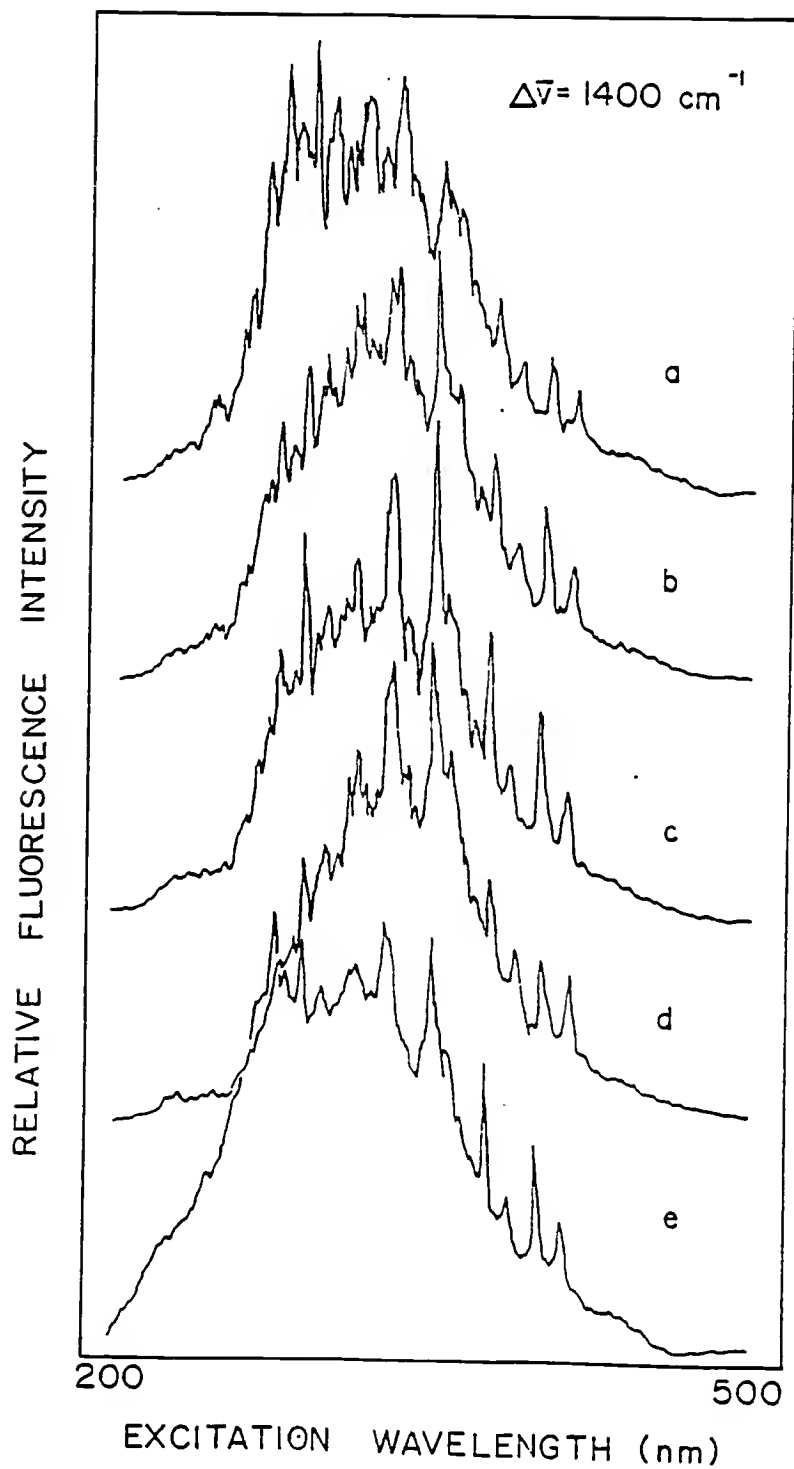


Figure 20. CESLS scan of exhaust from different gasoline samples obtained using a U-tube collection system ( $\Delta\bar{\nu} = 1400 \text{ cm}^{-1}$ ). Samples: (a) Brand A Super Unleaded, (b) Brand A Unleaded, (c) Brand B Super Unleaded with Ethanol, and (d) Brand B Unleaded with Ethanol, and (e) Brand C Regular.

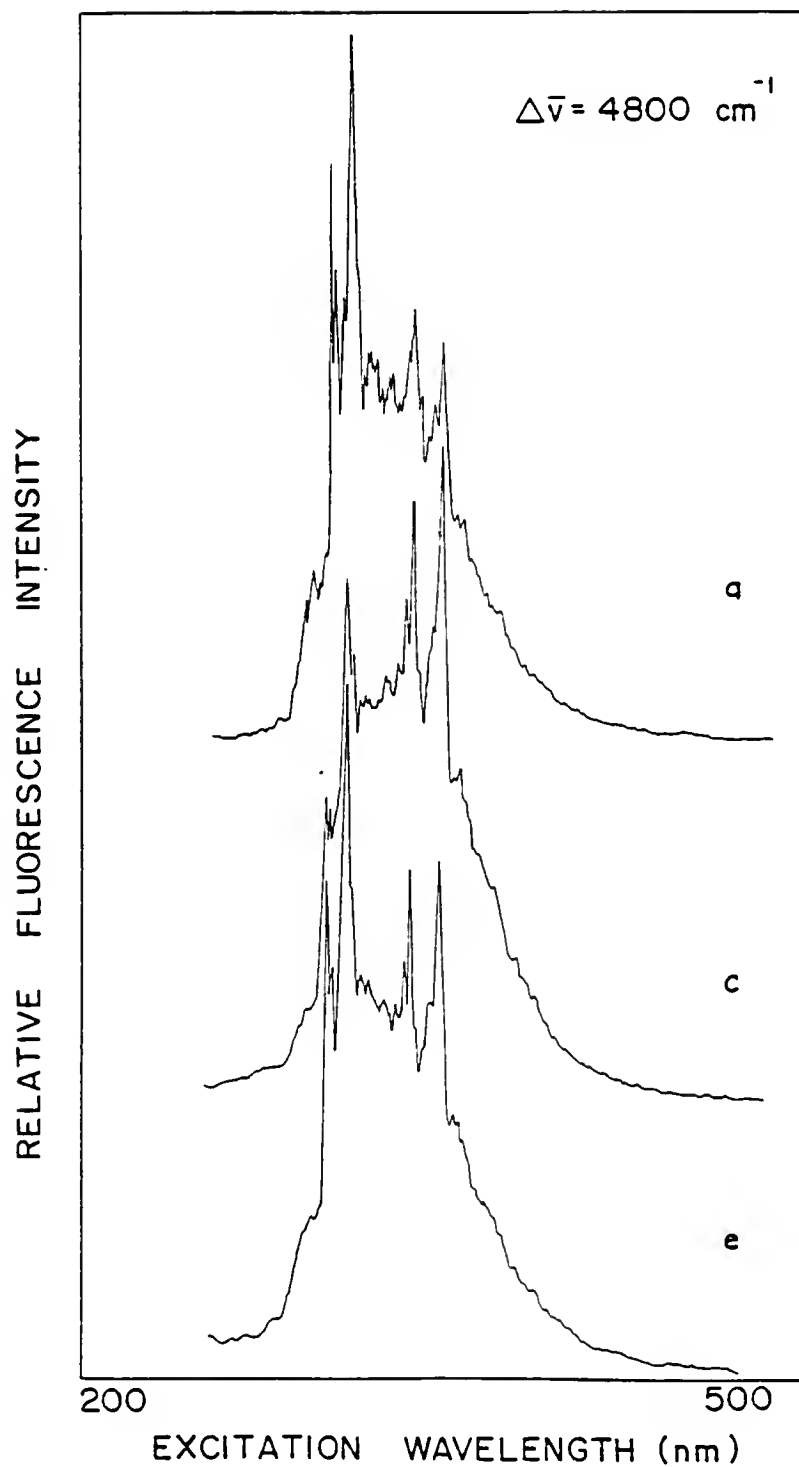


Figure 21. CESLS scan of exhaust from different gasoline samples obtained using a U-tube collection system ( $\Delta\bar{\nu} = 4800 \text{ cm}^{-1}$ ). Samples: (a) Brand A Super Unleaded, (c) Brand B Super Unleaded with Ethanol, and (e) Brand C Regular.

Tests to determine the efficacy of the extraction processes and sampling systems were not performed because the intent of this study was to demonstrate the sensitivity and selectivity of CESLS and not to propose a new sampling method. Also, the engine used in this study could not be optimized and reproducibly run to obtain controls and therefore prohibited the possibility of obtaining data necessary for a meaningful efficacy analysis.

The difference in the appearances of spectra obtained with the two different methods (Figures 18 and 19 compared to 20 and 21) can be attributed to the sampling procedures. In the second system the extracts contain all PAHs collected over the 120 cm length of tube while in the first system each extract contains only the PAHs condensed in a 3 cm interval of the tube.

Possible applications of this method include preliminary screening to evaluate systems proposed for reducing PAH emission and fingerprinting of samples to identify their origin.

#### Gasoline and Crude Oil Fingerprinting

##### Sampling Methodology

Gasoline samples were obtained from various service stations in the Gainesville, FL, area. They were stored at 4°C in amber glass vials prior to analysis. Crude oil samples were obtained from the Stazione Sperimentale dei Combustibile (Milano, Italy) through the Joint Research Centre of European Communities (Ispra, Italy). To achieve analyte concentrations within the linear dynamic range of the method, samples were diluted with hexane. For the gasolines and light crude oil fractions, a direct dilution was performed. For the heavier, more viscous crude oil fractions, samples were weighed and then

extracted by 25 mL of hexane in an ultrasonic bath. These samples were then centrifuged and spectra were obtained for the supernatant. When necessary, these samples were also further diluted with hexane. Dilution requirements were determined by first running the samples directly and then diluting and scanning until no significant spectral changes were observed. Once dilution requirements were established for the most complex, concentrated samples with the different methods all fingerprints were run at this concentration. However, dilutions for gasolines and crude oils were determined separately.

### Results and Discussion

Figures 22 and 23 demonstrate the ability of CESLS to identify several PAHs within gasoline samples. These scans were obtained at low temperature with energy differences of 1400 and 4800  $\text{cm}^{-1}$ , respectively. The synthetic mixtures were matched by comparing the unknown to a library of scans obtained for pure PAHs. Figures 22 and 23 also indicate the advantage of combining scans at different values. For the 1400  $\text{cm}^{-1}$  scan, anthracene (A) and benzo(a)pyrene (BAP) are easily identified, and the 4800  $\text{cm}^{-1}$  scan allows identification of pyrene (P) and fluoranthene (FLU).

Figures 24 through 27 contain scans obtained with  $\Delta\bar{\nu} = 1400 \text{ cm}^{-1}$ . They demonstrate the fingerprinting capabilities of CESLS as well as contrast room temperature versus low temperature measurements. Figures 24 and 25 show scans obtained for three different gasolines at 77 K and 298 K, respectively. Although brand names will not be given, it is especially interesting to note major spectral differences for Brand E super unleaded and regular gasoline (scans a and b).

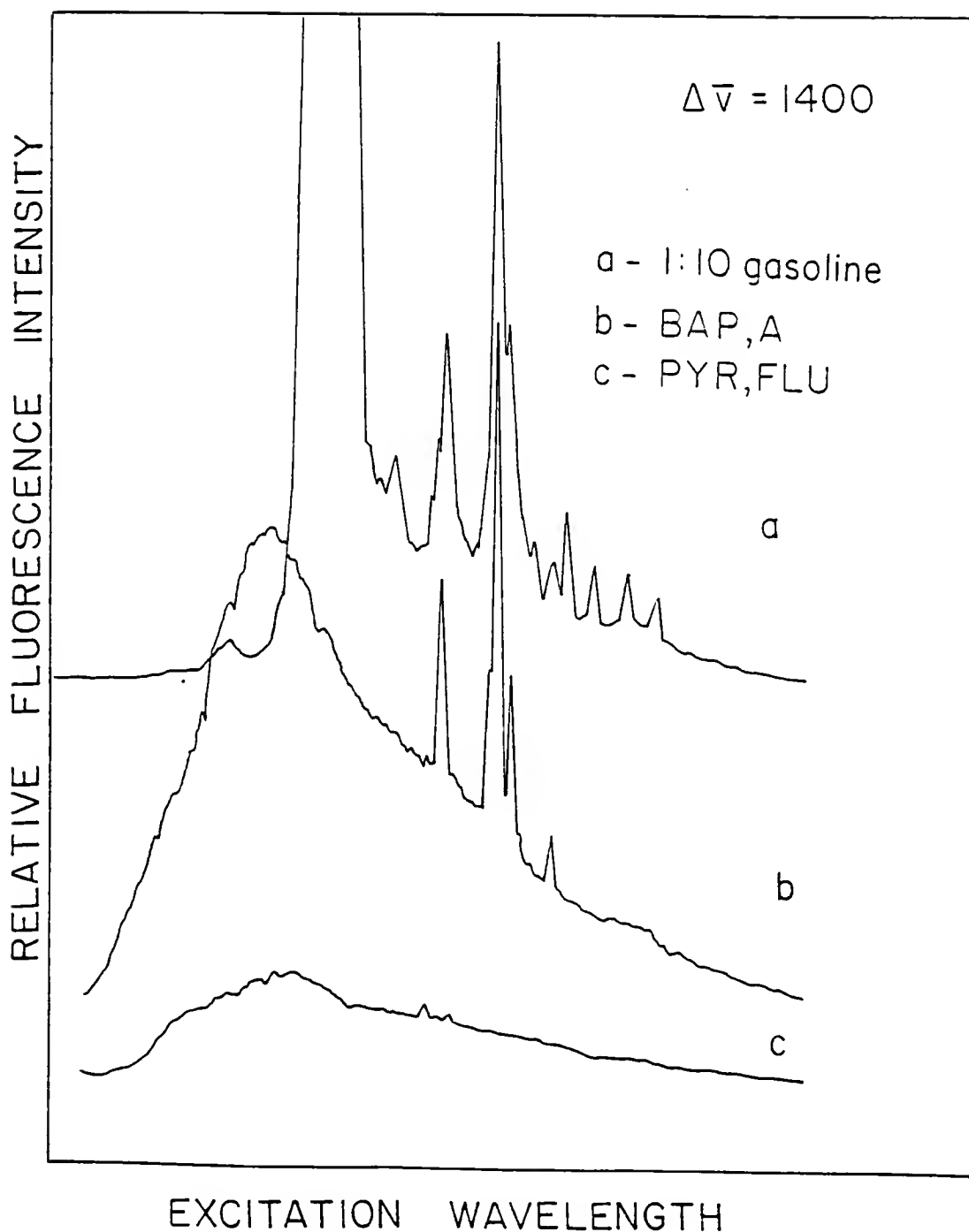


Figure 22. CESLS scans at 77 K and  $1400\text{ cm}^{-1}$  for a) Brand D gasoline (1:10 dilution), b) mixture containing benzo(a)pyrene (BAP) and anthracene (A), and c) mixture containing pyrene (PYR) and fluoranthene (FLU).

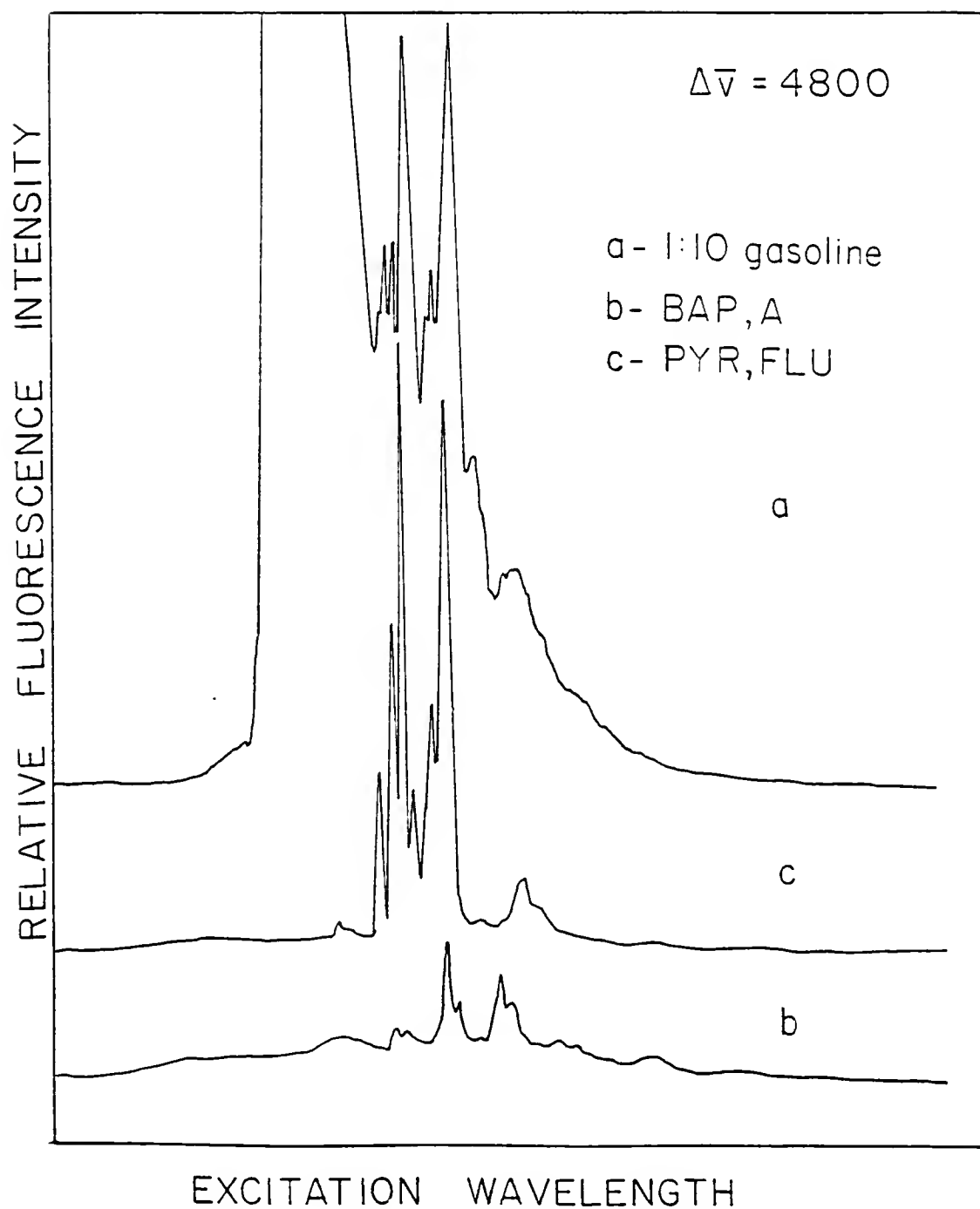


Figure 23. CESLS scans at 77 K and  $4800\text{ cm}^{-1}$  for samples identified in Figure 22.

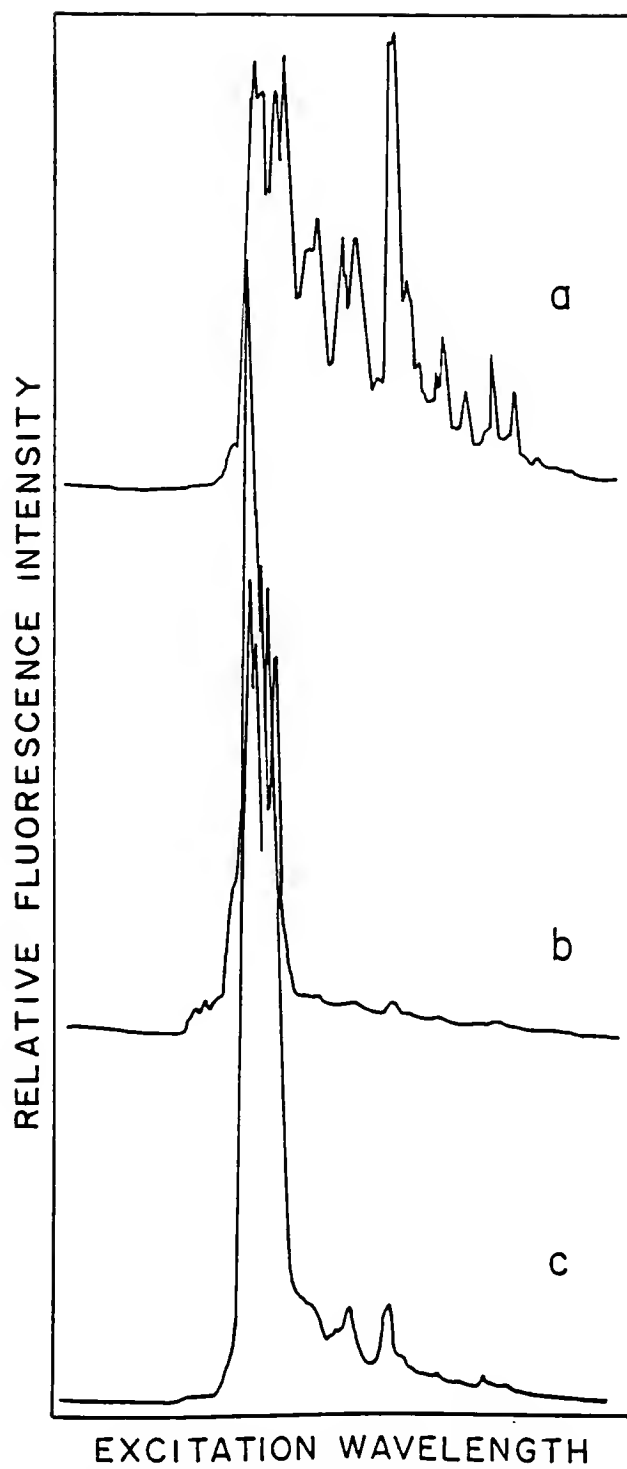


Figure 24. CESLS scans at 77 K and  $1400\text{ cm}^{-1}$  for 1:50 dilutions of a) Brand E Super Unleaded, b) Brand E Regular, and c) Brand F Regular.

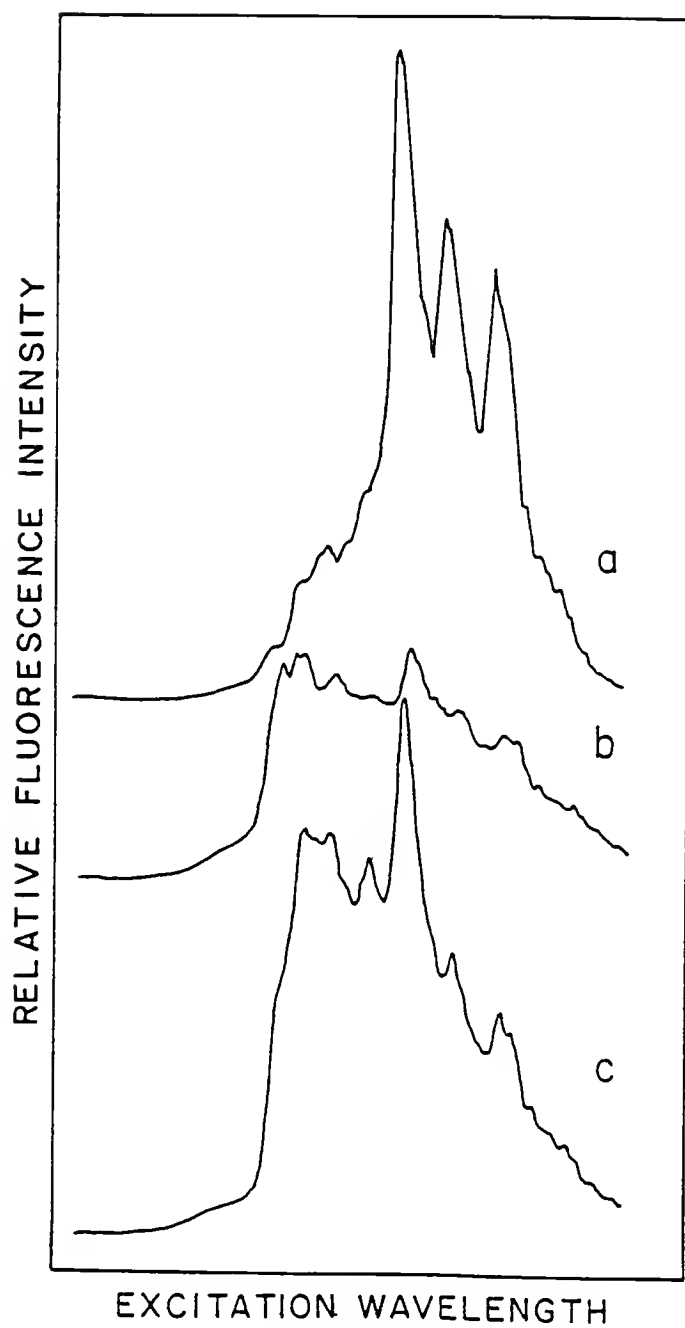


Figure 25. CESLS scans at 298 K and  $1400\text{ cm}^{-1}$  for samples identified in Figure 24 (no dilutions required).

Scans of Brand G regular and diesel obtained at 77 K and 298 K are shown in Figures 26 and 27, respectively. Once again the sensitivity and selectivity of CESLS are demonstrated. Also, these figures illustrate the feasibility of using CESLS to identify the source of an environmental hazard, for example a leak in a tank at a service station.

Figures 28 and 29 compare scans of selected fractions of crude oil number one at 77 K and 298 K, respectively. Scans are for fractions collected by distillation a) below 350°C, b) between 160 and 240°C, and c) between 240 and 350°C. Scans of the same temperature fractions of crude oil number two are presented at 77 K, Figure 30, and 298 K, Figure 31.

The spectra presented here are representative of results obtained for many different gasoline and crude oil samples which were analyzed. The different dilution requirements for the sample types (i.e., gasolines and crude oil fractions) and the methods (i.e., low temperature and room temperature) can be explained by variations in a) concentration of compounds contributing to the fluorescence fingerprint, b) sample matrices, and c) increase in quantum yields of fluorescing compounds at low temperature.

The room temperature scans on filter paper often yielded enough information for conclusive sample identification and are simpler to obtain than low temperature measurements, which require liquid nitrogen and dewars with quartz windows. These scans would be especially suited for distinguishing between known samples. The room temperature scans could also be used for preliminary sample screening and to provide complimentary information to that obtained at low temperature.

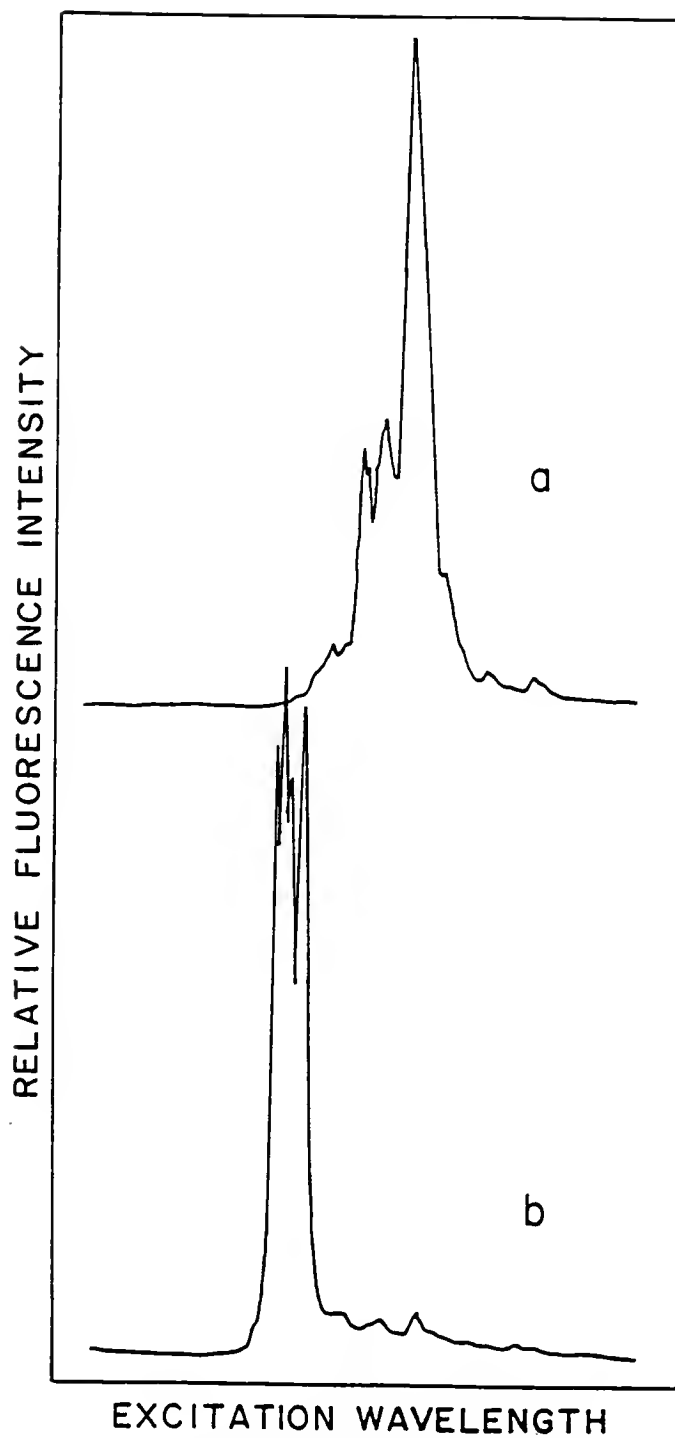


Figure 26. CESLS scans at 77 K and  $1400\text{ cm}^{-1}$  for 1:50 dilutions of a) Brand G Diesel and b) Brand G Regular Gasoline.



Figure 27. CESLS scans at 298 K and  $1400\text{ cm}^{-1}$  for samples identified in Figure 26 (no dilutions required).

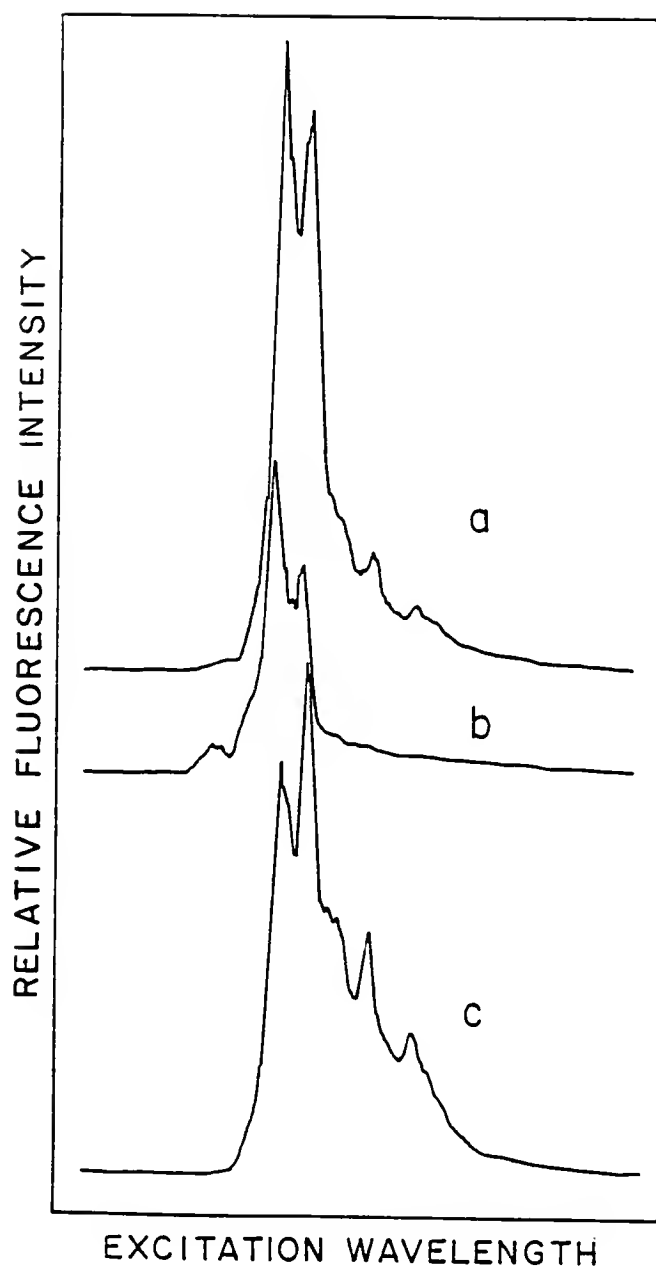


Figure 28. CESLS scans at 77 K and  $1400\text{ cm}^{-1}$  for 1:1000 dilutions of crude oil number one distillation fractions a) below  $350^{\circ}\text{C}$ , b)  $160$  to  $240^{\circ}\text{C}$ , and c)  $240$  to  $350^{\circ}\text{C}$ .

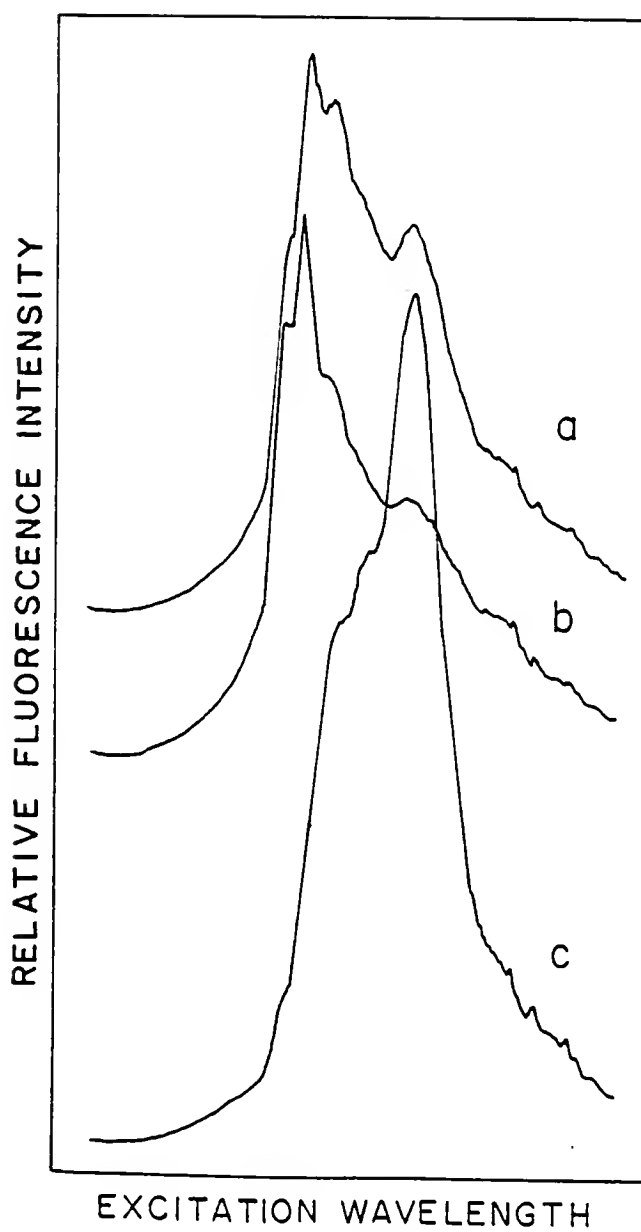


Figure 29. CESLS scans at 298 K and  $1400\text{ cm}^{-1}$  for 1:10 dilutions of crude oil number one fractions described in Figure 28.

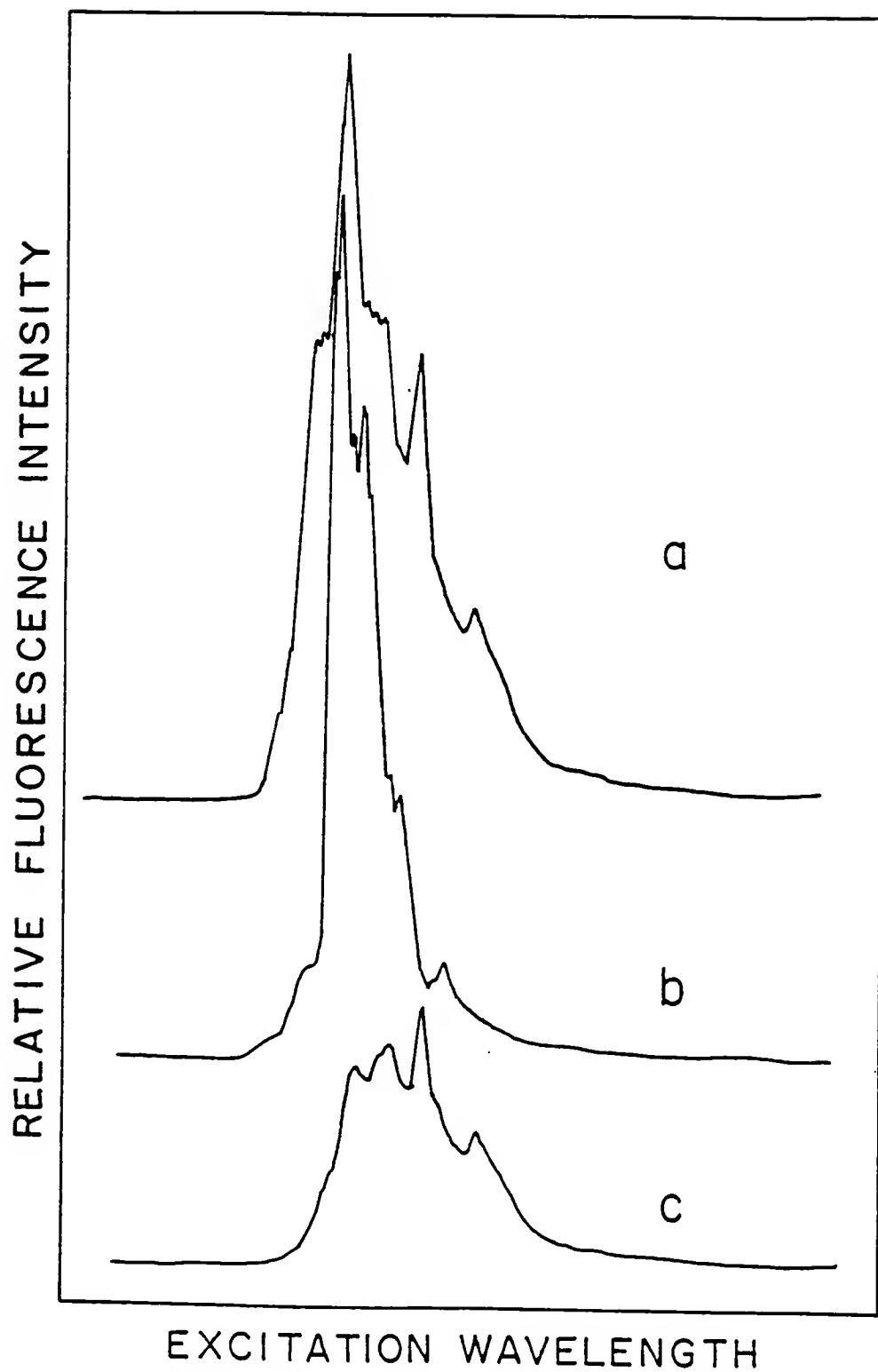


Figure 30. CESLS scans at 77 K and  $1400\text{ cm}^{-1}$  for 1:1000 dilutions of crude oil number two fractions a) below  $350^{\circ}\text{C}$ , b)  $160$  to  $240^{\circ}\text{C}$ , and c)  $240$  to  $350^{\circ}\text{C}$ .



Figure 31. CESLS scans at 298 K and  $1400\text{ cm}^{-1}$  for 1:10 dilutions of crude oil number two fractions described in Figure 30.

Measurements made at low temperature provide greater spectral resolution, and it has been demonstrated that this enhancement in resolution can allow identification of specific compounds and provide information necessary for distinguishing between samples which are very similar.

### Conclusions

The sensitivity and selectivity of CESLS for fingerprinting and identifying PAHs in environmental samples has been demonstrated. Reproducibility for all samples and methods was found to be excellent. CESLS is an inexpensive, simple, and reliable method, which is expected to have a wide range of applications for complex mixture analysis in the future.

CHAPTER 4  
FEASIBILITY STUDY OF  
CONSTANT ENERGY SYNCHRONOUS LUMINESCENCE SPECTROMETRY  
FOR PESTICIDE DETERMINATION

Introduction

Carbamate pesticides are widely used to protect plants from insects (55). Due to the toxicity of these compounds and the possibility of residual presence in the environment and crops, there is an obvious need for a sensitive and reliable method for determining them. A method for distinguishing pesticides from their hydrolysis products and/or metabolites could also have a wide variety of applications for studies involving optimizing application concentrations and times, as well as metabolism of pesticides by insects, animals, and humans.

Pesticide determination has been done by a wide variety of methods ranging from liquid chromatography followed by mass spectrometry (56) to room temperature phosphorescence (7), UV detection (8), and a variety of fluorescence techniques (9-12). Fluorescence techniques are among the most sensitive because of the high fluorescence quantum yields of many pesticides (12). Generally luminescence detection follows separation methods such as HPLC (9) or TLC (11). Separation is usually required due to overlap in conventional luminescence spectra of the compounds of interest.

The many advantages of CESLS over conventional luminescence measurements were evaluated theoretically in Chapter 2. CESLS was applied to determination of PAHs in Chapter 3 with very good results.

Based on previous success with mixture analysis, it was decided to extend the application of CESLS to the determination of pesticides.

The enhancement in selectivity achieved with CESLS at low temperature over conventional luminescence measurements will be demonstrated in this article. It will be shown that often CESLS allows analysis of compounds in a mixture without prior separation. This is a very attractive possibility since separation techniques generally increase the cost and time required for each analysis.

For this study carbaryl, naphthol (a hydrolysis product of carbaryl), and carbofuran were evaluated with respect to identification, limits of detection, and linear dynamic ranges. Bandpasses and constant energy differences were varied to evaluate their effect upon spectra obtained.

## Experimental Section

### Instrumentation

The experimental setup used for this study was described in Chapter 2 and shown in Figure 15. For this study spectral bandpasses were varied from 1.5 to 4 nm. Constant energy scans were obtained with an excitation range from 250 to 350 nm in approximately 2 min. Spectra were taken at low temperature (77 K) through the use of a liquid nitrogen dewar system, and round quartz sample tubes (3 mm i.d. and 5 mm o.d.).

### Sample Preparation

Stock solutions of 100 ppm carbaryl, naphthol, and carbofuran (obtained from EPA, Research Triangle Park, NC) were made in reagent grade ethanol (obtained from Aaper Alcohol & Chemical Co., Shelbyville, KY). These stock solutions were subsequently diluted in ethanol to

form samples for calibration curves and to obtain spectra for demonstration purposes.

### Results and Discussion

First, excitation and emission scans were obtained for the three compounds. Carbofuran luminescence scans yielded excitation peaks at 234 and 284 nm, and one broad emission peak centered at 299 nm. The width of the emission peak allowed determination at a wide range of energy differences, while the position of these peaks prevented overlap with constant energy scans of naphthol and carbaryl. Figures 32 and 33 show spectra for carbaryl and naphthol, respectively. Spectra were taken at low temperature and were not corrected for instrumental response. These spectra will be used here to demonstrate the results one can expect with constant energy scanning and variations in bandpasses.

From conventional luminescence excitation and emission spectra of the three compounds, tables of possible energy differences between each excitation and emission pair were calculated using the expression previously given for  $\Delta\bar{\nu}$ .

Tables V and VI contain results of these calculations for carbaryl and naphthol respectively. Based on these calculations, constant energy scans were obtained at a variety of energy differences. For example, naphthol has three transitions with an overall vibrational energy loss close to  $1400\text{ cm}^{-1}$  (see Table VI). Figure 34 shows the spectrum of naphthol obtained by scanning with  $\Delta\bar{\nu} = 1400\text{ cm}^{-1}$ . If one then compares both tables for naphthol and carbaryl (Table V), it can be seen that an energy difference of  $2650\text{ cm}^{-1}$  is a good compromise for identification

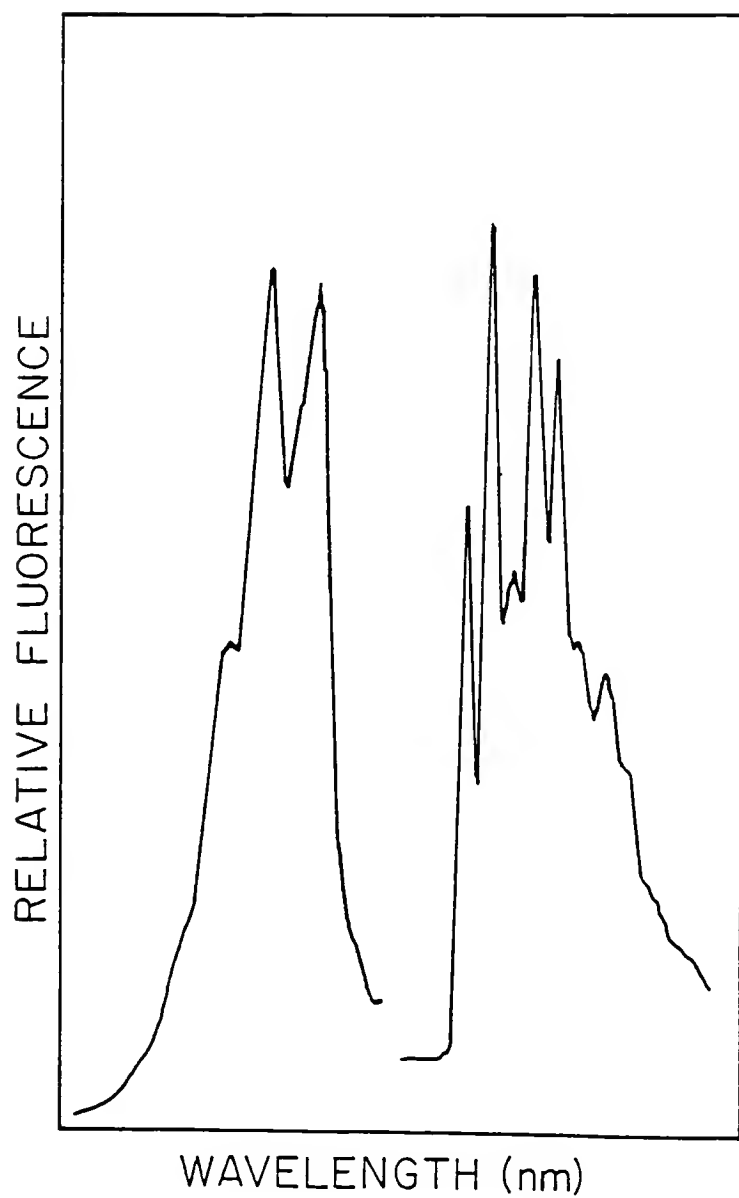


Figure 32. Excitation and emission scans of carbaryl. Prominent peaks are listed in Table V.

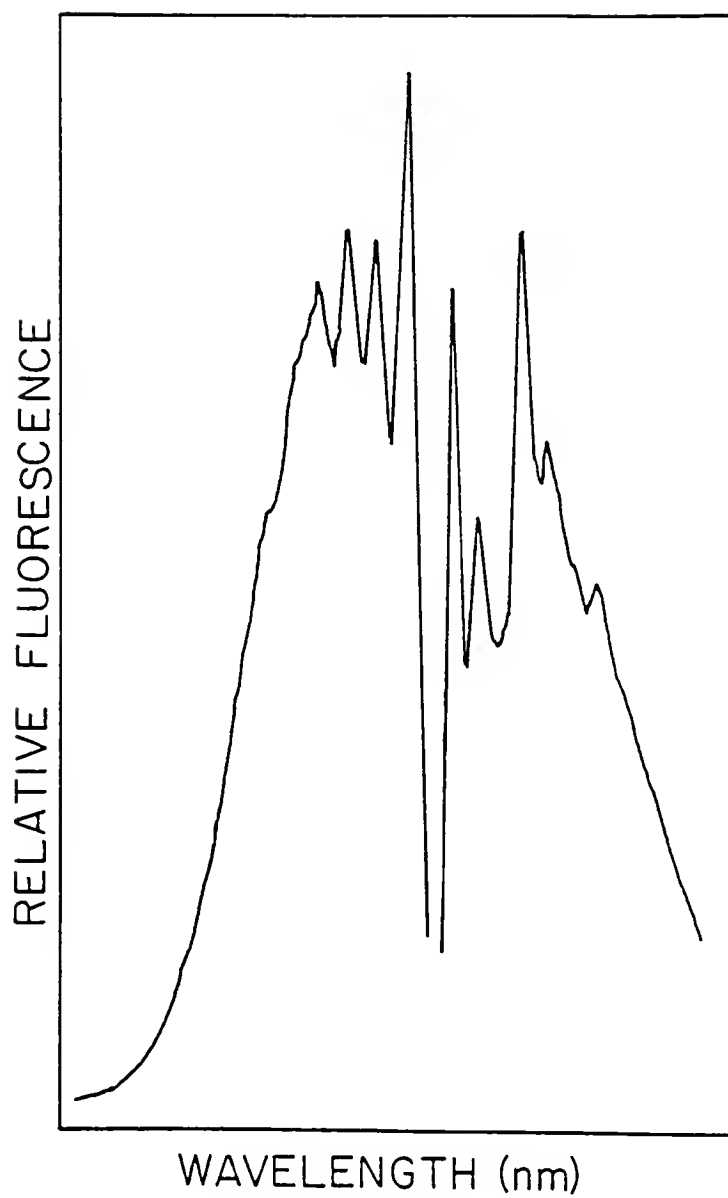


Figure 33. Excitation and emission scans of naphthol. Prominent peaks are listed in Table VI.

Table V. Calculated Energy Transitions (in  $\text{cm}^{-1}$ ) for Carbaryl.

Excitation peaks (nm)	Emission peaks (nm)			
	315.7	320.7	330.5	335.5
273.2	4926	5413	6347	6792
283.1	3650	4137	5070	5515
294.3	2310	2797	3730	4176

Table VI. Calculated Energy Transitions (in  $\text{cm}^{-1}$ ) for Naphthol.

Excitation peaks (nm)	Emission peaks (nm)				
	326.4	331.6	341.7	347.5	358.2
304.6	2193	2673	3565	4053	4913
311.8	1435	1915	2806	3295	4154
318.3	780	1260	2152	2640	3500
325.7	66	547	1438	1927	2786

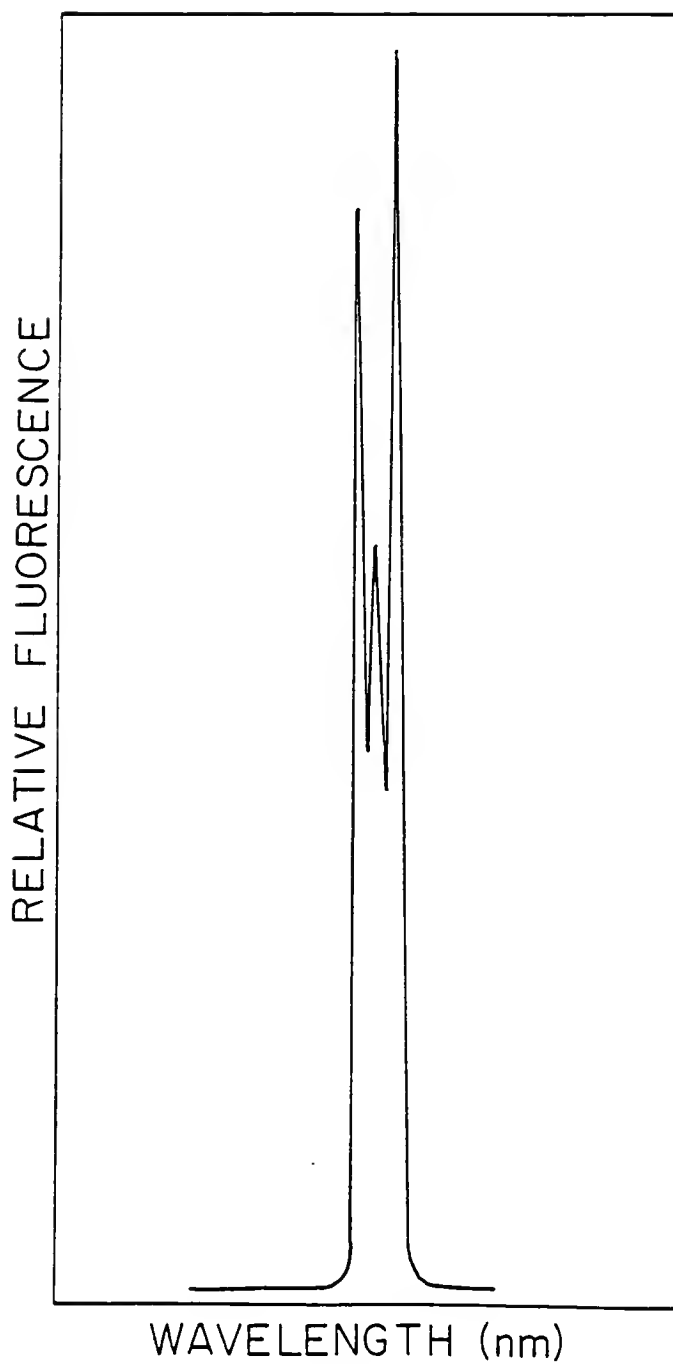


Figure 34. Constant energy scan of naphthol with  $\Delta\bar{\nu} = 1400 \text{ cm}^{-1}$ . Excitation wavelength range 250-350 nm. Excitation and emission bandpasses 1.5 nm.

of both compounds. As mentioned earlier, carbofuran could be determined at a wide range of constant energy differences. This fact is illustrated in Figure 35 which includes scans of a mixture of 4 ppm carbaryl, 4 ppm carbofuran, and 2 ppm naphthol at  $\Delta\bar{\nu} = 1400$  and  $2650\text{ cm}^{-1}$ . Also, this figure demonstrates the advantage of using a combination of constant energy scans for confirmation of identification. Peaks used for identification and limit of detection measurements are labeled. These scans were obtained with 1.5 nm bandpasses on the excitation and emission monochromators. Concentrations were calculated based on peak heights and comparison to standard calibration curves. The mixture was run in triplicate and peak heights were averaged to minimize variation in signal intensity due to effects such as solvent cracking and changes in sample tube alignment. Values determined in this manner gave results within 13% of the true value for all three compounds. In conventional luminescence, the accuracy and precision of such measurements is dependent on the relative concentrations of the compounds being quantitated, due to overlap in spectral characteristics. The excellent resolution obtained with CESLS minimizes this problem.

Theory presented in Chapter 2 indicated that it should be possible to maintain good resolution while increasing signals by opening either the excitation or emission monochromator and keeping the other narrow. Therefore, it was decided to evaluate these same compounds under varying conditions. Table VII gives limits of detection obtained for the three compounds at a variety of bandpasses and energy differences. Analytically useful ranges were approximately 3.5 orders of magnitude for the three compounds under all conditions, and included the limits

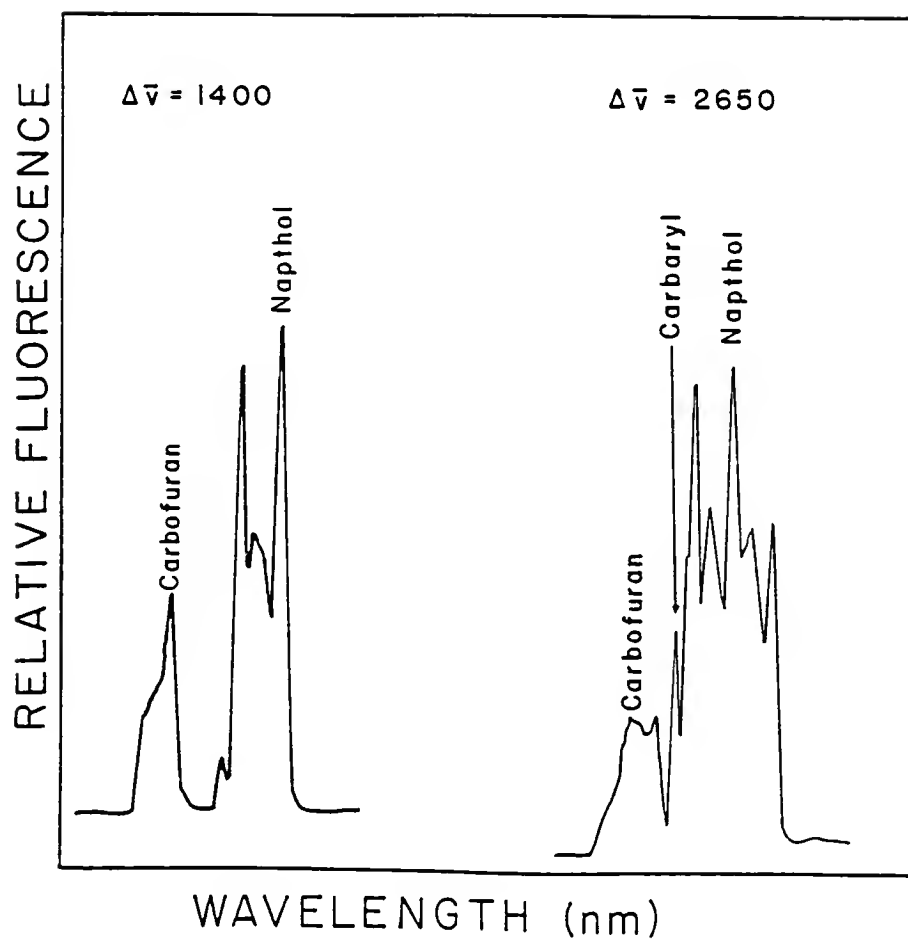


Figure 35. Constant energy scans of a mixture of carbaryl, naphthol, and carbofuran with  $\Delta\bar{\nu} = 1400$  and  $2650 \text{ cm}^{-1}$ . Excitation and emission bandpasses 1.5 nm.

Table VII. Limits of Detection for Pesticides with Variable Parameters.

Compound	(cm <sup>-1</sup> )	bandpasses <sup>a</sup>	LOD (ppb)
Carbaryl	2650	1.5,1.5	24
	2650	4.0,1.5	10
	2650	1.5,4.0	13
Naphthol	1400	1.5,1.5	6
	2650	1.5,1.5	7
	2650	4.0,1.5	2
	2650	1.5,4.0	3
Carbofuran	1400	1.5,1.5	20
	2650	1.5,1.5	45
	2650	4.0,1.5	13
	2650	1.5,4.0	18

<sup>a</sup> Bandpasses for excitation, emission monochromators in nm.

Note: Analytically useful ranges were approximately 3.5 orders of magnitude extending from the limit of detections for all conditions and compounds.

of detection. Figure 36 shows the effect on the constant energy spectra of naphthol when a) opening the excitation monochromator to a 4 nm bandpass and maintaining a 1.5 nm bandpass for the emission monochromator, and b) opening the emission monochromator to a 4 nm bandpass and maintaining a 1.5 nm bandpass for the excitation monochromator. The lower scans in Figure 36 were obtained with the same sensitivity scale and 1.5 nm bandpasses on both monochromators. Figure 37 shows the effect of the same variation in parameters on constant energy luminescence spectra of carbaryl. The effect of CESLS can be visualized in a simplified way as moving simultaneously across the excitation and emission spectra. (This would be an exact representation if the spectra were plotted in units of wavenumber and the separation between the points moving across these spectra was equal to the constant energy difference being maintained.) For naphthol, opening the excitation slit causes a loss in resolution in the constant energy peaks at higher wavelength. This loss can be correlated to the excitation and emission scans (see Figure 33). There is a broad emission peak at higher wavelength, and therefore the use of a narrow emission slit merely reduces light throughput. However, resolution is lost by opening the excitation slit because the higher wavelength excitation peaks are quite narrow. Resolution for naphthol is maintained very well by opening the emission slit and keeping the excitation slit narrow.

For carbaryl, in a  $2650\text{ cm}^{-1}$  scan, resolution is maintained by opening the excitation slit and keeping the emission slit narrow. Again this effect can be related back to the excitation (broad peaks) and emission (narrow peaks) scans for this compounds (see Figure 32).

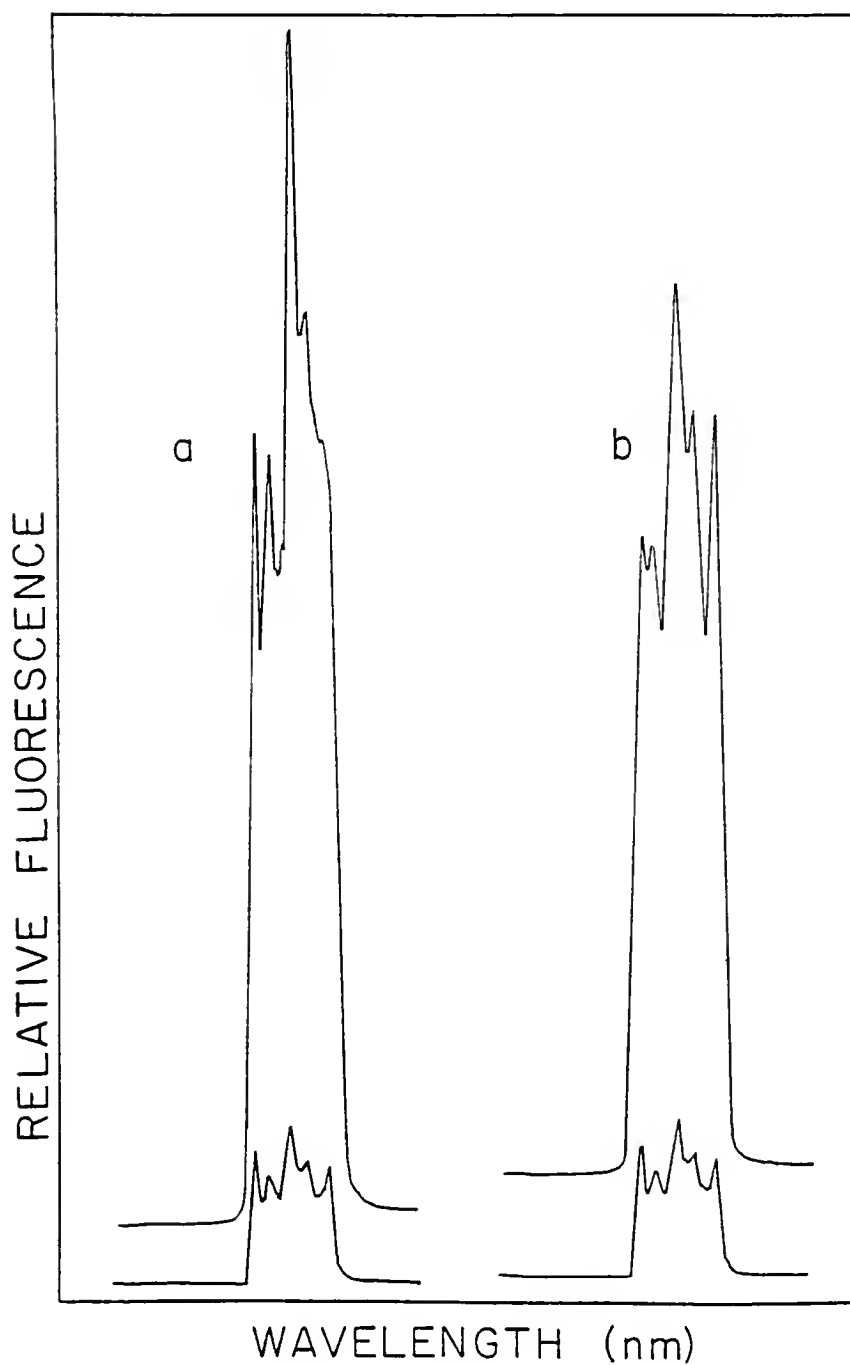


Figure 36. Constant energy scans of naphthol with  $\Delta\bar{\nu} = 2650 \text{ cm}^{-1}$ . Demonstrating the comparison between spectra obtained with bandpasses of 1.5 nm on both monochromators versus a) maintaining a 1.5 nm emission bandpass and opening the excitation bandpass to 4 nm, and b) maintaining a 1.5 nm excitation bandpass and opening the emission bandpass to 4 nm.

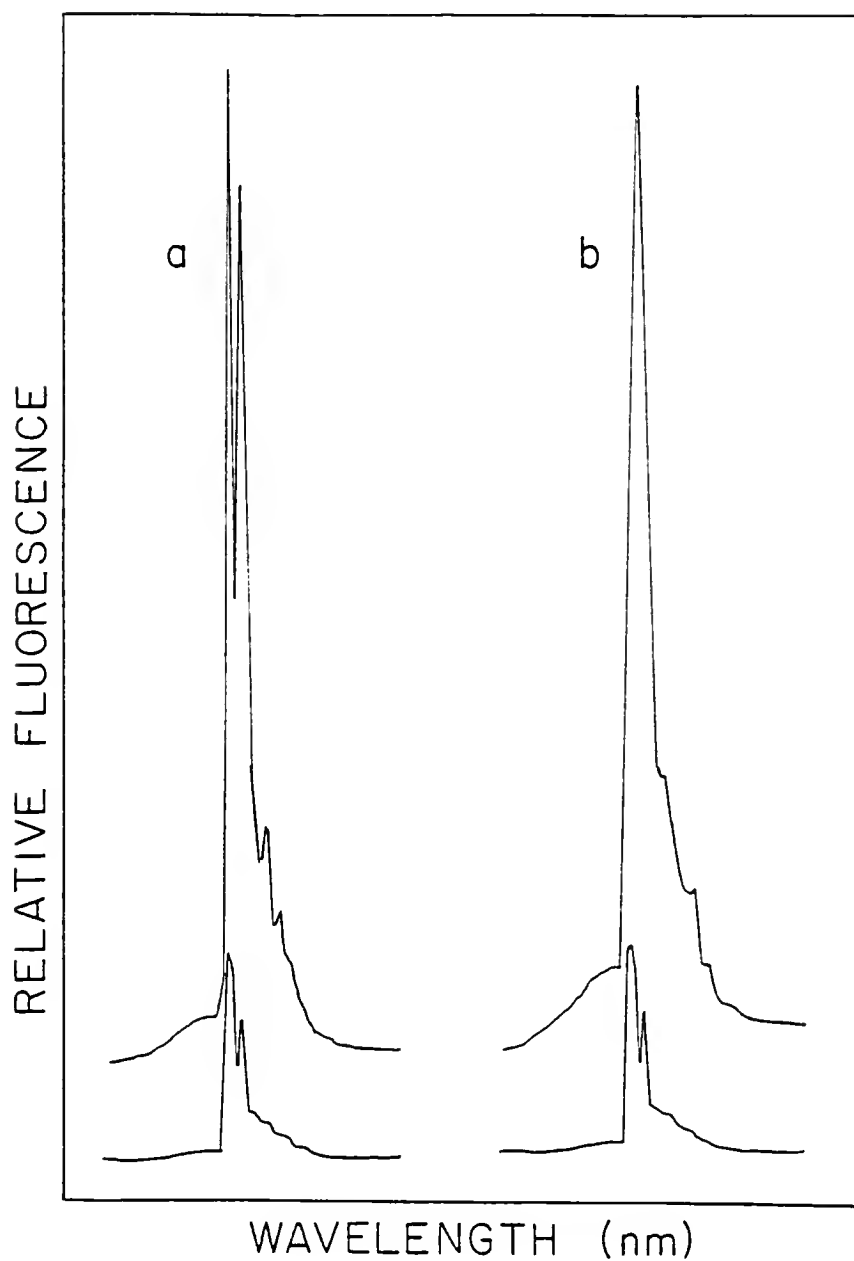


Figure 37. Constant energy scans of carbaryl with  $\Delta\bar{\nu} = 2650 \text{ cm}^{-1}$ . Showing the results obtained with the same variation in parameters described in Figure 36.

For carbofuran, the constant energy spectrum is superimposed on a solvent background peak at  $\bar{\nu} = 2650 \text{ cm}^{-1}$ . To minimize the solvent background interference and to optimize throughput and resolution based on excitation and emission scans, a  $1400 \text{ cm}^{-1}$  constant energy difference is used for detection of carbofuran. However, it should be noted that even in the presence of the solvent peak, carbofuran could be readily detected at concentrations only slightly higher than the limit of detection when a constant energy difference of  $1400 \text{ cm}^{-1}$  is used (see Table VII and Figure 35).

Figure 38 shows the effect of varying bandpasses on the excitation and emission monochromators for the three component mixture. For scan a) both monochromator bandpasses are 1.5 nm; for b) the excitation bandpass is 2.5 nm and the emission bandpass is 1.5 nm, and for scan c) the excitation bandpass is 1.5 nm and the emission bandpass is 2.5 nm. It can be seen that for these variations in bandpasses, signal intensities are increased while resolution is maintained for identification and quantitation purposes. Optimum parameter selection will be determined by the complexity of the mixture being studied, the specific components being determined, and the concentration of the analytes. Depending on the application, one may wish to trade resolution for increased sensitivity or vice versa.

In conclusion, we feel that we have demonstrated the sensitivity and selectivity of CESLS, an inexpensive and reliable method, for analysis of pesticides and hope that in the future this technique will find wide applicability to studies involving pesticides as well as other complex mixtures where physical separations may be avoided.

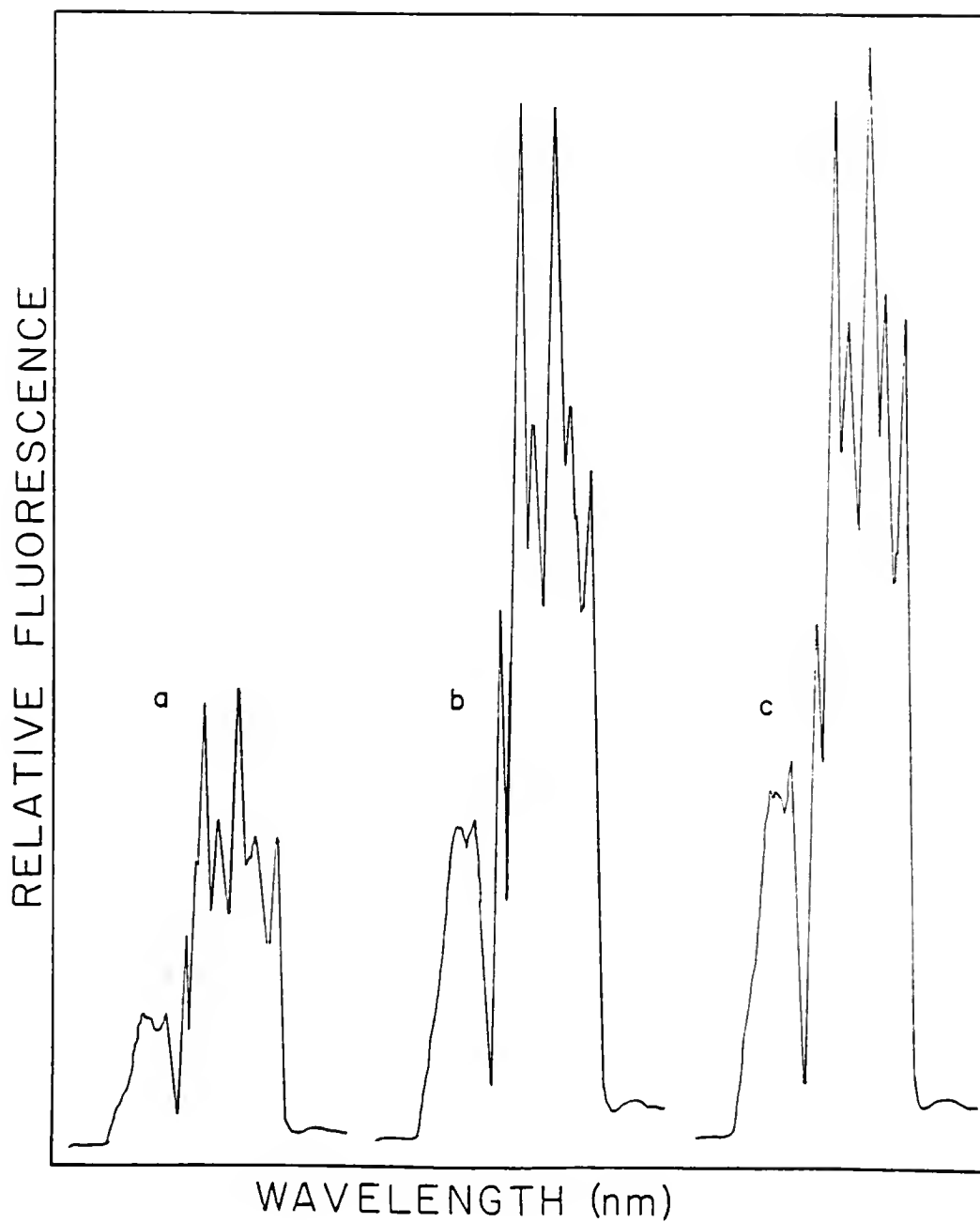


Figure 38. Constant energy scans of a mixture of carbaryl, naphthol, and carbofuran with a) bandpasses of 1.5 nm on both monochromators, b) excitation bandpass of 2.5 nm and emission bandpass 1.5 nm, and c) excitation bandpass 1.5 nm and emission bandpass 2.5 nm.

## CHAPTER 5 TIME RESOLVED PHOSPHORIMETRY

### Introduction

If a molecule absorbs light and is excited into a singlet excited state, it may then undergo intersystem crossing into the excited triplet state. If this molecule then decays radiatively to the ground state this transition is termed phosphorescence. This process is outlined in the Jablonski diagram presented in Figure 1, Chapter 1. The reader is referred to Vo-Dinh (57) and previous references (17-20) for a thorough explanation of parameters affecting phosphorescence, as well as descriptions of methods currently employed for measuring phosphorescence signals.

Phosphorimetry has a unique advantage over many analytical measurement methods. This advantage is the possibility of conducting time-resolved measurements to distinguish between compounds whose phosphorescence spectra overlap but which have different lifetimes. This possibility is graphically illustrated in Figure 39.

Time resolution measurements can be made by using many different types of devices. Mechanical choppers are the simplest and most common devices employed. The excitation radiation is periodically interrupted and the emission is observed after a time delay following the excitation cycle. The phosphorescence signal that persists after the excitation has ceased can therefore be detected without interference from scattered light and fluorescence emission. The time delay between the excitation cycle and emission measurement can be varied to

# PHOSPHORESCENCE

## Time Resolution

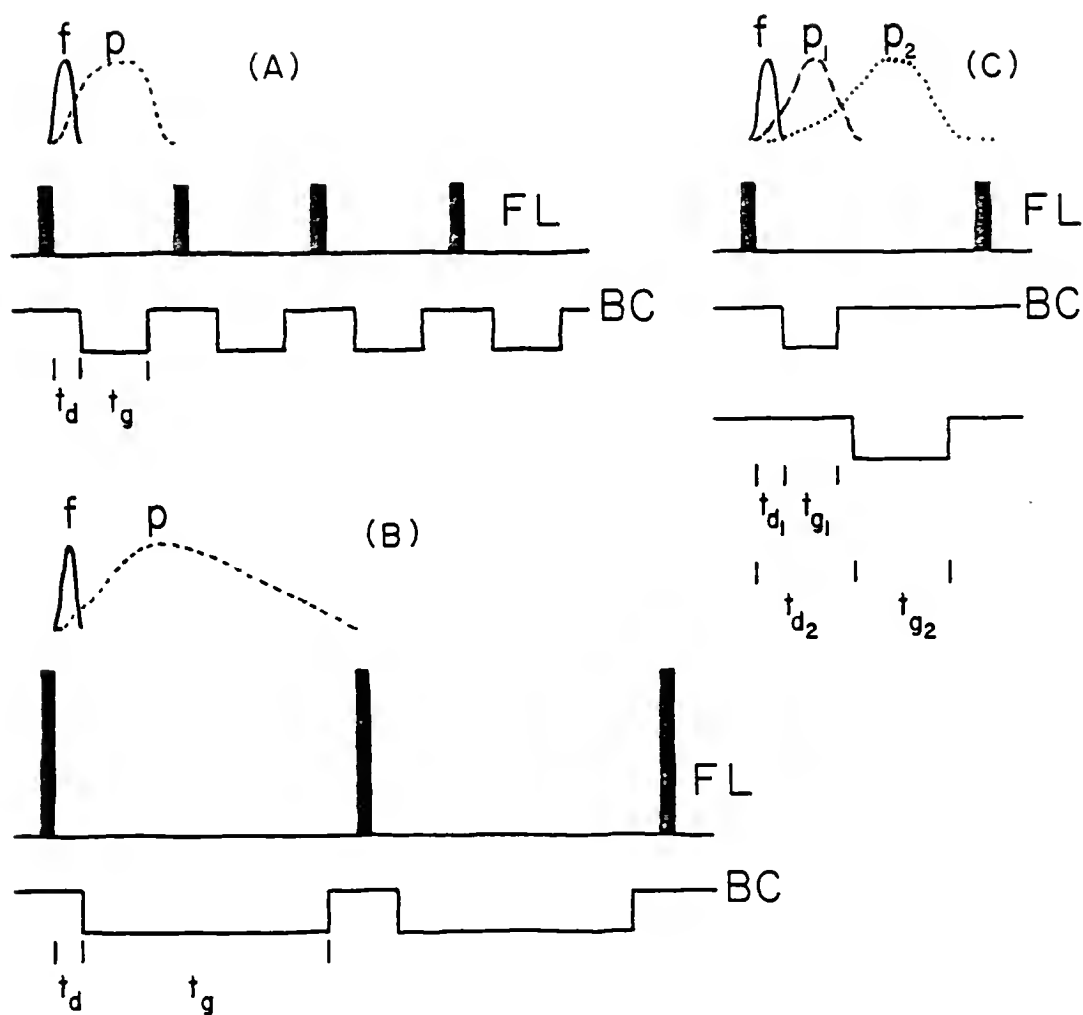


Figure 39. Illustration demonstrating the ability to obtain more selective spectra through the use of time-resolution. FL - flash lamp pulse, BC - boxcar, f - fluorescence, p - phosphorescence,  $t_d$  - delay time,  $t_g$  - gate time, Subscripts used to denote compounds with different excited state lifetimes.

distinguish between short and long lived phosphors. Mechanical devices used for chopping the excitation light include Becquerel discs (58), rotating cylinders (59), and rotating mirrors (60).

A method superior to those using mechanical choppers employs pulsed excitation and electronically gated detection. O'Haver and Winefordner, 1966, and Fisher and Winefordner, 1972, demonstrated the efficiency of pulsed-source time-resolved detection for analyzing mixtures of fast-decaying phosphors (59,61). Later Winefordner and coworkers improved the pulsed-source system by replacing the CW xenon arc lamp and a mechanical chopper with a pulsed xenon flash tube for excitation (62-64). A signal averager or a boxcar integrator was used for detection.

Systems using pulsed nitrogen lasers and flash-tube pumped dye lasers with electronically gated detection have been used to measure phosphorescence lifetimes in the submicrosecond range, record total luminescence, and obtain well resolved phosphorescence spectra (65-68).

Other devices which have been used for detection in time-resolved luminescence measurements are gated PM tubes (69-71), and silicon-intensified target (SIT) vidicons (72).

O'Donnell and Winefordner used time-resolution extensively for analysis of phosphors at low-temperature (77 K) (73). Low temperature is used to minimize non-radiative de-excitation processes of the first excited triplet state such as collisions with solute or solvent molecules. One disadvantage of working at low temperature is the requirement for liquid nitrogen and a dewar with quartz windows to allow passage of ultra violet radiation. A further disadvantage of the dewar system is the loss of energy at each interface in the system

(i.e. air to quartz, quartz to vacuum, vacuum to quartz, quartz to liquid nitrogen, etc.). Also, as the sample freezes it may form a clear glass, a cracked glass, or a snow. Many different variables can affect the appearance of the frozen sample matrix and reproducibility is often a problem. Spinning the sample tube as is done in NMR helps to increase reproducibility, but is not 100% effective.

Vo-Dinh (57) describes room temperature measurements and the many methods such as internal and external heavy atom effects and the use of a variety of substrates to enhance phosphorescence, thereby allowing measurement at temperatures greater than 77 K.

A new system is presented which combines sensitivity, selectivity, and resolution of spectra obtained using constant energy synchronous luminescence spectroscopy with the added selectivity of time-resolved phosphorimetry measurements.

## Experimental

### Instrumentation

The experimental setup was designed to allow maximum versatility. A schematic of the system is presented in Figure 40. Room temperature and low temperature measurements can be made with minimal rearrangement through the use of a room temperature cell attached to a cover which fits over the dewar holder. A pulsed flashlamp (EG&G Model FX-239E) is employed for excitation in phosphorescence measurements and a gated integrator is used for detection. A mirror on a kinematic mount allows one to change over to a continuous xenon arc lamp for excitation in fluorescence measurements, again the emphasis is on versatility.

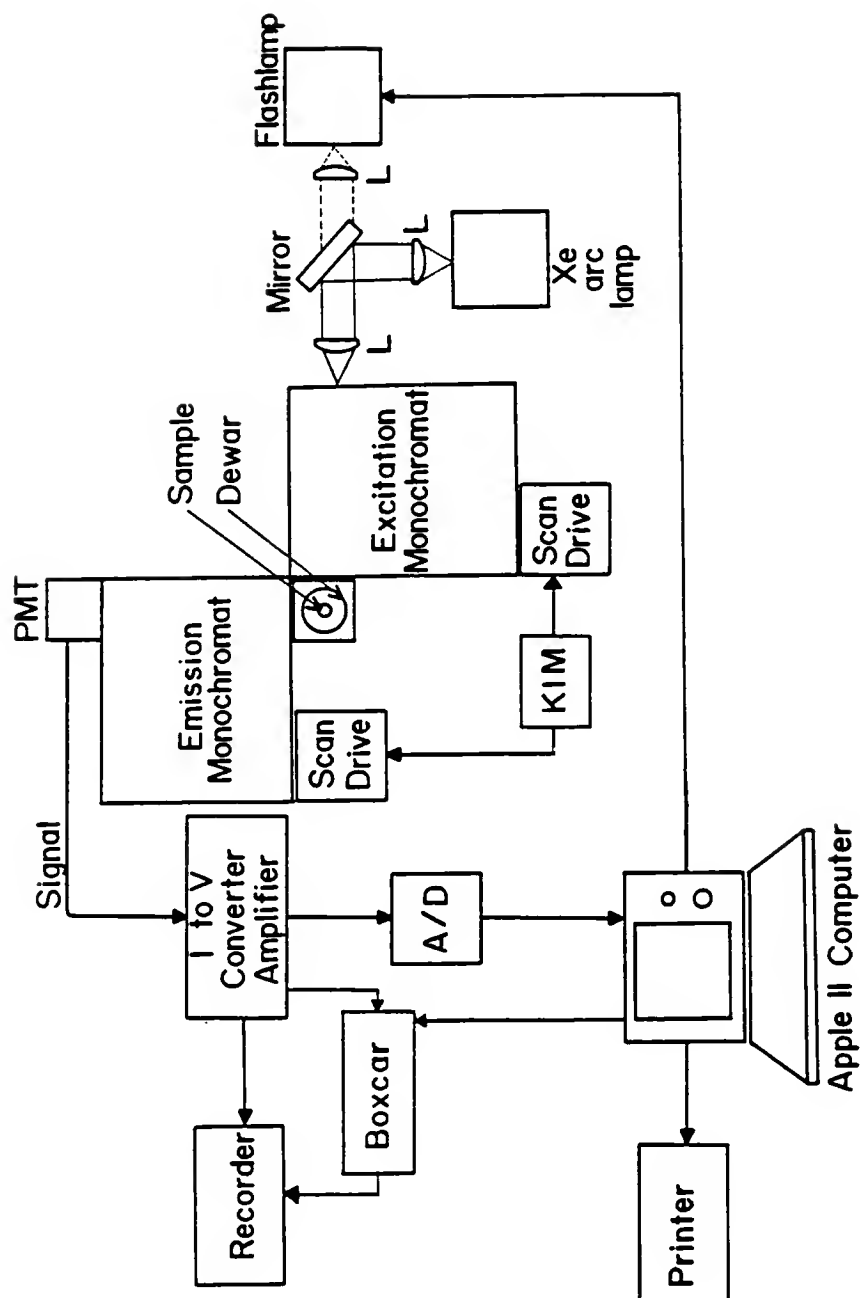


Figure 40. Schematic diagram of experimental system modified to allow time-resolved CESLS.

The synchronous scanning is controlled by a KIM microcomputer. An Apple II plus computer is used to control the pulsing of the source, the gating of the detection system, and to acquire data as the monochromators are scanned. Programs have been written to vary the repetition rate of the source, the time delay between the excitation and detection cycles, and the duration of the detection cycle.

### Sample Preparation

Stock solutions of 100 ppm polyaromatic hydrocarbons (PAHs) were made in hexane. These stock solutions were further diluted with hexane to form working standards. The sources of these materials were given in Chapter 3 of this work.

### Results and Discussion

The ability to employ time-resolved measurements to discriminate between fluorescence and phosphorescence transitions is demonstrated in Figure 41. Figure 41 contains constant energy spectra obtained for benzo(e)pyrene using (a) a continuous source and measuring emission directly, and (b) a flashlamp as the source and measuring emission with a boxcar averager which employs a delay between the excitation and detection cycles.

The constant energy difference for these scans was  $12,000 \text{ cm}^{-1}$ . This value was chosen to optimize detection of phosphorescence, and was calculated from excitation and emission scans using the equation given previously for  $\Delta\bar{\nu}$ .

Figures 42 and 43 illustrate the advantage of being able to combine constant energy fluorescence and phosphorescence scans with  $\Delta\bar{\nu} = 12,000 \text{ cm}^{-1}$  for PAH determination. Figure 42 contains scans for a mixture of phenanthrene and benzo(e)pyrene. Figure 43 contains scans

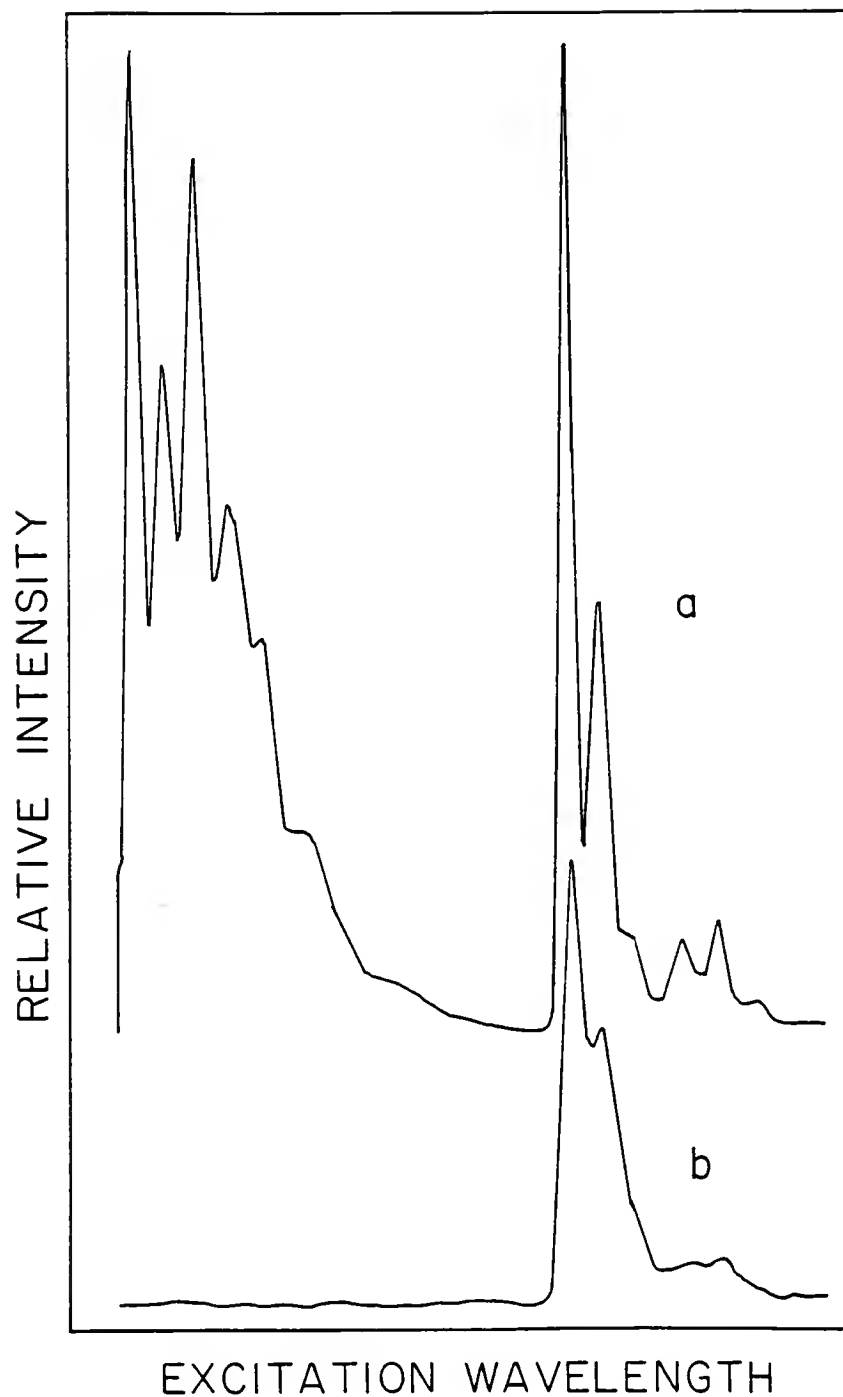


Figure 41. Constant energy scans with  $\Delta\bar{\nu} = 12,000 \text{ cm}^{-1}$  for benzo(e)pyrene obtained using (a) a continuous source and measuring emission directly, and (b) a flashlamp as the source and measuring emission with gated detection.

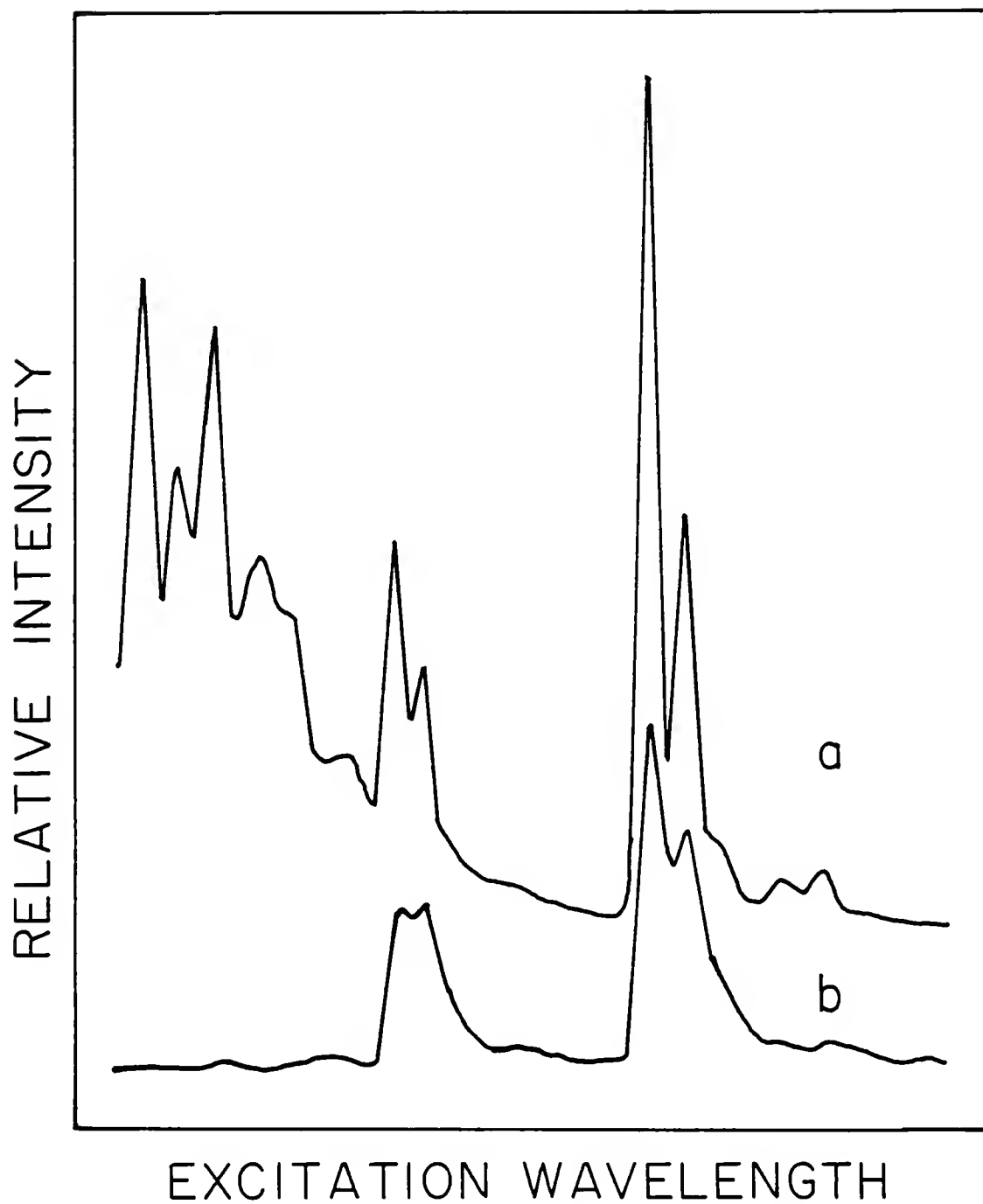


Figure 42. Constant energy scans with  $\Delta\bar{\nu} = 12,000 \text{ cm}^{-1}$  for a mixture of benzo(e)pyrene and phenanthrene obtained using (a) a continuous source and measuring emission directly, and (b) a flashlamp as the source and measuring emission with gated detection.

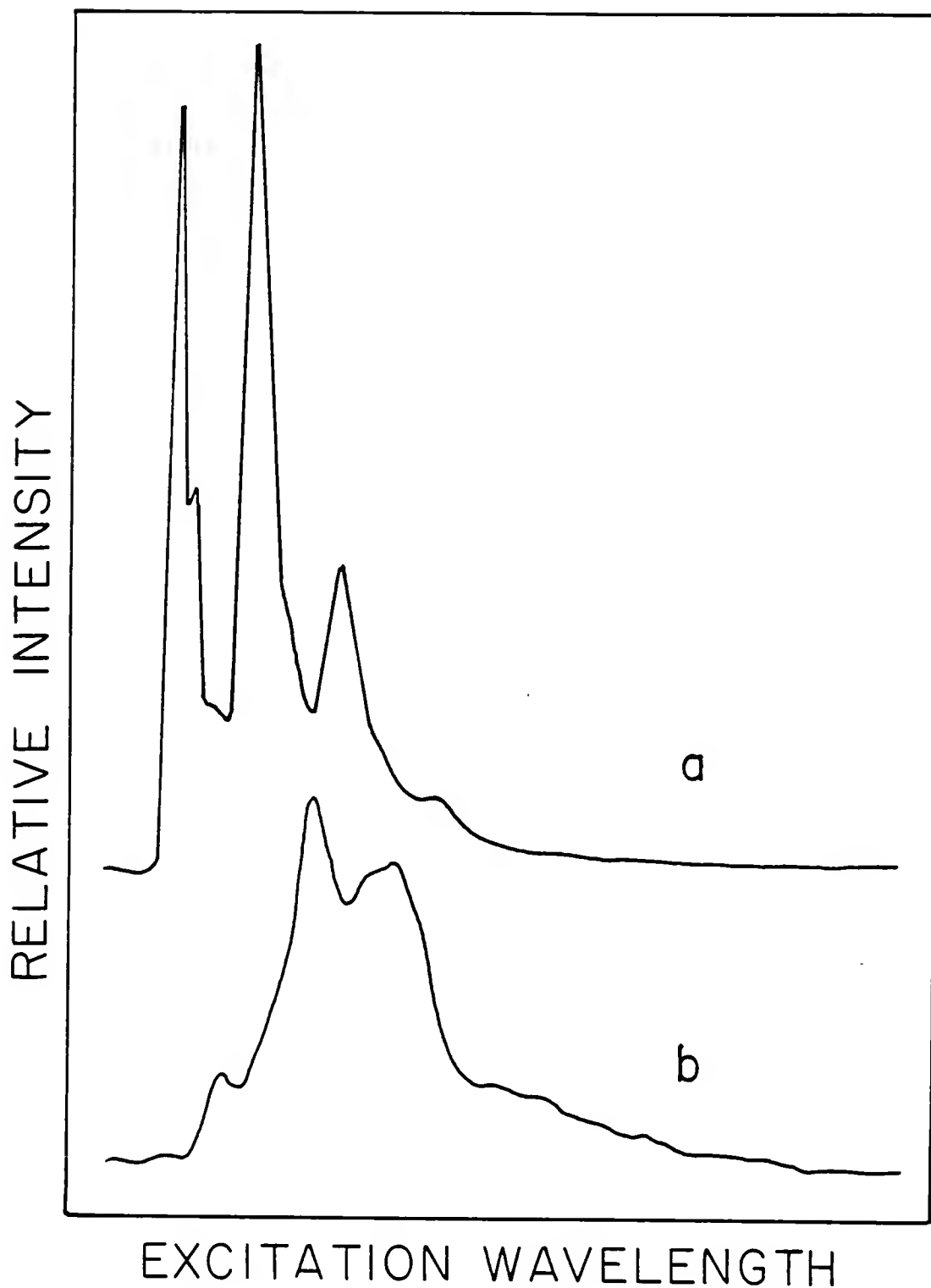


Figure 43. Constant energy scans with  $\Delta\bar{\nu} = 12,000 \text{ cm}^{-1}$  for a mixture of benzo(a)pyrene and carbazole obtained using (a) a continuous source and measuring emission directly, and (b) a flashlamp as the source and measuring emission with gated detection.

for a mixture of carbazole and benzo(a)pyrene. In both figures scans labelled a were obtained using a continuous source and direct detection of emission, while scans labelled b were obtained using a flashlamp and gated detection. Figure 42 demonstrates that although fluorescence peaks for phenanthrene and benzo(e)pyrene overlap, the phosphorescence peaks are well resolved. Compare Figures 41 and 42 to determine the contribution of benzo(e)pyrene to the emission spectra. The enhancement in selectivity obtained with time-resolved measurements allows identification and quantitation of both compounds, without physical separation being required.

Benzo(a)pyrene fluoresces very strongly, but exhibits no phosphorescence. Carbazole exhibits both fluorescence and phosphorescence. Scan a in Figure 43 demonstrates the overlap in the fluorescence and phosphorescence spectra of these compounds. Scan b illustrates the ability to discriminate between the fluorescence of both compounds and to detect only the phosphorescence of carbazole. Again the increase in information obtained through the use of scans obtained under different conditions has been demonstrated.

The results presented here were chosen to illustrate the selectivity enhancement obtained through the use of time-resolved measurements. The potential of constant energy scanning in combination with band narrowing techniques and time-resolved measurements is only beginning to be realized. In the future, the advantages of this system will be exploited to analyze complex mixtures. The ability to vary the delay and gate times of detection relative to excitation will allow one to obtain very selective spectra which can be optimized for specific

components in the mixture. Also, if samples are very complex a combination of spectral fingerprints obtained under a variety of conditions (i.e. different  $\Delta\bar{\nu}$  values, variable time delays and gates, room and low temperature measurements, etc) can be used to confirm identification which might be difficult if not impossible.

## CHAPTER 6 CONCLUSION

### Summary

A complete evaluation of constant energy synchronous luminescence spectroscopy (CESLS) parameters of peak wavelength maximum, intensity maximum, and peak bandwidth has been presented, with mathematical relationships derived for each parameter as it is affected by the luminescence excitation and emission spectral characteristics and the scan path. Computer plots were generated to graphically illustrate these relationships. Model compounds were used to demonstrate the application of these relationships, and to compare results obtained with constant energy and constant wavelength scanning. Results of this study demonstrated the band-narrowing achieved through synchronous scanning as well as the ability of CESLS to exploit the natural energy relationships fundamental to spectroscopic evaluation of luminescent compounds.

CESLS at low temperature (77 K) was applied to fingerprinting gasoline exhaust samples containing polyaromatic hydrocarbons (PAHs). One sampling system was used to obtain a single sample for the exhaust generated by different types of gasolines. Another system involved a crude sample separation based on temperature. The separation system provided increased selectivity and sample information. It also confirmed previous results demonstrating the effect sampling methodology can have on the number and quantity of PAHs found in engine exhaust.

This study demonstrated the sensitivity of CESLS for PAH analysis, especially for fingerprinting and screening samples. This method would be well suited for preliminary screening to evaluate systems proposed for reducing PAH emission from engines.

CESLS was also applied to environmental analysis involving gasoline and crude oil samples containing PAHs. Sample identification at low temperature (77 K) with quartz tubes and room temperature on filter paper was compared. The ability to identify individual PAHs in samples as well as fingerprint different samples based on total PAH content with CESLS was demonstrated.

The room temperature scans on filter paper often yielded enough information for conclusive sample identification and are simpler to obtain than low temperature measurements. These scans would be especially useful for distinguishing between known samples. The room temperature scans could also be used for preliminary sample screening and to provide information complimentary to that obtained at low temperature.

Measurements made at low temperature provide greater spectral resolution, and it was demonstrated that this enhancement in resolution was usually necessary to identify specific PAHs and to provide information required to distinguish between samples which were very similar.

This study indicated the feasibility of using CESLS to identify the source of an environmental hazard such as an oil spill or a leak at a service station.

Due to the documented high quantum yields of many pesticides, CESLS at low temperature was proposed for determining compounds in this

class. Based on theoretical calculations involving optimization of experimental parameters, carbaryl, naphthol, and carbofuran were evaluated under a variety of bandpasses and constant energy differences. Limits of detections and analytically useful ranges were established for these compounds under varying conditions. Results indicated that optimum parameter selection will be determined by the complexity of the mixture being studied, the specific components being determined, and the concentration of the analytes. Depending on the application, one may wish to trade resolution for increased sensitivity or vice versa.

CESLS was demonstrated to be both sensitive and selective enough for analysis of pesticides. Hopefully, based on results such as these CESLS will find wide applicability to studies involving pesticides as well as other complex mixtures where physical separation may be avoided.

Finally, a system was established to allow combining CESLS with time-resolved measurements. The emphasis in the design of the system was in maintaining versatility. The arrangement allows one to choose between a continuous xenon arc lamp for fluorescence and a flashlamp for phosphorescence. Also, the cell holder was designed to allow room and low temperature measurements. The added selectivity of time-resolution allows one to discriminate between compounds which have similar luminescence spectral characteristics, but whose excited state lifetimes are different.

Time-resolved CESLS was applied to analysis of synthetic mixtures containing PAHs to demonstrate the added selectivity and information enhancement achieved with this technique.

### Future Work

The CESLS design currently allows room and low temperature measurements and the ability to conduct fluorescence and phosphorescence analysis. In the future more system modifications are expected to aid in fully realizing the potential of CESLS. One device which is under consideration for use in conjunction with CESLS is a refrigeration system which allows one to choose and maintain a sample temperature between 77 and 323 K. This device operates on the Joule-Thompson effect and cools a small sample stage. The ability to vary the sample temperature can be used to conduct more extensive studies into the effect of temperature on luminescence spectral characteristics. Also, solid samples as well as liquid samples on different substrates can be analyzed with this system.

In the future, it is also expected that CESLS will be combined with data manipulation techniques such as factor analysis. Such techniques will help to enhance the usefulness of the data obtained using CESLS.

The sensitivity and selectivity of CESLS will be applied to analysis of mixtures containing a wide variety of compounds. CESLS has already been applied successfully to PAH and pesticide analysis, and has shown promise in preliminary experiments involving pharmaceuticals.

Special emphasis will be placed on utilizing the versatility of the experimental design. Combinations of spectra obtained under a variety of experimental conditions will be used to maximize sample information. It is expected that combining information in this manner will allow sample identification which might be difficult if not impossible otherwise.

## GLOSSARY

$\lambda_i$	- excitation wavelength (nm)
$\lambda_j$	- emission wavelength (nm)
$\lambda_{i_o}$	- peak excitation wavelength (nm)
$\lambda_{j_o}$	- peak emission wavelength (nm)
$\bar{\nu}_i$	- energy equivalent to $\lambda_i$ ( $\text{cm}^{-1}$ )
$\bar{\nu}_j$	- energy equivalent to $\lambda_j$ ( $\text{cm}^{-1}$ )
$\bar{\nu}_{i_o}$	- energy equivalent to $\lambda_{i_o}$ ( $\text{cm}^{-1}$ )
$\bar{\nu}_{j_o}$	- energy equivalent to $\lambda_{j_o}$ ( $\text{cm}^{-1}$ )
$x_i$	- excitation intensity at $\lambda_i$ or $\bar{\nu}_i$
$x_{i_o}$	- excitation intensity at $\lambda_{i_o}$ or $\bar{\nu}_{i_o}$
$y_j$	- emission intensity at $\lambda_j$ or $\bar{\nu}_j$
$y_{j_o}$	- emission intensity at $\lambda_{j_o}$ or $\bar{\nu}_{j_o}$
$M_{ij}$	- luminescence intensity at $\lambda_i, \lambda_j$ or $\bar{\nu}_i, \bar{\nu}_j$
$M_{ijs}$	- luminescence intensity of synchronous scan at $\lambda_i, \lambda_j$
$M_{ijs_o}$	- luminescence intensity maximum of synchronous scan
$M_o$	- luminescence intensity at $\lambda_{i_o}, \lambda_{j_o}$
$\sigma_i$	- standard deviation of excitation peak ( $\text{cm}^{-1}$ )
$\sigma_j$	- standard deviation of emission peak ( $\text{cm}^{-1}$ )
$\sigma_s$	- standard deviation of synchronous peak ( $\text{cm}^{-1}$ )
$\Delta\lambda$	- wavelength difference in conventional synchronous scan (nm)
$\Delta\bar{\nu}$	- energy difference in CESLS scan ( $\text{cm}^{-1}$ )
$\lambda_{s_o}$	- wavelength of synchronous maximum (nm)
$\bar{\nu}_{s_o}$	- energy equivalent to $\lambda_{s_o}$ ( $\text{cm}^{-1}$ )
$\delta\lambda_i$	- luminescence excitation bandwidth (nm)

## Glossary. Continued.

$\delta\lambda_j$	- luminescence emission bandwidth (nm)
$\delta\lambda_s$	- synchronous luminescence bandwidth (nm)
$\delta\bar{\nu}_i$	- luminescence excitation bandwidth ( $\text{cm}^{-1}$ )
$\delta\bar{\nu}_j$	- luminescence emission bandwidth ( $\text{cm}^{-1}$ )
$\delta\bar{\nu}_s$	- synchronous luminescence bandwidth ( $\text{cm}^{-1}$ )

## For geometric model

x	= $\bar{\nu}_i - \bar{\nu}_{i_o}$ ( $\text{cm}^{-1}$ )
y	= $\bar{\nu}_j - \bar{\nu}_{j_o}$ ( $\text{cm}^{-1}$ )
a	= $\delta\bar{\nu}_i/2$ ( $\text{cm}^{-1}$ )
b	= $\delta\bar{\nu}_j/2$ ( $\text{cm}^{-1}$ )

## REFERENCES

- (1) A. Colmsjo and U. Stenberg, Anal. Chem. 51, 145 (1978).
- (2) R. J. Hurtubise and J. D. Phillip, Anal. Chim. Acta 52, 159 (1978).
- (3) T. Nielsen, J. Chromatogr. 170, 147 (1979).
- (4) G. F. Kirkbright and C. G. deLima, Analyst (London) 99, 338 (1974).
- (5) L. M. Shabad and G. A. Smirnov, Atmos. Environ. 6, 153 (1972).
- (6) E. Sawicki, T. W. Staley, W. C. Elbert, and J. D. Pfaff, Anal. Chem. 36, 497 (1964).
- (7) E. B. Asafu-Adjaye, J. I. Yun, and S. Y. Su, Anal. Chem. 57(4), 904 (1985).
- (8) E. M. Sparacino and J. W. Hines, J. Chromatogr. Sci. 14, 549 (1976).
- (9) R. J. Argauer and J. D. Warthen, Anal. Chem. 47(14) 2472 (1975).
- (10) G. G. Guilbaut and M. H. Sadar, Anal. Chem. 41(2) 366 (1969).
- (11) R. W. Frei and J. F. Lawrence, J. Chromatogr. 67, 87 (1972).
- (12) M. J. Larkin and M. J. Day, Anal. Chim. Acta 108, 425 (1979).
- (13) W. R. McLeod and G. N. Vaughan, J. Chromatogr. 275, 21 (1985).
- (14) C. Parkanyi, D. Bouin, D. C. Shieh, S. Tunbrant, J. J. Aaron, and A. Tine, J. Chim. Phys. 81, 21 (1985).
- (15) I. W. Tsina, M. Fass, J. A. Debban, and S. B. Martin, Clin. Chem. 28, 1137 (1982).
- (16) S. C. J. Cole, R. J. Flanagan, A. Johnston, and D. W. Holt, J. Chromatogr. 218, 621 (1981).
- (17) S. G. Schulman, Molecular Luminescence Spectroscopy, Methods and Applications: Part 1, John Wiley & Sons, Inc., New York (1985).
- (18) N. J. Turro, Modern Molecular Photochemistry, Benjamin/Cummings Publishing Company, Inc., Menlo Park, CA (1978).

- (19) C. A. Parker, Photoluminescence of Solutions, Elsevier Publishing Company, New York (1968).
- (20) J. D. Winefordner, T. C. O'Haver, and S. G. Schulman, Luminescence Analysis, in Analytical Chemistry, John Wiley & Sons, New York (1972).
- (21) E. L. Wehry and G. Mamantov, in Modern Fluorescence Spectroscopy Vol. 4, E. L. Wehry, ed., Plenum Press, New York (1981).
- (22) H. H. Jaffe and M. Orchin, Theory and Applications of Ultraviolet Spectroscopy, John Wiley & Sons, New York (1962).
- (23) I. B. Berlman, Handbook of Fluorescence Spectra of Aromatic Molecules, Academic Press Inc., New York (1965).
- (24) W. Karcher, R. J. Fordham, J. J. Dubois, P. G. J. M. Glaude, and J. A. M. Ligthart, Spectral Atlas of Polycyclic Aromatic Compounds, P. Reidel Publishing Company, Dordrecht, Holland (1985).
- (25) E. L. Inman, Ph.D. dissertation, University of Florida, Gainesville, FL (1984).
- (26) T. Vo-Dinh in Modern Fluorescence Spectroscopy Vol. 4, E. L. Wehry, ed., Plenum Press, New York (1981).
- (27) J. N. Miller, Analyst 109, 191 (1984).
- (28) B. J. Clark, A. F. Fell, K. T. Milne, D. M. G. Pattie, and M. H. Williams, Anal. Chim. Acta 170, 35 (1984).
- (29) E. L. Inman and J. D. Winefordner, Anal. Chem. 54, 2018 (1982).
- (30) M. J. Kerkhoff, Ph.D. dissertation, University of Florida, Gainesville, FL (1984).
- (31) T. Vo-Dinh, Anal. Chem. 50, 396 (1978).
- (32) A. C. Andre, M. Bouchy, and M. L. Viriot, Anal. Chim. Acta 105, 297 (1979).
- (33) E. L. Inman and J. D. Winefordner, Anal. Chim. Acta 138, 245 (1982).
- (34) J. B. F. Lloyd and I. W. Evett, Anal. Chem. 49, 1710 (1977).
- (35) J. C. Andre, M. Bouchy, M. Niclaude, and Ph. Baudot, Anal. Chim. Acta 92, 369 (1977).
- (36) J. C. Andre, Ph. Baudot, and M. Niclaude, Clin. Chim. Acta 76, 55 (1977).

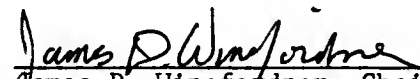
- (37) I. M. Warner, G. D. Christian, E. R. Davidson, and J. B. Callis, Anal. Chem. **49**, 564 (1977).
- (38) D. W. Johnson, J. B. Callis, and G. D. Christian, Anal. Chem. **49**, 747A (1977).
- (39) E. L. Inman and J. D. Winefordner, Anal. Chim. Acta **141**, 241 (1982).
- (40) M. J. Kerkhoff, L. A. Files, and J. D. Winefordner, Anal. Chem. **85**, 1673 (1985).
- (41) G. Grimmer, Environmental Carcinogens: Polycyclic Aromatic Hydrocarbons, CRC Press, Inc., Boca Raton (1983).
- (42) M. Cooke and A. J. Dennis, Polynuclear Aromatic Hydrocarbons: Formation, Metabolism and Measurement, Battelle Press, Columbus, OH (1983).
- (43) J. Jacob, W. Karcher, J. J. Belliardo, and P. J. Wagstaffe, Fresenius Z Anal. Chem. **317**, 101 (1986).
- (44) J. Jacob, W. Karcher, J. J. Belliardo, and P. J. Wagstaffe, Fresenius Z Anal. Chem. **323**, 1 (1986).
- (45) D. Schuetzle, Environmental Health Perspectives **47**, 65 (1983).
- (46) M. Yu and R. A. Hites, Anal. Chem. **53**(3), 951 (1981).
- (47) M. J. Kerkhoff, T. M. Lee, E. R. Allen, D. A. Lundgren, and J. D. Winefordner, Environ. Sci. Technol. **19**, 695 (1985).
- (48) M. J. Kerkhoff, E. L. Inman, E. Voigtman, L. P. Hart, and J. D. Winefordner, Appl. Spectrosc. **38**, 239 (1984).
- (49) J. J. Aaron, M. Andino, and J. D. Winefordner Anal. Chim. Acta **160**, 171 (1984).
- (50) S. I. Lamb, C. Petrowski, I. R. Kaplan, and B. R. T. Simoneit J. Air Pollut. Control Assoc. **30**, 1098 (1980).
- (51) W. N. Billings and T. F. Bidleman, Environ. Sci. Technol. **14**, 679 (1980).
- (52) B. C. Turner and D. E. Glotfelty, Anal. Chem. **49**, 7 (1977).
- (53) T. Braun and A. B. Farag, Anal. Chem. **99**, 1 (1978).
- (54) W. Cautrells and K. Van Cauwenbergh, Atmos. Environ. **12**, 1133 (1978).

- (55) P. T. Haskell, Pesticide Application: Principles and Practice, Clarendon Press, Oxford University Press, New York (1985).
- (56) R. D. Voyksner and J. T. Bursey, Anal. Chem. 56, 1582 (1984).
- (57) T. Vo-Dinh, Room Temperature Phosphorimetry for Chemical Analysis John Wiley & Sons, New York (1984).
- (58) C. A. Parker and C. G. Hatchard, Trans. Farad. Soc. 57, 1894 (1961).
- (59) T. C. O'Haver and J. D. Winefordner, Anal. Chem. 38, 682 (1966).
- (60) T. Vo-Dinh, G. L. Walden, and J. D. Winefordner, Anal. Chem. 49, 1126 (1977).
- (61) R. P. Fisher and J. D. Winefordner, Anal. Chem. 44, 948 (1972).
- (62) C. M. O'Donnell, K. F. Harbaugh, R. P. Fisher, and J. D. Winefordner, Anal. Chem. 45, 607 (1973).
- (63) K. F. Harbaugh, C. M. O'Donnell, and J. D. Winefordner, Anal. Chem. 45, 39 (1973).
- (64) K. F. Harbaugh, C. M. O'Donnell, and J. D. Winefordner, Anal. Chem. 46, 1206 (1974).
- (65) T. Vo-Dinh, R. Paetzold, and U. P. Wile, Zeit. Phys. Chem. 251, 395 (1972).
- (66) T. Vo-Dinh and U. P. Wild, Appl. Opt. 12, 1286 (1973).
- (67) G. D. Boutillier and J. D. Winefordner, Anal. Chem. 51, 1384 (1979a).
- (68) G. D. Boutillier and J. D. Winefordner, Anal. Chem. 51, 1391 (1979b).
- (69) T. D. S. Hamilton and R. K. Razi Naqui, Anal. Chem. 45, 1581 (1973).
- (70) G. B. Strambini and W. C. Galley, Canadian J. Spectrosc 21, 1 (1976).
- (71) E. Lue-Yen Bower, G. D. Boutillier, and J. D. Winefordner, Canadian J. Spectrosc. 22, 120 (1977).
- (72) D. E. Goeringer and H. L. Pardue, Anal. Chem. 51, 1054 (1979).
- (73) C. M. O'Donnell and J. D. Winefordner, Clin. Chem. 21, 285 (1975).

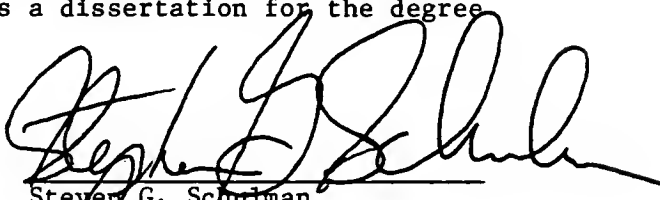
#### BIOGRAPHICAL SKETCH

Leigh Ann Files was born on March 31, 1960, in Brinkley, Arkansas. She grew up in Hunter, Arkansas, and graduated in May 1978 from Brinkley High School. She received a Bachelor of Science degree in chemistry from Arkansas State University in May 1982. Leigh Ann participated in a research project at the University of Alabama during the summer of 1981. The interest in research generated by this project was instrumental in her decision to attend graduate school. Leigh Ann began graduate school at the University of Florida in August 1982, and she is currently a candidate for a Doctor of Philosophy degree in analytical chemistry.

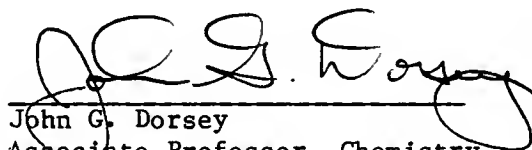
I certify that I have read this study and that in my opinion it conforms to acceptable standards of scholarly presentation and is fully adequate, in scope and quality, as a dissertation for the degree of Doctor of Philosophy.

  
James D. Winefordner, Chairman  
Graduate Research Professor,  
Chemistry

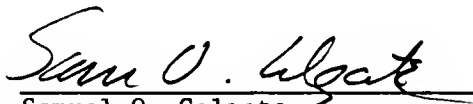
I certify that I have read this study and that in my opinion it conforms to acceptable standards of scholarly presentation and is fully adequate, in scope and quality, as a dissertation for the degree of Doctor of Philosophy.

  
Steven G. Schulman  
Professor, Pharmacy

I certify that I have read this study and that in my opinion it conforms to acceptable standards of scholarly presentation and is fully adequate, in scope and quality, as a dissertation for the degree of Doctor of Philosophy.

  
John G. Dorsey  
Associate Professor, Chemistry

I certify that I have read this study and that in my opinion it conforms to acceptable standards of scholarly presentation and is fully adequate, in scope and quality, as a dissertation for the degree of Doctor of Philosophy.

  
Samuel O. Colgate  
Associate Professor, Chemistry

I certify that I have read this study and that in my opinion it conforms to acceptable standards of scholarly presentation and is fully adequate, in scope and quality, as a dissertation for the degree of Doctor of Philosophy.

A. F. Brajter-Toth  
Anna F. Brajter-Toth  
Assistant Professor, Chemistry

This dissertation was submitted to the Graduate Faculty of the Department of Chemistry in the College of Liberal Arts and Sciences and to the Graduate School and was accepted as partial fulfillment of the requirements for the degree of Doctor of Philosophy.

August 1986

Dean, Graduate School

